2

NAS 12-602
CR-86186

R-628

IMPROVING AUTOMATIC LANDING SYSTEM PERFORMANCE USING MODERN CONTROL THEORY AND INERTIAL MEASUREMENTS

by
Duncan MacKinnon

January 1969

INSTRUMENTATION LABORATORY

MASSACHUSETTS INSTITUTE OF TECHNOLOGY

Cambridge 39, Ma

R-628

IMPROVING AUTOMATIC LANDING SYSTEM PERFORMANCE USING MODERN CONTROL THEORY AND INERTIAL MEASUREMENTS

by

Duncan MacKinnon

January 1969

INSTRUMENTATION LABORATORY
MASSACHUSETTS INSTITUTE OF TECHNOLOGY
CAMBRIDGE, MASSACHUSETTS 02139

Approved by: _____
Deputy Associate Director

Approved by: _____
Associate Director

Approved by: _____
Deputy Director

ACKNOWLEDGEMENT

The author wishes to acknowledge the sponsorship of Robert Pawlak of the Electronics Research Center of the National Aeronautics and Space Administration, whose interest in the applications of inertial navigation to all-weather landing resulted in the establishment of the project reported herein. We are also indebted to Paul Fahlstrom of the Federal Aviation Agency whose interest in the problem was also instrumental in establishing the project.

The author also wishes to acknowledge the many helpful suggestions and guidance provided by Charles Broxmeyer. The mathematical models of the vehicle were derived by Paul A. Madden. The author acknowledges the programming help provided by Eugenia Freiburghouse.

This report was prepared under DSR Project 55-30500, sponsored by the Electronics Research Center of the National Aeronautics and Space Administration through Contract NAS 12-602 with the Instrumentation Laboratory of Massachusetts Institute of Technology in Cambridge, Massachusetts.

The publication of this report does not constitute approval by the National Aeronautics and Space Administration of the findings or the conclusions contained therein. It is published only for the exchange and stimulation of ideas.

R-628

AUTOMATIC LANDING SYSTEM OPTIMIZATION USING MODERN CONTROL THEORY AND INERTIAL MEASUREMENTS

ABSTRACT

Conventional automatic landing system designs for commercial transports have been primarily based on the utilization of Instrument Landing System (ILS) information to provide the position information required for acquisition and tracking of the landing glide path. Lateral position relative to a vertical plane passing through the runway centerline is derived from the localizer receiver output. Position relative to a vertical reference path is generated by processing the output of the glideslope receiver.

The spacial reference surfaces defined by the ILS signals are ideally plane, however, as a result of reflections from objects on the ground illuminated by the localizer and glideslope transmitter antennae, irregularities, referred to as "beam bending" or "beam noise", are superimposed on the planar surfaces. Beam irregularities are the most significant source of noise in a conventional landing system. The amplitude of the noise is large enough to produce significant performance limitations on the landing system as a result of filtering and gain limitations which must be introduced due to saturation limits on vehicle effectors.

Inertial navigator position and velocity is relatively free from the high frequency noise which plagues ILS information, however, erroneous, low frequency, gyro-drift induced, variations in position and velocity exist. The position error after a typical flight is measured in nautical miles, for example. This error would appear to preclude the application of inertial position for flight trajectory control during the terminal phases of flight. The possibility of combining the desirable low frequency characteristics of the ILS sensor with the broad bandwidth of the inertial information then suggests itself. By applying a systematic mathematical estimation technique to the signals from the ILS and inertial navigator it is possible to correct the inertially measured position and velocity. The result is position and velocity information which is relatively free from noise compared to the information provided by the ILS.

In order to obtain maximum advantage from the noise free corrected inertial position and velocity data a complete review of the lateral and vertical position control systems was carried out. Primary attention was focused on improving the

magnitude characteristics of the open loop transfer functions of the vertical and lateral position regulators to increase bandwidth and minimize the effects of environmental disturbances. The ability of the control system to follow a desired trajectory in space was increased by feedforward compensation. Maximum resistance to disturbances is achieved if the control effectors are always operated in an unsaturated condition. Optimization theory is applied to synthesize trajectories which the vehicle can follow (in the absence of disturbances) without saturating the effectors. This report develops the new control system structures and compares the performances of new and conventional automatic landing systems.

Duncan MacKinnon
January 1969

TABLE OF CONTENTS

TABLE OF CONTENTS (cont.)

TABLE OF CONTENTS (cont.)

CHAPTER 1

INTRODUCTION

1.1 Introduction

Routine all-weather landing of transport aircraft is one of the outstanding unsolved problems of present-day technology. The importance of the problem and its implications both for passenger safety and for economic operation of airlines have been recognized for decades. Now that the jumbo-type transport and the supersonic transport are soon to be introduced into passenger service the problem of all-weather landing may be considered to be a critical factor limiting the full utilization of these aircraft.

Over the past ten years, important strides have been made in the direction of the goal of all-weather landing. Of these, the most important has undoubtedly been the actual implementation of aircraft control systems which use Instrument Landing System (ILS) information and which have successfully performed thousands of automatic landings. An outstanding example is the system developed by the Blind Landing Experimental Unit (BLEU) of the Naval Aircraft Establishment, United Kingdom (see ref (1)).* It is highly probable that the basic concepts of control in what might be termed a classical automatic landing system such as the BLEU system will provide the conceptual framework for the systems that will eventually be adopted. It does not appear, however, that systems exist which will provide the invariable accuracy, reliability and independence from external disturbances, which will be mandatory for routine all-weather landing of transport aircraft.

The point of view of the study described in this report is twofold. The study is concerned with the implications of inertial navigation technology for the all-weather landing problem. As a corollary, the study is concerned with the application of control theory, both classical and modern, for the effective utilization of the inertial equipment. The study is directed particularly towards the development of an all-weather landing system for the supersonic transport (SST). The SST presents a particularly challenging landing problem as a result of its high approach speed and its aerodynamic characteristics. It should be emphasized, however, that the results of the study may be applied to any aircraft.

*References (1) to (25) were referred to in reference 26 and are included in the table of references for completeness.

Over the past twenty years, an increasingly sophisticated technology of inertial navigation and guidance systems has grown up. This technology has been grounded on the continuous development of extremely precise reference components, principally floated gyros and accelerometers and a parallel development of support technology, such as gimbal structures, angular encoders, and thermal control systems. The concurrent advances in computer technology have been indispensible to the rapid advances made in inertial systems. The developments in inertial navigation and guidance have been almost entirely motivated by military requirements. While the utility of inertial navigation systems for commercial aircraft has been recognized, the participation of commercial aircraft users in inertial navigation development has been a minor factor because of the costs involved. It is now considered, however, that the accuracy, reliability and production costs of inertial navigation equipment originally developed for military pruposes are such that they are appropriate for commercial use. Plans for the large commercial transports soon to be introduced invariably include one or more inertial navigation systems per aircraft. It is planned, for example, that the SST will carry three inertial navigation systems to provide redundancy.

Search of the available literature fails to show that any significant application of inertial navigation technology has been made to the automatic landing problem. A primary purpose of the present study, as noted, has been to demonstrate, by computer simulation, the implications of inertial navigation for the automatic landing problem. On the basis of work performed to date, it is believed that significant advantages will accrue from appropriate use of inertial navigation equipment. This contention is fully described and documented in the subsequent chapters.

1.2 Aircraft Landing

The problem of landing an aircraft can be defined as a general problem in control theory. The control system, human or automated, must generate a set of commands which transfer the vehicle from some rather general initial state x_i to a terminal state x_f. The initial state is usually on a linear trajectory inclined at some angle ψ_i relative to a vertical reference plane which contains the runway centerline. The terminal state, for the purposes of this discussion, is on a linear path described by the center of gravity of the aircraft in the vertical reference plane as it rolls down the runway centerline. The transfer between these states is usually divided into a number of clearly defined stages which are illustrated in Fig. 1.2.1.

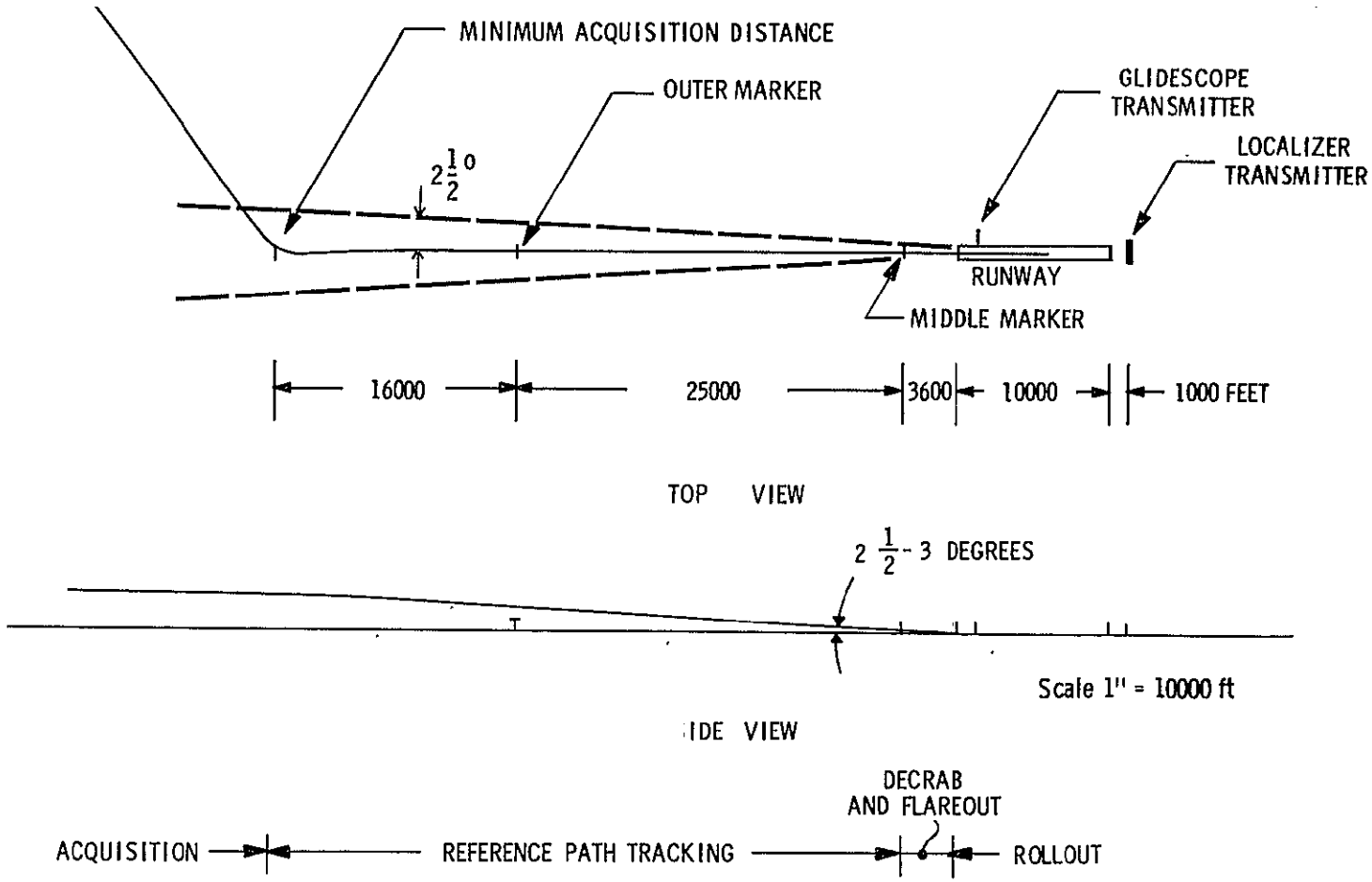

Fig. 1.2.1 Nominal geometrical relationships at the initiation of localizer acquisition.

1. Acquisition· During the acquisition phase the aircraft trajectory is changed to a path coincident with a reference defined by the terminal navigation system: In the case of an ILS system the path is specified by the intersection of two planes defined by the Localizer and Glideslope signals.

2. Reference Path Tracking: During the path tracking phase the vehicle follows the reference defined by the terminal navigation system. The reference path is followed until the vehicle is 70-100 feet above the runway elevation. During this phase a jet transport aircraft descends at approximately 10 feet/second.

3. Flareout: The flareout maneuver occurs during the final phase of flight. The primary purpose of flare is to reduce the vertical rate of descent from approximately 10 feet/second to approximately 2.5 feet/second. Flareout is initiated at the termination of the Reference Path tracking phase.

4. Decrab: If a component of wind perpendicular to the runway centerline exists the aircraft is normally flown at a slight "crab" angle into the crosswind to reduce the lateral component of ground velocity to zero. The decrab maneuver, which occurs during flareout, aligns the longitudinal axis of the aircraft with the runway by rotating the vehicle in an uncoordinated fashion (roll $\phi = 0$).

5. Rollout: Rollout Control is the final phase of vehicle guidance during a landing. The aircraft is on the ground, rolling along the runway. The rollout control system attempts to keep the center of gravity of the vehicle in the vertical reference plane. Thus the landing system must be capable of solving a relatively large assortment of control problems. The next section introduces criteria which may be applied to landing system performance.

1.3 Performance Criteria for Automatic Landing Systems

Before the question of improving a system is approached, it is important to establish the exact nature of the indices which will be used to measure performance. These criteria should reflect the qualities which are normally desirable in flight control systems. In addition, special performance measures must be introduced which pertain to the problems peculiar to automatic landing. A set of measures which reflect these goals is:

Table 1.3-1

List of Specific Performance Requirements

Phase	Requirement
Acquisition	1. Acquire the ILS localizer and glide-slope centers as quickly as possible with minimum overshoot. 2. Perform this maneuver within the restrictions imposed on roll and roll rate.
ILS Reference Line Tracking	1. Minimize the error between the actual path of the aircraft and the ideal location of the ILS reference line.
Flareout	1. Minimize the error between a desired vertical velocity profile and the actual vertical velocity profile.
Decrab	1. Minimize the lateral components of aircraft velocity and position at touchdown. 2. Minimize the angular difference between a vertical plane through the runway center line and the aircraft's longitudinal axis at touchdown. 3. Attempt to achieve zero roll angle at touchdown.
Rollout	1. Minimize the distance between the path of the aircraft and the runway center line.

1. Sensitivity to environmental disturbances.
2. Accuracy of flight relative to a desired reference trajectory.
3. Control effector activity caused by noise.
4. Physical limitations imposed by the aircraft structure.
5. Human factors.

The first two performance measures deal specifically with landing accuracy. A reduction in the effects of external disturbances ensures that landings may be repeated with small dispersion in spite of large changes in ambient atmospheric conditions. The ability to track a desired path accurately is obviously a particularly important item and will undoubtedly provide a key to winning the confidence of aircrews and the acceptance of the new automatic landing systems by the airlines. Accurate path tracking also provides the greatest margin of safety, since a comparatively small deviation from the path may be interpreted as an incipient failure and an appropriate warning transmitted to the pilot.

Control effector activity resulting from noise levels in the sensors which provide the information for control-loop closure must be restricted to a fairly low level to reduce wear on the effectors, decrease drag and limit undesired inputs into the pilots controls.

The control system must also operate without exceeding the structural limitations of the vehicle. This implies control within a particular flight envelope and special care to ensure that the flexible bending modes of the vehicle are not excited.

Human factors are particularly important in a passenger aircraft. Restrictions on variables such as roll, roll rate and vertical acceleration must be incorporated into the design. An automatic landing system should optimize items 1 through 5 while working within these restrictions.

The above criteria may be interpreted as a set of specific performance requirements applicable to each control stage of an automatic landing. Such a set of specific requirements is given in Table 1. 3-1.

1. 4 Automatic Landing Systems

As indicated above, automatic landing systems have been under development for some time. A conventional automatic landing system is shown in Fig. 1. 4. 1. The terminal navigation aid (ILS) provides position information x_r relative to the approach reference trajectory. This information is usually quite noisy as a result of fluctuations in the reference path due to random reflections from objects on the ground illuminated by the localizer and glideslope antennae. The output from the ILS is fed to a coupler which operates on the signal to provide inputs m_0 to the auto-

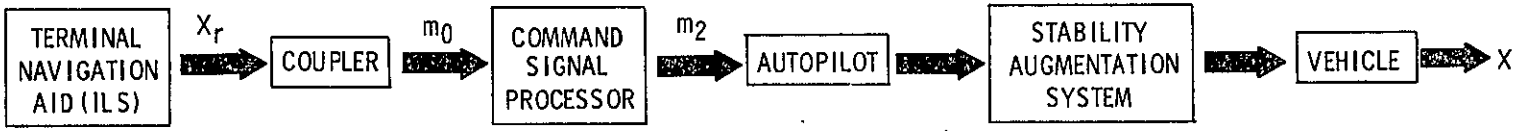

Fig. 1.4.1 Conventional automatic landing system.

pilot which are linear combinations of the position error, the integral of the position error and the derivative of the position error. The output from the coupler m_0 is fed to a signal processor which limits the signal to account for human factors and flight envelope restrictions. The control signal m_2 is then applied to the aircraft autopilot which modifies the vehicle attitude to effect the trajectory changes required for ILS reference path tracking. The aircraft is placed under landing system control when it is initially on a linear path inclined at some heading angle ψ_a relative to the runway centerline. The control system automatically acquires the reference path and guides the aircraft along it until control is tranferred to a human operator or the decrab and flareout control systems at an altitude of 70-100 feet relative to the runway.

While the simplicity of the conventional system is very attractive it suffers from a number of disadvantages.

1. The open loop gains are restricted due to filtering which must be used to reduce the high noise level in the ILS signals.
2. The control system tends to operate in saturation much of the time due to the high ILS noise level and the linear relationship between lateral position error and signal processor input. As a result the control system sensitivity to environmental disturbances is increased.

The goal of this study is to improve the overall performance of a landing system by utilizing information provided by the inertial navigator and the contributions of modern control theory. This object is achieved by the application of four concepts

a) Inertial filtering of the ILS reference signals
b) Inertial stabilization of the aircraft control system
c) Generalized trajectory control
d) Nonlinear trajectory generation

The concepts a-d form the basis for a new system which satisfies the criteria outlined in section 1.3.

A block diagram of the MIT/IL automatic landing system is shown in figure 1.4.2. The command input to the system is the instruction I which selects the operating mode of the landing system from the phases described in section 1.2. The nonlinear trajectory generator develops a new spacial reference trajectory which interacts with the terminal approach reference trajectory to satisfy the

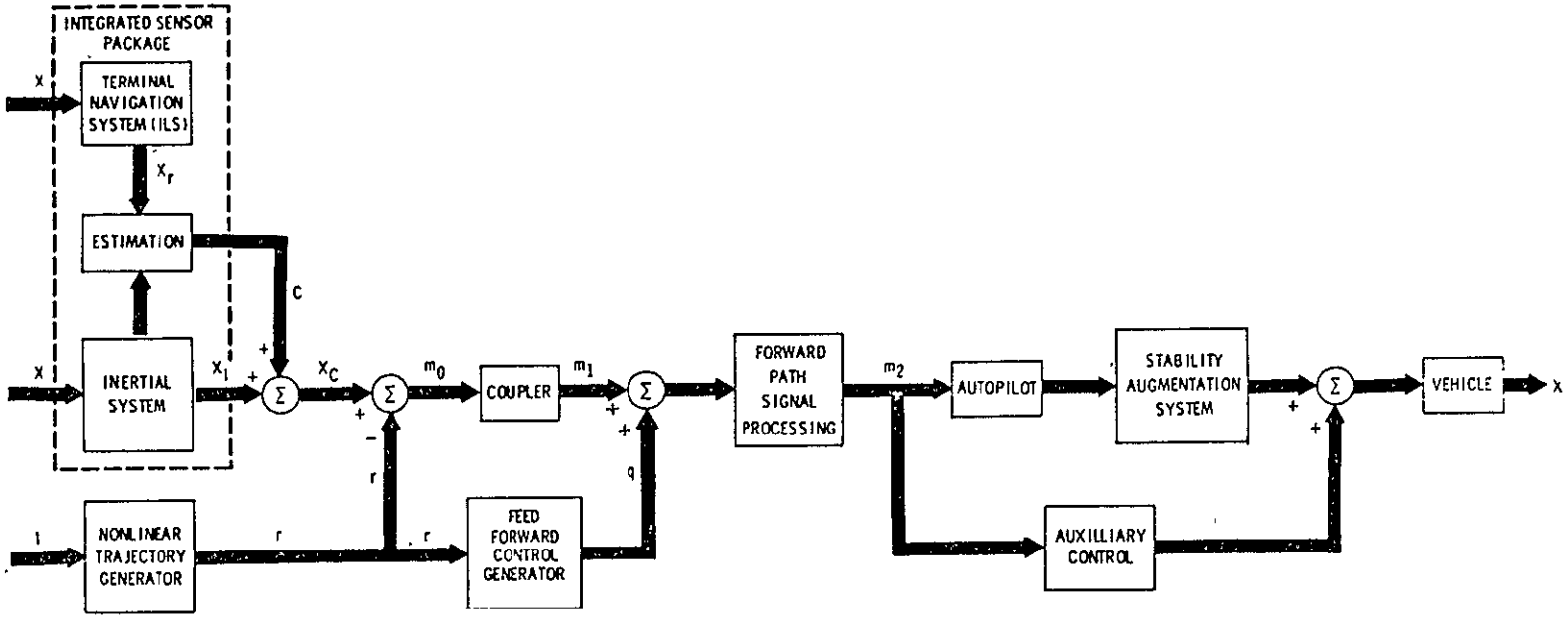

Fig. 1.4.2 Modernized automatic landing system

instruction I. The reference path r produced by the nonlinear trajectory generator accounts for

1. Saturation constraints imposed by effectors and/or human factors.
2. The bandwidth limitations of the closed loop position control system.

As a result the vehicle is able to follow the trajectory precisely without saturating the effectors or the limits imposed by human factors. The utilization of trajectory generation has another very important implication since it permits the designer to select the system gains without considering the affect of gain values on gross response characteristics, permitting in general the utilization of higher gains. The output from the trajectory generator consists of a set of reference position, velocity and accelerations signals r.

The position, velocity and lagged acceleration of the vehicle are generated by an integrated sensor package consisting of an inertial navigator, an estimator, and the terminal navigation aid (ILS). The output x_c of the integrated sensor is a corrected set of inertial system measurements x_i which provide relatively noise free vehicle state data. The velocity, position, and acceleration components of x_c are compared with corresponding components of r to generate a feedback control m_0. By exercising simultaneous control in this fashion over position, velocity and acceleration the affect of feedback path dynamics is eliminated and a considerable improvement in trajectory following precision achieved. A detailed discussion of nonlinear trajectory generation and its application can be found in chapter 4.

In addition to the control component generated by comparing desired and actual values of position, velocity and acceleration a feedforward component q is produced to eliminate steady state errors. For example, a signal, in the vertical channel is generated to provide the vehicle pitch angle required to maintain a desired rate of descent.

The total control signal is then applied to a signal processor which plays the same role as the command signal processor in the conventional automatic landing system. However as a result of careful trajectory generation and low sensor noise levels the limits in the signal processor are normally not exceeded. As a result the control system primarily operates in an unsaturated state reducing the sensitivity to environmental disturbances as explained in chapter 4.

Subsequent chapters will discuss various aspects of the design of the MIT/IL Landing system in more detail.

CHAPTER 2

INERTIAL - TERMINAL NAVIGATION SYSTEM INTEGRATION

2.1 Introduction

Inertially measured position and velocity are characterized by very low noise levels at high frequencies in spite of the wide bandwidth of the measuring instrument. As a result inertial position and velocity would appear to be ideal feedback variables for position control system synthesis. Unfortunately the position and velocity information provided by the inertial system are subject to low frequency gyro excited errors which increase in amplitude with time. The magnitude of the error in position roughly increases one nautical mile for each hour of operation in a system of the type currently considered for commercial aircraft operation. As a result the errors at the termination of a typical flight will preclude the use of position and possibly velocity as feedback control variables.

A terminal navigation system such as ILS on the other hand, provides relatively accurate position information which is corrupted by severe high frequency noise. ILS position and derived velocity are thus rather unsuited for control applications.

The possibility of combining the desirable features of the ILS and inertial information then suggests itself. Such an integrated sensor unit would combine the low frequency characteristics of the ILS with the wide noise free dynamic range of the inertial system. The equations of integrated sensor providing corrected velocity and position information were developed in reference 26. This chapter extends the technique to encompass acceleration correction and examines the properties of the solution in more detail.

2.2 Initial Inertial System Correction

The modern approaches to navigation system design utilize the total information provided by all the navigation sensors such as DME, VOR, VORTAC, LORAN, etc. and combines them using a systematic estimation technique such as Kalman Filtering or integral square error minimization. As a result it is possible to update the inertial system during flight and it will probably be possible to reduce the position error of the inertial system below one nautical mile before the aircraft

enters the terminal control area. Additional initial corrections may be made based on the data provided by the ILS system. Such initial corrections play an important role during the acquisition phase of an automatic landing as shown in chapter 6 of reference 26.

The lateral position relative to the vertical reference plane is the most important variable during the initial phases of an automatic landing. The lateral position may be estimated by examining the geometrical properties of a radius drawn from the ILS Localizer transmitter to the vehicle. Let r_y be the length of the radius and α_y the angular deflection of the radius from the vertical reference plane. The lateral distance y from vehicle to vertical reference plane is then given by

$$y = \alpha_y r_y \tag{2.2-1}$$

Assume that α_y is measured by the localizer receiver while r_y is generated by a distance measuring device (DME) located at the localizer antenna. The angle and distance measurements are subject to errors $e_{\alpha y}$ and e_{ry} respectively. The actual measured distance y_m is then given by

$$y_m = \alpha_y r_y + \alpha e_{ry} + r_y e_{\alpha y} + e_{\alpha y} e_{ry} \tag{2.2-2}$$

The first term on the right hand side is the actual distance y. The last term is very small relative to the second and third terms and may be neglected. The error e_y in y is then approximately

$$e_y \approx \alpha_y e_{ry} + r_y e_{\alpha y} \tag{2.2-3}$$

If $e_{\alpha y}$ and e_{ry} are uncorrelated, the mean square value of the error $E(e_y)$ may be written

$$E(e_y) \approx \alpha_y^2 E(e_{ry}) + r_y^2 E(e_{\alpha y}) \tag{2.2-4}$$

Assuming typical values at the initiation of acquisition

$$E(e_{\alpha y}) = 1 \times 10^{-4} \text{ rad}^2$$

$$\alpha_y^2 = 36 \times 10^{-4} \text{ rad}^2$$

$$E(e_{ry}) = 4 \times 10^6 \text{ ft}^2$$

$$r_y^2 = 36 \times 10^8 \text{ ft}^2$$

it is apparent that the second term in equation (2. 2-4) will dominate $E(e_y)$ and

$$E(e_y) \approx r_y^2 E(e_{\alpha y}) = 36 \times 10^4 \text{ ft}^2 \qquad (2.2\text{-}5)$$

Since the mean square value of the error in inertial position $E(e_{yi})$ on entering the terminal area will range from 10^6 to 10^9 ft^2 depending on the duration of flight, updating techniques and so forth, it is advantageous to perform an initial inertial position correction based on ILS - DME information by setting inertial lateral position $y_i = y_m$.

Velocity data provided by the ILS - DME terminal navigation system, on the other hand, is generally much less accurate than the inertial velocity information. Thus an initial velocity correction based on terminal navigator data would not normally be made.

A similar approach may be used to correct the vertical position if it is measured by the inertial system. In this case it is generally advantageous to use the radio altimeter and/or barimetric altitude as the reference variable since the errors in these measurements are generally much smaller than the errors in the glideslope signal.

While instantaneous inertial velocity and acceleration correction using ILS and DME information is not feasible it is possible to generate very precise inertial system corrections using mathematical estimation theory. This approach is discussed in the next section.

2. 3 Estimation of Inertial System Errors

While instantaneous correction of inertial system position in 2. 2 results in a reduction in position error a more sophisticated approach must be utilized if a further correction in inertial position and corrections in inertial velocity and acceleration are desired. Mathematical estimation theory provides the techniques for accomplishing these goals. A least integral squared error technique is a relatively simple approach to this problem which requires only a modest quantity of computer memory.

Let a set of inertially measured variables corresponding to motion along one axis be represented by a vector

$$x_i = \begin{bmatrix} x_{i1} \\ x_{i2} \\ x_{i3} \end{bmatrix} \qquad (2.3\text{-}1)$$

where

x_{i1} is inertially measured position

x_{i2} is inertially measured velocity

x_{i3} is inertially measured acceleration

A simplified set of relationships which models the inertial system is then

$$\dot{x}_{i1} = x_{i2}$$

$$\dot{x}_{i2} = x_{i3} \qquad (2.3\text{-}2)$$

subject to the initial conditions $x_{i1}(0)$, $x_{i2}(0)$. Since the time interval during an automatic landing is short compared to the dynamics of the inertial system the errors in position and velocity may be attributed to errors in the initial values $x_{i1}(0)$ and $x_{i2}(0)$ and an accelerometer bias error in $x_{i3}(0)$ (as a result of stable member misalignment and deflections of the local vertical). Thus

$x_{i1}(0)$ = (position at t = 0) + (error in position at t = 0)

$x_{i2}(0)$ = (velocity at t = 0) + (error in velocity at t = 0)

$x_{i3}(0)$ = (acceleration at t = 0) + (bias error)

Knowledge of the errors in initial position and velocity and the bias error in acceleration is sufficient to correct all subsequent inertial data during the landing maneuver.

Consider the system shown in Fig. 2.3.1. The inertial system described in equation (2.3-2) is modelled by two integrators. The input to the inertial system is x_{i3} which is the sum of the true acceleration x_3 and the accelerometer bias b. The output inertial position x_{i1} is fed to a model of the ILS receiver. The true position is fed to the actual ILS receiver. The outputs of the ILS receiver and its model are multiplied by range to the ILS transmitter r to convert to measured distance and compared at a summing junction. It is apparent that the resultant error ϵ will be zero for all $t > 0$ providing

1. The ILS model and ILS system outputs coincide at t = 0.
2. The ILS model accurately represents the ILS receiver.

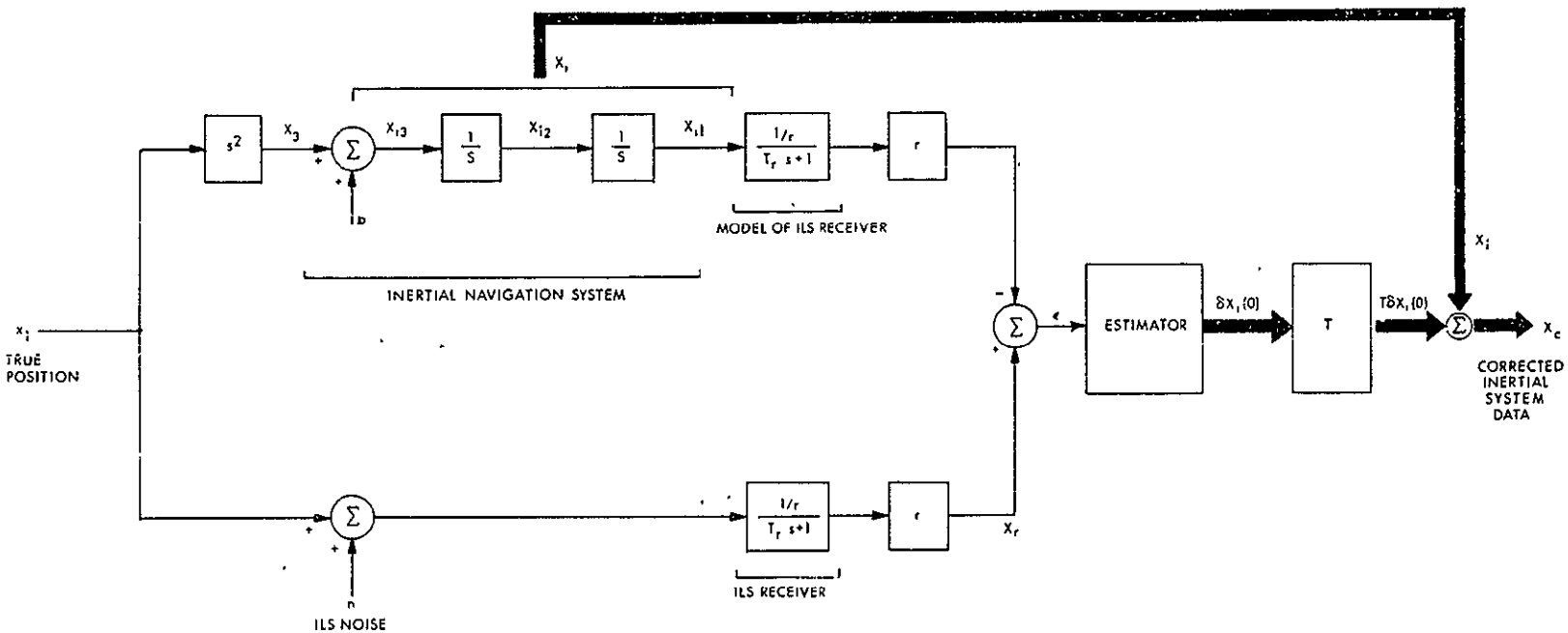

Fig. 2.3.1 Integrated sensor block diagram.

3 The errors in inertially measured position, velocity and the accelerometer bias are zero

4. The noise input n is zero

It is assumed that the first two requirements are satisfied. Satisfaction of the third shall now be investigated.

Let the vector describing the inertial system x_i be perturbed at $t = 0$ by $\delta x_i(0)$. Since the system is linear the effect $\delta\epsilon$ of the perturbation $\delta x_i(0)$ on the error ϵ may be written

$$\delta\epsilon(t) = h(t)' \, \delta x_i(0) \tag{2.3-3}$$

where h is a vector of responses. The element $h_k(t)$ is the step response measured at ϵ to a step in x_{ik} applied at $t = 0$. The new error is then

$$\epsilon(t) = \epsilon(t) + \delta\epsilon(t) \tag{2.3-4}$$

The estimation of the best perturbation in $\delta x_i(0)$ may be accomplished by solving the following optimization problem

Problem: Find a vector of perturbations $\delta x_i(0)$ which minimizes the integral performance index

$$J = \int_0^t \left[\epsilon(\alpha) + \delta\epsilon(\alpha)\right]^2 d\alpha \tag{2.3-5}$$

Expanding $\left[\epsilon(\alpha) + \delta\epsilon(\alpha)\right]^2$ using equation (2.2-3) gives*

$$J = \int_0^t \Big[\epsilon(\alpha)^2 + 2\,h(\alpha)' \, \delta x_i(0)\, \epsilon(\alpha) + \delta x_i(0)' \, h(\alpha).h(\alpha)' \, \delta x_i(0)\Big] d\alpha \tag{2.3-6}$$

The first variation with respect to $\delta x_i(0)$ in the performance index J is given by

*The notation x′ denotes the transpose of the vector x.

$$\delta J = \delta x_i'(0) \int_0^{-} \Big[2h(\alpha)\, \epsilon(\alpha) + 2h(\alpha)\, h(\alpha)'\, \delta x_i(0) \Big]\, d\alpha \qquad (2.3\text{-}7)$$

The first necessary condition of the calculus of variations requires δJ to vanish. This condition is satisfied if

$$\delta x_i(0) = -\left[\int_0^t h(\alpha)\, h(\alpha)'\, d\alpha\right]^{-1} \int_0^t h(\alpha)\, \epsilon(\alpha) d\alpha \qquad (2.3\text{-}8)$$

The validity of equation (2.3-8) becomes apparent if the ILS sensor noise is assumed to be zero: The error $\epsilon(\alpha)$ then reduces to

$$\epsilon(\alpha) = h(\alpha)' \left[x_i(0) - x(0) \right] \qquad (2\ 3\text{-}9)$$

Substituting into (2.3-8) yields

$$\delta x_i(0) = -\left\{\left[\int_0^t h(\alpha)\, h(\alpha)'\, d\alpha\right]^{-1} \int_0^t h(\alpha)\, h(\alpha)'\, d\alpha \left[x_i(0) - x(0)\right]\right\} \qquad (2.3\text{-}10)$$

or

$$x_i(0) + \delta x_i(0) = x(0) \qquad (2.3\text{-}11)$$

the desired solution. The success of the solution hinges on the nonsingularity of the matrix

$$H = \int_0^t \left[h(\alpha)\, h(\alpha)'\right]\, d\alpha \qquad (2.3\text{-}12)$$

If t is small, $t = \delta t$, integral 2.3-12 may be approximated by

$$H = \left[h(0)\, h(0)'\right] \delta t \qquad (2.3\text{-}13)$$

Since δt is a scalar the determinant $|H|$ at $t = \delta t$ is

$$|H| = |h(0)\, h(0)'|\ \delta t \qquad (2.3\text{-}14)$$

Since the $|h(0)\, h(0)'|$ is zero the matrix H approaches singularity as

$t \to 0$. This explains the transient behavior of the solution shown in Fig. 2.5.1. As time increases $|H|$ will exist and a solution for $\delta x_i(0)$ generated.

The noise n associated with reference signal x_r introduces disturbances into the computation which affect the accuracy of the solution. An interesting property of the estimation algorithm is its ability to attenuate the effects of ILS noise n as time progresses. This effect is a result of the averaging process inherent in the minimization of the integral (2.3-5). The effect of ILS noise is illustrated in section 2.7.

The new initial conditions $x_i(0) + \delta x_i(0)$ may be used to calculate a corrected set of inertial information $x_c(t)$ by using the relation

$$x_c(t) = x_i(t) + T(t)\, \delta x_i(0) \tag{2.3-15}$$

where the matrix T(t) is defined

$$T(t) = \begin{bmatrix} 1 & t & \frac{t^2}{2} \\ 0 & 1 & t \\ 0 & 0 & 1 \end{bmatrix} \tag{2.3-16}$$

A block diagram of this estimation procedure is shown in Fig. 2.3.1. This technique may be used to correct vertical or lateral position, velocity and acceleration information using the ILS localizer and glideslope signals.

2.4 Simplified Estimation of the Inertial System Position and Velocity Errors

The general estimation procedure presented in the previous section may be simplified if the corrections are restricted to position and velocity. This is merely a specialization of the method developed previously and may be arrived at by redefining the following variables

$$x_i = \begin{bmatrix} x_{i1} \\ x_{i2} \end{bmatrix} \tag{2.4-1}$$

$$h = \begin{bmatrix} h_1 \\ h_2 \end{bmatrix} \tag{2.4-2}$$

Neglecting the accelerometer bias the perturbation $\delta\epsilon(t)$ becomes

$$\delta\epsilon(t) = h(t)' \, \delta x_i(0) \qquad (2.4\text{-}3)$$

Substituting (2.4-1), (2.4-2) and (2.4-3) into (2.3-5) and minimizing the integral gives

$$\delta x_i(0) = -\left[\int_0^t h(\alpha)\, h(\alpha)' \, d\alpha\right]^{-1} \int_0^t h(\alpha)\, \epsilon(\alpha)\, d\alpha \qquad (2.4\text{-}4)$$

The effect of an acceleration bias $x_{i3}(0)$ creates an effective nonstationarity in the estimated initial value errors $-\delta x_i$. The effect of acceleration bias is illustrated in the next section. The corrected inertial velocity and position may be computed once $\delta x_i(0)$ is known

$$x_i(t) = x_i(t) + T(t)\, \delta x_i(0) \qquad (2.4\text{-}5)$$

where

$$x_c(t) = \begin{bmatrix} x_{c1} \\ x_{c2} \end{bmatrix} \qquad (2.4\text{-}6)$$

and

$$T(t) = \begin{bmatrix} 1 & t \\ 0 & 1 \end{bmatrix} \qquad (2.4\text{-}7)$$

The response characteristics of this estimation technique are illustrated in the next section.

2.5 Response Characteristics of an Integrated Sensor Unit

The behaviour of the estimation algorithm in section 2.4 may be demonstrated by individually introducing errors in position velocity and acceleration. The results of a sequence of runs of this form are shown in Figs. 2.5.1, 2.5.2 and 2.5.3. It is evident that the estimation process must continue for some time before useful information may be derived from the updated inertial position and velocity. To prevent the premature application of the information the corrections are multiplied by a matrix of functions U(t) before being applied to the inertial information. Thus

$$x_c(t) = x_i(t) + T(t)\, U(t)\, \delta x_i(0) \qquad (2.5\text{-}1)$$

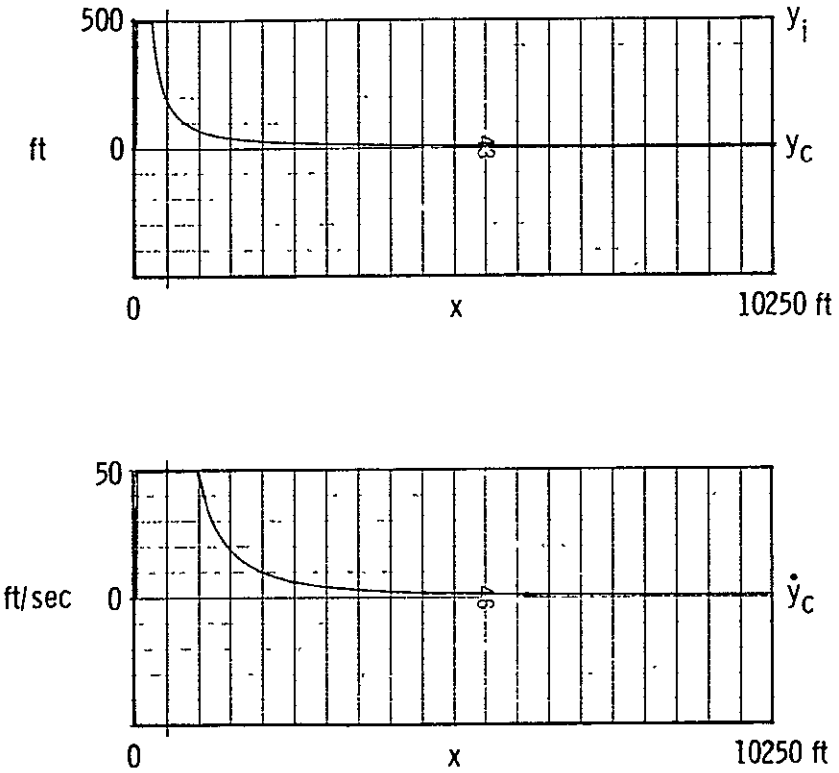

Fig. 2.5.1 Corrected inertial position, y_c, and velocity, $\dot{y}_c$, in response to an initial error in inertial position. ($y = \dot{y} = 0$, $\dot{y}_i = 0$, $y_i = 500$ ft)

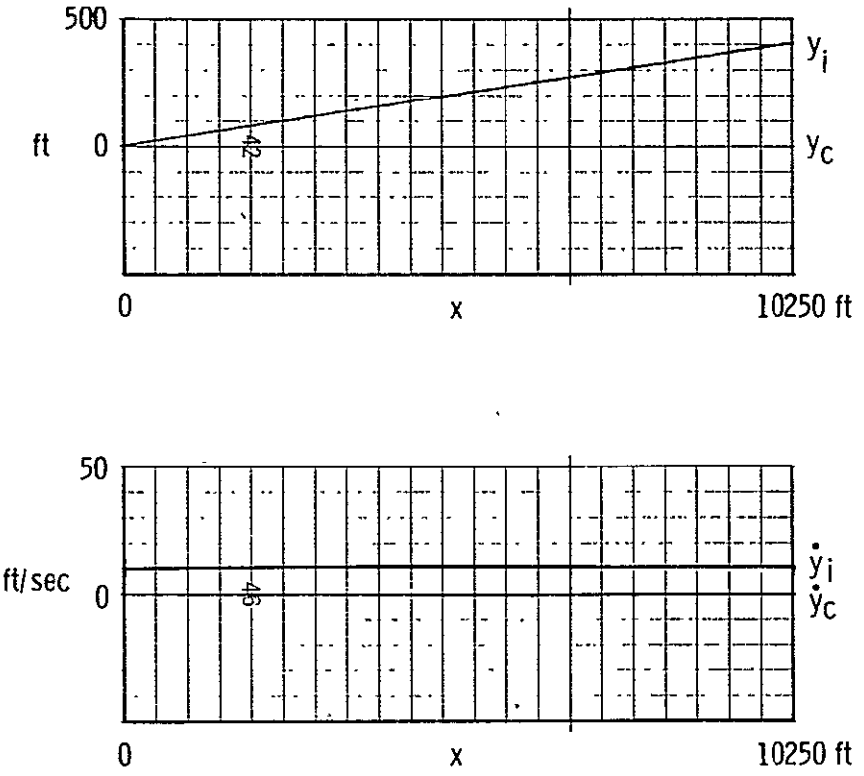

Fig. 2.5.2 Corrected inertial position, y_c, and velocity, $\dot{y}_c$, in response to an initial error in inertial velocity. ($y = \dot{y} = 0$, $\dot{y}_i = 10{:}0$ ft/sec, $y_i = 10.0$ t ft)

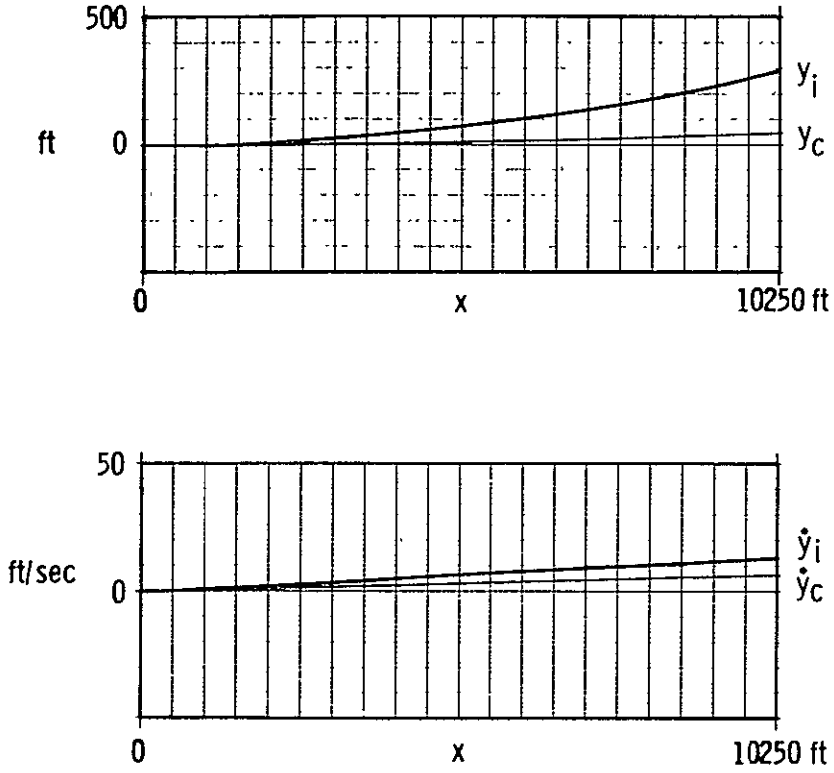

Fig. 2.5.3 Corrected inertial position, y_c, and velocity, $\dot{y}_c$, in response to an initial acceleration bias. ($y = \dot{y} = 0$, $\ddot{y}_i = 0.322$ ft/sec^2, $\dot{y}_i = 0.322t$ ft/sec $y_i = 0.161\ t^2$ ft)

The matrix U(t) is a diagonal matrix. The elements $u_{ii}(t)$ on the diagonal of U(t) are currently of the form

$$u_{ii}(t) = \begin{cases} 0 & t \leq t_1 \\ \dfrac{t - t_{1i}}{t_{2i} - t_{1i}} & t_1 < t \leq t_2 \\ 1 & t > t_2 \end{cases} \qquad (2.5\text{-}2)$$

The times t_{1i} and t_{2i} are constants with respect to the initiation of estimation ($t = 0$ in preceding sections of chapter 2). Equation (2.5-2) shows that the correction $\delta x_{ik}(0)$ is gradually applied over the time interval (t_{1k}, t_{2k}). This procedure reduces control system disturbances resulting from estimator transients.

2.6 The Nature of Sensor Noise

The primary source of sensor noise once estimator convergence is achieved in an ILS based integrated sensor unit is ILS beam center fluctuation. Changes in the glideslope and localizer beam center planes occur as a result of reflections from objects on the ground illuminated by the localizer and glideslope antennas. While the effect is deterministic in nature the three dimensional complexity of the pattern currently precludes the application of an analytic solution to eliminate the effects of the fluctuations.* As a result the perturbations in beam center position are usually characterized by an extraneous stochastic input to the ILS receivers. The receiver generally possesses a low pass filter which, for the purposes of our investigation, is depicted by a simple time lag with time constant T_r. A typical localizer receiver output resulting from beam noise is shown in Fig. 2.6.1. The power spectrum of this signal is illustrated in Fig. 2.6.2.

In order to investigate the effects of beam noise on integrated sensor performance fluctuations in the beam center were simulated by exponentially correlating the output of a gaussian random number generator using a simple first order filter. The resultant signal in Fig. 2.6.3 was added to the input of the localizer receiver simulation to produce the output shown in Fig. 2.6.4. Figure 2.6.4 may be compared to the beam noise illustrated in Fig. 2.6.1 to verify the validity of the simulated noise. The power spectrum of the simulated receiver output is compared to the actual power spectrum in Fig. 2.6.2.

Sensor noise level is conveniently quantized by generating the mean square value of the noise using equation (2.6-1).

---

*By storing the pattern, for example.

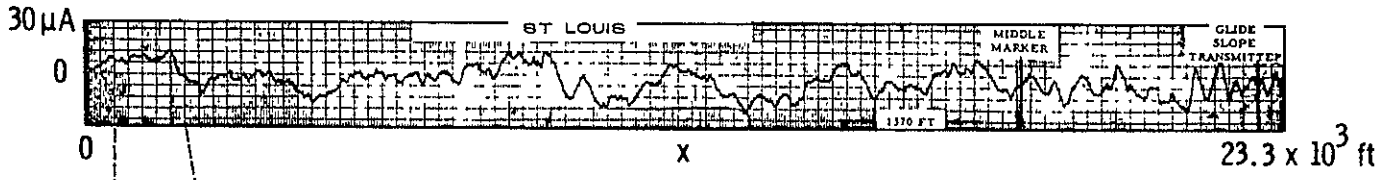

Fig. 2.6.1 Typical localizer beam noise. (St Louis facility)

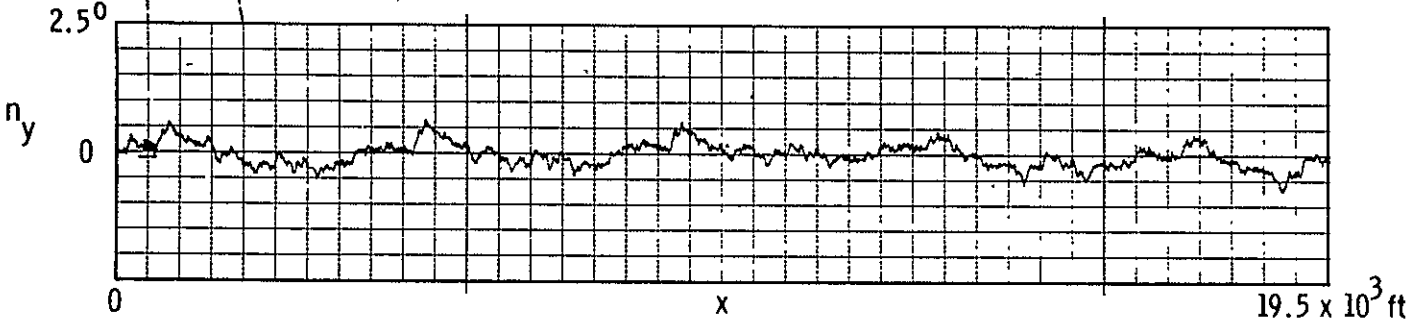

Fig. 2.6.3 Simulated localizer beam noise.

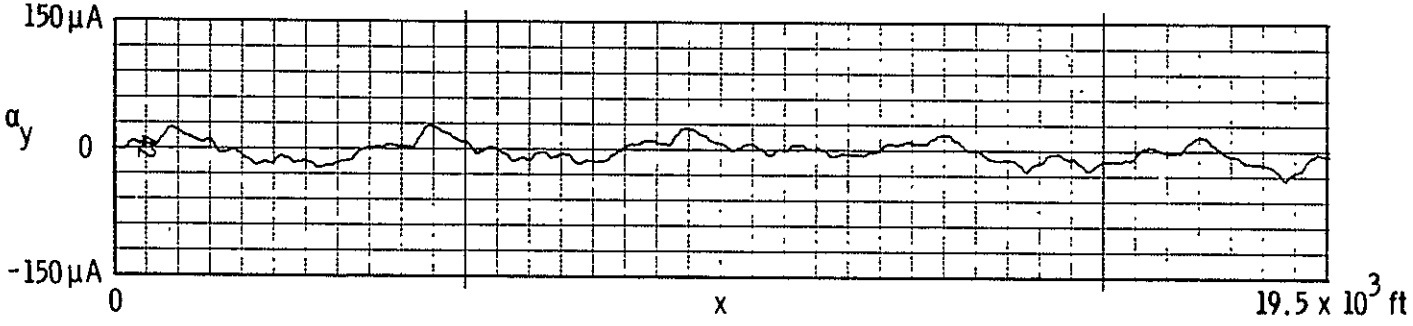

Fig. 2.6.4 Localizer receiver output as a result of simulated beam noise input (T_r = 0.4 sec)

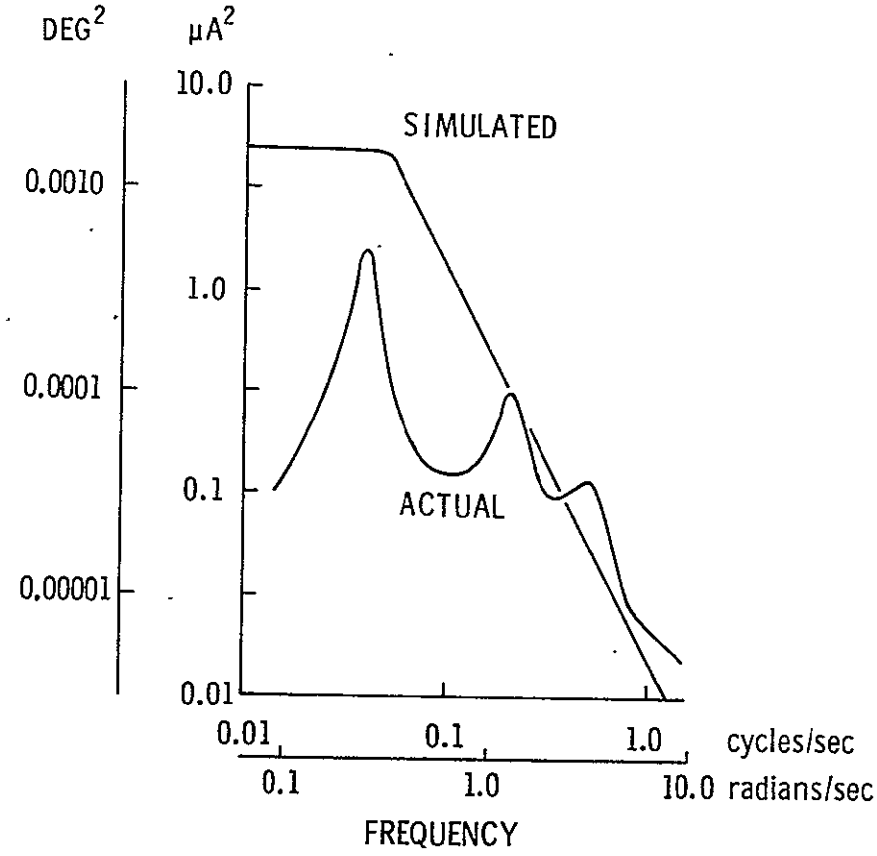

Fig. 2.6.2 Simulated and actual localizer power spectra.

$$E(x) = \lim_{T \to \infty} \frac{1}{T} \int_0^T x^2 \, d\alpha \qquad (2.6\text{-}1)$$

If the random variable x is ergodic the limit (2.6-1) exists and is equal to the statistical mean of x^2. As a result of the relationships discussed in section 2.2 it is apparent that the mean square value $E(e_y)$ of the error e_y in y is related to the localizer output α_y, the distance to the localizer transmitter r_y and the error e_{ry} in r_y by the formula

$$E(e_y) \approx \alpha_y^2 E(e_{ry}) + r_y^2 E(e_{\alpha y}) \qquad (2.6\text{-}2)$$

While $E(e_r)$ and $E(e_\alpha)$ may be considered constant during an automatic approach α_y and r are subject to variation. Thus the expectation $E(e_y)$ is time varying and the process e_y is nonstationary. Since α_y is usually very small after acquisition it shall be assumed that

$$E(e_y) \approx r_y^2 E(e_{\alpha y}) \qquad (2.6\text{-}3)$$

A similar expression may be derived for the mean square value of the error in vertical position $E(e_z)$.

$$E(e_z) \approx r_z^2 E(e_{\alpha z}) \qquad (2.6\text{-}4)$$

where r_z is the distance to the glideslope antenna

α_z is the angular deviation from the ideal glideslope reference plane

The nonstationarity of e_y and e_z with respect to distance indicated in equations (2.6 2) and (2.6 3) creates difficulties when two systems are to be compared. Thus it is more convenient to compare $E(e_{\alpha y})$ and $E(e_{\alpha z})$ which may be generated from the relationships.

$$E(e_{\alpha y}) \approx r_y^{-2} E(e_y) \qquad (2.6\text{-}5)$$

$$E(e_{\alpha z}) \approx r_z^{-2} E(e_z) \qquad (2\ 6\text{-}6)$$

2.7 Integrated Sensor Noise Levels

One of the most significant improvements achieved by sensor integration is a significant reduction in noise level. Noise originating in the ILS in introduced

into the inertial corrected system output as a result of the correction algorithm in section 2.4.

Since the noise is introduced in a linear fashion the noise contents in the corrected inertial position will vary as a function of the distances from the ILS localizer and glideslope antennas. In order to obtain meaningful statistical information stationarity must be re-established by dividing the corrected position by antenna distance before averaging. The response of the integrated sensor to the noise signals shown in Figs. 2.6.4 is illustrated in Fig. 2.7.1 The normalized responses are shown. The resultant averages may be compared with the values computed using equations (2.6-4) and (2.6-5). A similar procedure may be used to compare the ILS velocity estimates (obtained by differentiating the ILS position signals) with the corrected inertial velocity estimate. The resultant averages are given in table 6.2-1.

2.8 Summary

A systematic procedure has been presented for correcting inertial system errors by combining ILS and inertial data utilizing mathematical estimation procedure. A general algorithm is presented which simultaneously estimates errors in inertial position velocity and acceleration. This result is specialized to yield a simplified procedure for estimating position and velocity errors. The transient behavior of the solution is investigated by generating responses to initial errors in position, velocity and acceleration in the absence of ILS noise. The effects of ILS noise on the Integrated Sensor are introduced and the resultant position and velocity errors are compared to the corresponding errors in the ILS signal by generating mean square statistical averages. The results show that the noise level of the integrated sensor package outputs is quite small compared to the ILS signal noise.

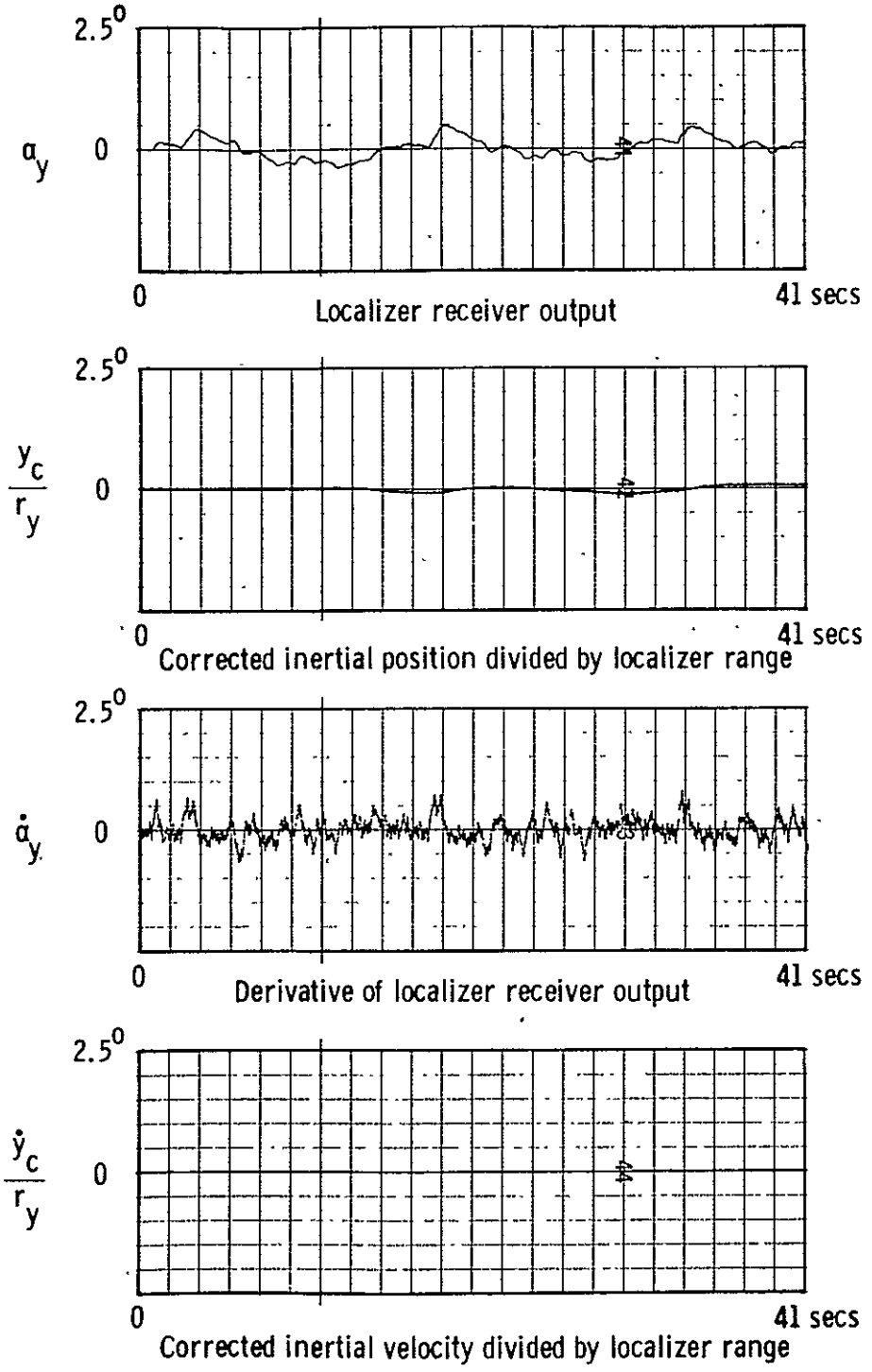

Fig. 2.7.1 Response characteristics of the integrated sensor unit to localizer beam noise. ($t_{11} = t_{12} = 15.0$ sec, $t_{21} = t_{22} = 25.0$ sec)

CHAPTER 3

LINEAR POSITION CONTROL SYSTEM SYNTHESIS AND PERFORMANCE LIMITATIONS

3. 1 Introduction

This chapter presents the pertinent elements of the synthesis and optimization of a new set of trajectory control systems which utilize the superior information provided by the integrated sensor package. The chapter also explores limitations imposed on the vertical and lateral position regulators by the dynamic characteristics of the vehicle and its effectors, the structure of the feedback control laws and the noise characteristics of the sensors. Error between the desired and actual values of controlled variables, sensitivity to disturbances emanating from the environment and control surface noise levels provide the basic criteria for this investigation.

3. 2 Inertial Stabilization

The integrated sensor unit, described in chapter 2, produces lateral and vertical position, velocity and lagged acceleration components which are relatively free from noise compared to the ILS localizer and glideslope signals. In order to effectively utilize this improved information a redesign of the lateral and vertical position control systems was undertaken. As shown in reference 26 the fundamental landing problem may be defined as a guidance problem in two orthogonal planes corresponding to the localizer reference plane, and a vertical plane containing the runway centerline. The intersection of the two planes defines the ideal ILS reference path. This approach separates the control problem into two distinct areas, lateral guidance relative to the vertical plane and vertical guidance with respect to the localizer reference plane. As a result of the decoupling inherent in the simplified vehicle equations of motion an accurate system design may be achieved by separating the two problems using the techniques presented in chapter 5 of reference 26. A convenient set of coordinates is an earth fixed reference frame originating at the point where the glideslope intersects the runway centerline. The x-axis lies along the centerline, y is horizontal while z is directed downward. The fundamental linearized relationships on which control system synthesis is based are then

$$\ddot{y} \approx g \cdot \varphi \tag{3.2-1}$$

$$\dot{z} \approx v_p \ (\alpha - \theta) \tag{3.2-2}$$

where

y is the lateral acceleration

g is the gravitational constant

φ is the roll angle

$\dot{z}$ is the vertical velocity

v_p is the path velocity

α is the angle of attack

θ is the pitch angle

Lateral vehicle control is effected by modifying the roll angle φ using the roll angle autopilot.[26] Vertical control results from modification of θ and α using the pitch control system and/or direct lift control devices, such as spoilers. The pertinent linearized forward path transfer functions are

$$\frac{y}{\varphi_d} = \frac{g}{s^2}\left[\frac{\varphi}{\varphi_d}\right] \tag{3.2-3}$$

and

$$\frac{z}{\theta_d} = \frac{v_p}{s}\left[\frac{\alpha}{\theta_d} - \frac{\theta}{\theta_d}\right]_{u=0} \tag{3.2-4}$$

where

φ_d, θ_d are desired roll and pitch angles respectively

$\left[\frac{\varphi}{\varphi_d}\right]$ is the roll control system transfer function

$\left[\frac{\theta}{\theta_d}\right]_{u=0}$ is the pitch control system transfer function at constant path velocity

$\left[\frac{\alpha}{\theta_d}\right]_{u=0}$ is a transfer function relating the perturbation in angle of attack α to θ_d

The control variables, φ_d and θ_d are constructed by linearly combining the outputs of the integrated sensor unit, a feedforward compensation signal and a desired reference trajectory.

FEEDBACK COMPENSATION

$$\varphi_d = -\left[\frac{K_y(K_{iy} + s)}{s} + K_{\dot{y}}s + \frac{K_{\ddot{y}}s^2}{T_{as} + 1}\right] y_c$$

FEEDFORWARD COMPENSATION

$$+\left[\frac{K_y(K_{iy} + s)}{s} + K_{\dot{y}}s + K_{\ddot{y}}s^2\right] y_r$$

$$+ \frac{s^2}{\ddot{g}} y_r \qquad (3.2\text{-}5)$$

FEEDBACK COMPENSATION

$$\theta_d = \left[\frac{K_z(K_{iz} + s)}{s} + K_{\dot{z}}s + \frac{K_{\ddot{z}}s^2}{T_{as} + 1}\right] z_c$$

FEEDFORWARD COMPENSATION

$$-\left[\frac{K_z(K_{iz} + s)}{s} + K_{\dot{z}}s + K_{\ddot{z}}s^2\right] z_r$$

$$- \frac{s}{v_p} z_r \qquad (3.2\text{-}6)$$

where

y_c, z_c are corrected values of y and z

y_r, z_r are desired values of y and z

K_y, K_z are adjustable position control loop parameters

K_{iy}, K_{iz} are adjustable integral compensator gains

$K_{\dot{y}}$, $K_{\dot{z}}$ are adjustable velocity control loop parameters

$K_{\ddot{y}}$, $K_{\ddot{z}}$ are adjustable acceleration control loop parameters

The differentiations shown in the feedforward component are avoided by explicit computation of the required derivatives as shown in section 4. 3. The structure of the reference components is based on the analysis in section 4. 4. (The small time constant T_a is neglected.)

Thus it is apparent that the control signals φ_d and θ_d are formed by simultaneously comparing the desired and actual values of position, velocity and acceleration. Any discrepancy generates a command which corrects the error. The integral compensators (K_{iy}/s, K_{iz}/s) weigh errors in position heavily as time progresses reflecting the emphasis on precise position control. The feedforward component $s^2 y_r/g$ provides the roll angle required to maintain the desired lateral acceleration based on relation 3. 2-1. The constant component of pitch required to maintain a steady rate of descent is generated by the term sz_r/v_p.

Since the structure of the control laws is fixed, analysis and synthesis leads to the definition of the feedback component parameters. Thus the designer is presented with a parameter optimization problem. The criteria and constraints associated with this problem are the topics of the next two sections.

3. 3 Disturbances, Errors, Bandwidth and Open Loop Gain

Two important criteria discussed in section 1. 3 are minimization of the effect of environmental disturbances on the system and the ability to follow a trajectory precisely. These phenomena are investigated by studying linear relationships using Laplace transform theory. A typical control system is shown in Fig. 3. 3. 1. The object of the control system is accomplished if the controlled variable C follows the reference input R. The system is subject to disturbances D which interfere with the control process. The fixed elements in the control system are G_1 and G_2 while G_0 and H are subject to modification.

The transfer function between C and R is

$$\frac{C}{R} = \frac{G_0 G_1 G_2}{1 + G_0 G_1 G_2 H} \qquad (3.3\text{-}1)$$

The dynamic response characteristics of the system depend upon the location of the zeros of the denominator. The location of the zeros may be modified by altering the transfer functions G_0 and H. The zeros are normally located to yield an overdamped step response. The rapidity of the response is primarily determined by the magnitude characteristics of $G_0 G_1 G_2 H$.

The ability to follow a trajectory precisely in space is an important requirement for an automatic landing system. Control system accuracy is measured by constructing the error between the desired and actual responses.

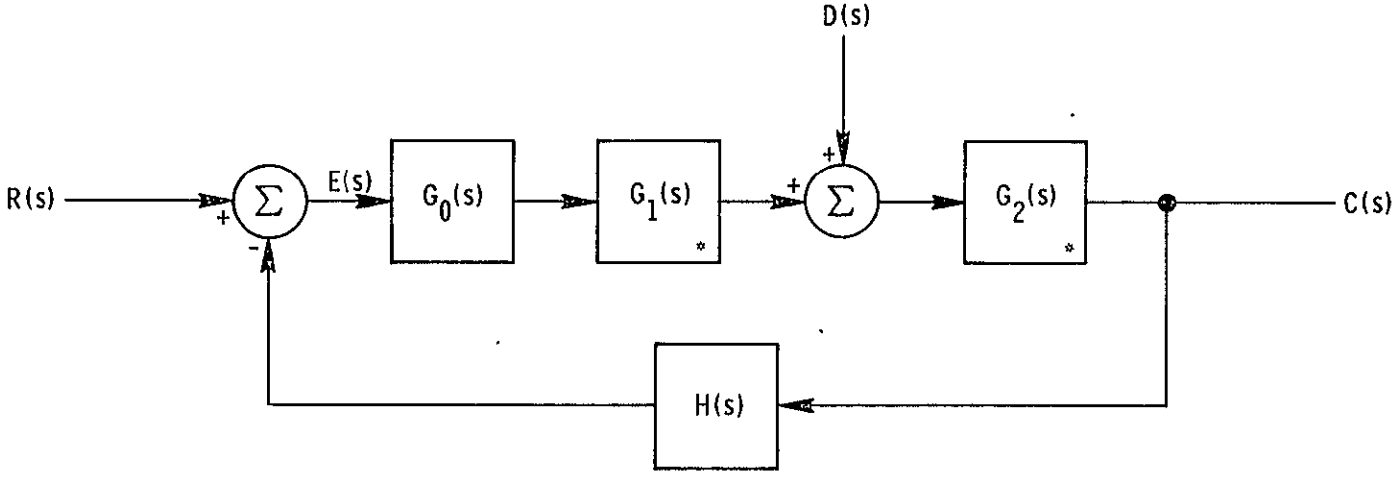

Fig. 3.3.1 Block diagram of a control system with a reference input, R(s), a controlled output, C(s) and a disturbance input, D(s).

$$E = R - C \tag{3.3-2}$$

The transfer function relating E to R is given by

$$\frac{E}{R} = \frac{1}{1 + G_0G_1G_2H} \tag{3.3-3}$$

The effect of external disturbances must also play an important role in control system design. Such effects are considered by examining the transfer function between the controlled output C and the disturbance D.

$$\frac{C}{D} = \frac{G_2}{1 + G_0G_1G_2H} \tag{3.3-4}$$

The open loop transfer function of the system is defined by the expression

$$G_{ol} = G_0G_1G_2H \tag{3.3-5}$$

One of the most important control system parameters is the Open Loop Gain which may be defined as follows:

Definition: The Open Loop Gain of the control system shown in Fig. 3.3.1 at $s = s_0$ is defined by the limit

$$\left|G_{ol}\right| = \lim_{s \to s_0} \left| G_0G_1G_2H \right| \tag{3.3-6}$$

As a result of the magnitude signs the value of the limit is independent of the direction in which s_0 is approached if G_{ol} is a rational fraction.

In most physical systems the response to a sinusoidal signal of frequency ω is of particular interest. In this case the general gain definition in equation (3.3-6) reduces to the more common form

$$\left|G_{ol}\right| = \lim_{s \to j\omega} \left| G_0G_1G_2H \right| \tag{3.3-7}$$

The effect of variations in the magnitude and phase of the open loop transfer function may be determined by evaluating the magnitudes of (3.3-3) and (3.3-4).

$$\left|\frac{E}{R}\right| = \left|\frac{1}{1 + G_{ol}}\right| \tag{3.3-8}$$

$$\left|\frac{C}{D}\right| = \left|\frac{G_2}{1 + G_{ol}}\right| \tag{3.3-9}$$

Three cases are of interest

1. $|G_{ol}| \gg 1$ The value of $|1 + G_{ol}| \approx |G_{ol}|$ and $\left|\frac{E}{R}\right| \approx \left|\frac{1}{G_{ol}}\right|$, $\left|\frac{C}{D}\right| \approx \left|\frac{G_2}{G_{ol}}\right|$. An increase in G_{ol} in this range reduces the error and sensitivity to disturbances.

2. $|G_{ol}| \approx 1$ The variation in $|1 + G_{ol}|$ depends on the arg G_{ol}. $\left|\frac{E}{R}\right|$ and $\left|\frac{C}{D}\right|$ may increase, decrease or remain stationary as $|G_{ol}|$ varies.

3 $|G_{ol}| \ll 1$ $|1 + G_{ol}| \approx 1$, $\left|\frac{E}{R}\right|$ and $\left|\frac{C}{D}\right|$ are essentially independent of variations in $|G_{ol}|$

The first case is the most important since it defines the spectral range where beneficial effects are obtained by feedback control. It is apparent that the frequency range where $|G_{ol}| > 1$, the bandwidth, should be as wide as possible. The $|G_{ol}|$ should also be as large as possible within the bandwidth of the system. Thus the designer is presented with two related optimization goals The maximization of bandwidth and open loop gain is subject to a number of constraints which are considered in the next section.

3.4 Limitations on Open Loop Gain and Bandwidth

In general it is not possible to increase the open loop gain indefinitely. The factors which limit the open loop gain are

1. The basic dynamic characteristics of the aircraft, effectors, and the signals available for control system stabilization.

   For a given set of fixed elements and a set of signals available for stabilization, there is a limit on the open-loop gain that can be achieved if the system is to be stable.

2. The permissible control effector activity resulting from sensor noise.

   Residual noise in the position and stabilization signals further restricts the gain because of the limitations that must be placed on effector activity due to effector saturation and permissible levels of control energy.

3. The accuracy of the linearized model.

Approximations are generally involved in the derivation of a linear mathematical model. Higher frequency dynamics which are usually ignored in the construction of a model become increasingly significant as the open loop gain is increased possibly invalidating the results of analysis.

The stability of the control system shown in Fig. 3. 3. 1 may be explored using the Nyquist Stability Criterion. For the purposes of our investigation it is sufficient to assume that the open loop transfer function is equal to unity at one discrete frequency ω_0 and the magnitude approaches zero as ω approaches infinity. In this case the Nyquist criterion states that the control system is stable (i.e., all the zeros of $1 + G_{ol}$ lie in the left half of the complex plane) if the arg G_{ol} is less than 180° and $\frac{\partial}{\partial\omega}$ arg G_{ol} is negative at $\omega = \omega_0$.

Consider the transfer functions G_f of the fixed elements and G_v of the variable elements in the control system shown in Fig. 3. 3. 1.

$$G_f = G_1 G_2 \tag{3.4-1}$$

$$G_v = G_0 H \tag{3.4-2}$$

Since $G_v = G_f$ at a unique frequency ω_0 it is apparent that the system is stable provided that

$$|G_v| > |G_f|^{-1} \quad \omega < \omega_0 \tag{3.4-3}$$

$$\left.\begin{aligned} |G_v| &= |G_f|^{-1} \\ \arg G_v &> -\arg G_f - 180 \end{aligned}\right\} \omega = \omega_0 \tag{3.4-4}$$

$$\frac{\partial}{\partial\omega} \arg G_v G_f < 0$$

$$|G_v| < |G_f|^{-1} \quad \omega > \omega_0 \tag{3.4-5}$$

While equations 3. 4-3 to 3. 4-5 guarantee stability the transient response of the control system will be unsatisfactory unless the angle $[180 - \arg G_v G_f]$ at ω_0, the phase margin, has a positive value. A phase margin of 30° to 60° is generally required to insure satisfactory transient response characteristics.

The second limitation pertains to the level of control effector activity resulting from random noise originating in the vehicle sensors as a result of internal

processes and stochastic environmental effects. The noise level is usually measured by evaluating the time average of the value of the noise squared.

$$E(x) = \lim_{T \to \infty} \frac{1}{T} \int_0^T \dot{x}^2 \, dt \qquad (3.4\text{-}6)$$

If the random processes are ergodic the integral (3.4-6) will exist and will equal th statistical expectation of the squared value of x. Since E(x) is proportional to the average value of x^2 rather than the deviation in x itself it is usually more convenier to compare the square root of E(x) which is designated e(x) and referred to as the root mean square value of x in this report.

Let δ be an effector deflection. As a result of effector saturation and control energy constraints the mean square value of effector deflection must be limited.

$$E(\delta) < E(\delta)_{max} \qquad (3.4\text{-}7)$$

The mean square value of effector deflection may be expressed as a function of the mean square values associated with the sensors and the parameters associated with G_v. Thus in order to satisfy inequality (3.4-7), restrictions must be impose on the magnitude of the parameters in G_v. The character of these constraints will become apparent when specific control systems are studied in subsequent sections.

The accuracy of a mathematical analysis is measured by comparing the actual behavior of the physical system with the predicted behavior based on the equations which are used to model the system. Since every physical system is distributed, it is impossible to exactly model it with a finite set of differential equations. However, the solution of a finite set of equations may be sufficiently close to the actual solution for a restricted set of inputs to provide a useful prediction of actual vehicle performance. Increasing the bandwidth of a control syster results in the excitation of vehicle dynamics (such as bending modes) which lead to significant differences between predicted and actual behavior. As a result a more refined mathematical model must be used if a valid analysis is required.

3.5 Lateral Control System Synthesis and Performance Limitations

A general synthesis procedure which defines limitations on the bandwidth ω_0 and the open loop gain G_{ol} is now illustrated by application to the synthesis of a lateral position control system. A control system may be separated into fixed an variable sections. In the case of the lateral control system the transfer function relating lateral displacement y to desired roll φ_d is assumed to be fixed and is designated G_{fy}. This transfer function is shown in Fig. 3.5.1.

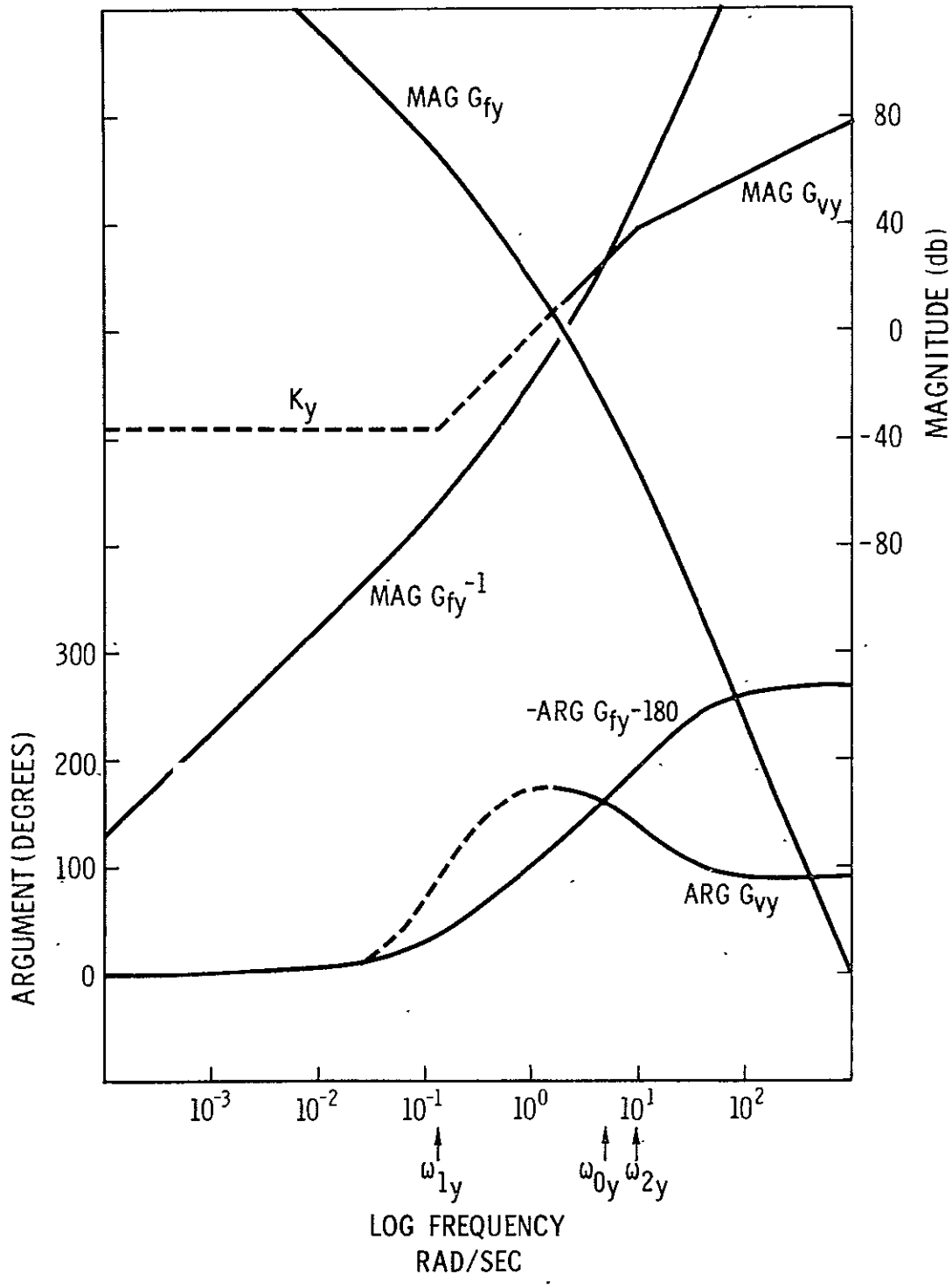

Fig. 3.5.1 Magnitude and phase characteristics for the lateral position control system.

$$G_{fy} = \frac{\varphi}{\varphi_d} = \left[\frac{y}{\varphi_d}\right] \frac{g}{s^2} \qquad (3.5\text{-}1)$$

The second area contains all the elements which the designer can modify to improve performance within the constraints discussed in section 3.4. In this case the transfer function relating φ_d to y is subject to variation and is designated G_{vy}

$$G_{vy} = \frac{\varphi_d}{y} = \left[K_y \frac{s + K_{iy}}{s} + K_{\dot{y}} s + \frac{K_{\ddot{y}} s^2}{T_a s + 1} \right] \qquad (3.5\text{-}2)$$

While the structure of equation (3.5-2) is assumed to be fixed variation is made possible by changing the values of the parameters K_y, $K_{\dot{y}}$, $K_{\ddot{y}}$ and K_{iy}.

In the case of an automatic landing system the lateral position response to atmospheric disturbances is of prime importance. Response to disturbances and system stability is determined by the feedback component of the control law (3.2-5). Therefore attention shall now be focussed on the definition of the adjustable feedback parameters. A subsequent section will discuss the specification of a suitable reference trajectory.

Consider the limitation imposed on bandwidth by stability. The lateral control system is stable if the criteria imposed by equations (3.4-3) to (3.4-5) are satisfied. These criterias are satisfied if

$$\arg G_{vy} > - \arg G_{fy} - 180 \qquad \omega = \omega_{0y} \qquad (3.5\text{-}3)$$

The value of ω_{0y} is determined by the intersection of $|G_{vy}|$ and $|G_{fy}|^{-1}$. Bandwidth maximization is achieved by moving ω_{0y} as far to the right as possible by manipulating arg G_{vy}. It is apparent from the structure of (3.5-2) that the bandwidth is maximized if the break frequency ω_{1y} associated with the G_{vy} is at zero frequency. This would imply that $K_y = 0$, an unsatisfactory solution. Thus some compromise is required between maximizing ω_{0y} while maintaining a reasonable value for ω_{1y}. Assuming that $\omega_{1y} \ll \omega_{2y} = T_a^{-1}$ the following relationships exist between the gains K_y, $K_{\dot{y}}$ and $K_{\ddot{y}}$:

$$\omega_{2y} = \frac{1}{T_a} \qquad (3.5\text{-}4)$$

$$\omega_{1y} \approx \left[\frac{K_y}{K_{\ddot{y}}}\right]^{1/2} \qquad (3.5\text{-}5)$$

$$K_{\ddot{y}} \approx \frac{K_y}{\omega_{1y}^2} \qquad (3.5\text{-}6)$$

$$K_{\dot{y}} \approx \frac{2\xi_{1y} K_y}{\omega_{1y}} \qquad (3.5\text{-}7)$$

where ζ_{1y} is the damping coefficient associated with the second order break frequency ω_{1y}. A reasonable compromise is achieved by setting $\omega_{1y} = 0.2$ rad/sec. The value of ω_{0y} is then approximately 2.0 rad/sec. The corresponding gains for $\zeta_{1y} = 1.00$ are

$$K_y = 1.13 \text{ degrees/ft}$$

$$K_{\dot{y}} = 11.3 \text{ degrees/ft}$$

$$K_{\ddot{y}} = 28.3 \text{ degrees/ft/sec}^2 \qquad (3.5\text{-}8)$$

The response characteristics of a lateral control system using these gains will be unsatisfactory as a result of the oscillatory nature of the system. The values in (3.5-8) do, however, provide a well defined upper limit on the parameter magnatudes.

Sensor noise introduces a further limitation of open loop gain and bandwidth by placing direct restrictions on the size of the adjustable parameters K_y, $K_{\dot{y}}$ and $K_{\ddot{y}}$.

While the general solution for the exact value of mean square control movement is extremely complicated, requiring precise knowledge of the statistical characteristics of all the disturbances acting on a system and the internally generated design purposes using the following theorem.

Theorem: Let $a_1 \sim a_n$ be any set of variables possessing finite autocorrelation and cross-correlation functions. Then the mean square value of their sum exists and is bounded

$$E\left(\sum_{i=1}^{n} a_i\right) \leq 2 \sum_{1=1}^{n} E(a_i) \qquad (3.5\text{-}9)$$

A proof of this theorem is given in Appendix B.

Referring to chapter 5 of reference 26 and equation (3.2-9) the mean square aileron deflection may be bounded

$$E(\delta_a) \leq 2 \left[K_y^2 E(y) + K_{\dot{y}}^2 E(\dot{y}) + K_{\ddot{y}}^2 E(\ddot{y}) + E(\varphi) \right] K_\varphi^2 + 2K_{\dot{\varphi}}^2 E(\dot{\varphi}) \qquad (3.5\text{-}10)$$

where

$E(x)$ is the mean square value of the variable x

K_x are control system parameters

A typical set of worst case noise parameters for the new lateral control system is

$$E(y) = 400.0 \text{ ft}^2$$

$$E(\dot{y}) = 25.0 \text{ ft}^2/\text{sec}^2$$

$$E(\ddot{y}) = 4.0 \text{ ft}^2/\text{sec}^4$$

$$E(\varphi) = 0.01 \text{ deg}^2$$

$$E(\dot{\varphi}) = 0.01 \text{ deg}^2/\text{sec}^2$$

Suppose that the maximum permissible mean square aileron deflection is

$$E(\delta_a) = 2500.0 \text{ deg}^2$$

and the parameters associated with the gains are

$$K_\varphi = 1.0$$

$$K_{\dot{\varphi}} = 2.0 \text{ sec}$$

$$\omega_{1y} = 0.200 \text{ rad/sec}$$

$$\zeta_{1_y} = 1.00$$

The corresponding maximum set of gains may then be computed using eqs. (3.5-5), (3.5-7) and (3.5-3). It is apparent that the terms in equation (3.5-10) contributed by roll and roll rate are comparatively small. Thus attention is focussed on the first three terms which are simplified using equation (3.5-5) and (3.5-6) to eliminate $K_{\dot{y}}$ and $K_{\ddot{y}}$.

$$E(\delta_a) < 10800\, K_y^2$$

therefore

$$K_{y\,\max}^2 \approx \frac{E(\delta_a)_{\max}}{10800} \qquad (3.5\text{-}11)$$

$$K_y \approx 0.481 \text{ degrees/ft}$$

$$K_{\dot{y}} \approx 4.81 \text{ degrees/ft/sec}$$

$$K_{\ddot{y}} \approx 12.02 \text{ degree/ft/sec}^2 \qquad (3.5\text{-}12)$$

Since the gains in (3.5-12) are less than the gains in (3.5-8) limitations on bandwidth and open loop gain are imposed by noise in this example.

The integral compensator gain K_{iy} may now be selected. Since the integral compensator always introduces phase lag the break frequency $\omega = K_{iy}$ must be selected so that the phase shift and magnitude effects introduced by the compensator

at the crossover frequency are small. This condition is satisfied if

$$K_{iy} < \frac{\omega_{0y}}{10}$$

Thus the value of K_{iy} should be less than 0. 20.

The final gains in table 5. 2-1 are based on the values in (3. 5-12) which were modified during simulation to achieve satisfactory transient response characteristics. The actual control system configuration is described in chapter 5.

3. 6 Vertical Control System Synthesis and Optimization

Conventional vertical position control systems utilize vehicle pitch to effect changes in the vertical plane. Thus the transfer function of the fixed elements G_{iz} in the control system relates vertical position z to desired pitch angle θ_d (eq 3. 2 -4). This transfer function is delineated in Fig. 3. 6. 1. The bandwidth limitations imposed by stability and noise are explored by plotting $|G_{vz}|^{-1}$, - (arg G_{vz} +180) and the control lay characteristics G_{vz} imposed by the structure in equation (3. 2-6). This leads to the following conclusions

1. The maximum crossover frequency ω_{0z} lies between 1. 0 and 10. 0 rad/ sec as a result of the phase restrictions on G_{vz}.
2. The slope of $|G_{iz}|^{-1}$ is approximately 40 db/decade for $1.0 < \omega < 10.0$. Since the maximum slope of G_{vz} is 40 db/decade any increase in ω_{0z} in this frequency range, by acceleration feedback occurs at essentially constant open loop gain $|G_{vz}\ G_{iz}| = 1.0$.
3. The break frequency ω_{iz} should be as high as possible to maximize the gain K_z.

As a result of 2 the application of acceleration feedback to increase bandwidth will not lead to a significant decrease in sensitivity to environmental disturbances Thus acceleration feedback may be eliminated and the control law reduced to

$$G_{vz} = \frac{\theta_d}{z} = \left[K_z \frac{s + K_{iz}}{s} + K_z^{\bullet} s \right] \qquad (3.6\text{-}1)$$

Assuming that the integral compensator has a negligible effect at ω_{0z} the maximum value of ω_{0z} is approximately 2 rad/sec. The value of ω_{iz} may be computed from the relation

$$\omega_{iz} = K_{iz} < \frac{\omega_{0z}}{10} \qquad (3.6\text{-}2)$$

The integral compensator must produce negligible phase shift at ω_{0z}. This condition is satisfied if

$$K_{iz} < \frac{\omega_{0z}}{10} \qquad (3.6\text{-}3)$$

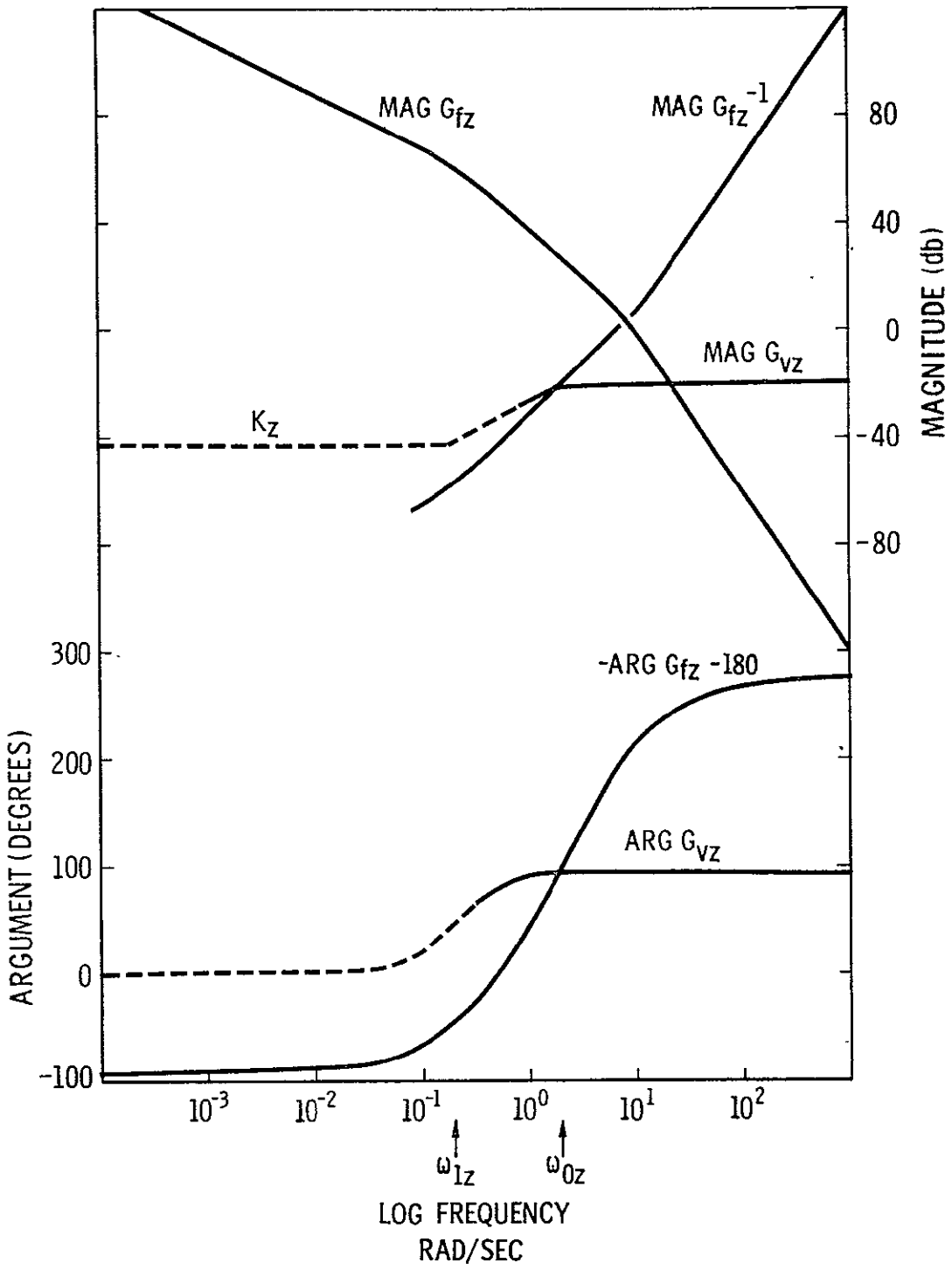

Fig. 3.6.1 Magnitude and phase characteristics for the vertical position control system.

The upper bound on mean square elevator effector activity is estimated using the relationship

$$E(\delta_e) \leq 2\ \left[K_z^2\ E(z) + K_{\dot{z}}^2\ E(\dot{z})\right]\ K_\theta^2$$

$$2\left[K_\theta^2\ E(\theta) + K_{\dot{\theta}}^2\ E(\dot{\theta})\right] \qquad (3.6\text{-}4)$$

where $K_\theta, K_{\dot{\theta}}$ are gains associated with the pitch autopilot described in reference 26 and $E(x^2)$ is the mean square value of the variable x. The second term in equation (3.6-4) is comparatively small and may be neglected.

Substituting

$$E(\delta_e)_{max} = 900 \text{ degrees}^2$$

$$E(z) = 100 \text{ ft}^2$$

$$E(\dot{z}) = 25 \text{ ft}^2/\text{sec}^2$$

$$K_{\dot{z}} = 0.2\ K_z \text{ (from equation 3.6-2)}$$

$$K_\theta = 7.10$$

yields

$$K_z \leq 0.351 \text{ degrees/ft}$$

This value of K_z is much larger than the level imposed by stability considerations ($K_z < 0.287$ degrees/ft). Thus the control system is stability limited and a value of $K_z < 0.287$ must be used.

As a result of the limited performance improvement attainable using the conventional vertical control configuration the conventional approach was abandoned and a new technique which utilizes direct lift control adopted. The results of this investigation are presented in section 3.7.

3.7 Improving Vertical Control System Performance by Direct Lift Control

While vertical position control is not as critical as lateral position control an improvement in vertical trajectory accuracy, particularly during the final landing phases, leads to important reductions in longitudinal touchdown dispersion. Investigations in the past have dealt with the synthesis of a vertical path controller which uses pitch angle as the primary control variable. The sequence of phenomena which occur when a change in vertical path is effected by a pitch attitude modification may be summarized as follows

1. An upward deflection command is fed to the elevator.
2. The lift produced by the horizontal stabilizer decreases as the elevator

deflects up producing a positive pitch moment about the y axis. Since the SST horizontal stabilizer provides a significant portion of the total lift the vehicle begins to sink.

3. The positive pitch moment leads to an increase in pitch angle which increases the angle of attack of the wing, increasing the lift.

4. In response to the increase in lift the vehicle begins to climb.

It is apparent that vertical control by means of pitch attitude is subject to two important disadvantages.

1. The required elevator deflection produces an undesirable control reversal at the initiation of the vertical maneuver. (This is a particularly serious problem during a landing abort maneuver.)

2. The relatively slow response of the pitch control system compared to the response of the vehicle effectors severely limits the bandwidth of the vertical position control loop.

The disadvantages described above may be circumvented by effecting vertical control using the direct lift spoilers. The direct lift spoilers are aerodynamic devices mounted on the top surface of the vehicles wings which may be deflected to disturb the air flow over the wings. This disturbance results in a change in the total lift force. By operating with the spoiler deflection at a fraction of their maximum deflection during the approach, positive or negative increments in lift may be generated by appropriate spoiler motion. The effect of spoiler operation is revealed by examining the linearized vehicle equations for angle of attack α and pitch rate q given on page 234 of reference 26. The transfer function relating α to direct lift spoiler δ_{sd} deflection is derived in Appendix A. If the spoiler effector is modelled by a simple time lag with a 0.05 second time constant T_{sd} the transfer function between z and the spoiler command δ_{sdc} may be written

$$G_{fz} = \frac{z}{\delta_{sdc}} = \frac{1}{T_{sd}s+1} \left[\frac{\alpha}{\delta_{sd}}\right]_{q=0} \frac{V_p}{s} \qquad (3.7\text{-}1)$$

This transfer function is shown in Fig. 3.7.1. The bandwidth limitations imposed by stability and sensor noise are investigated using the techniques in section 3.5. The control structure is defined by equation (3.2-6). Referring to Fig. 3.7.1 it is apparent that

1. The maximum possible bandwidth is approximately $\omega_{0z} \approx 20$ rad/sec compared to $\omega_{0z} \approx 4$ rad/sec for the conventional system.

2. The break frequency ω_{1z} should be as high as possible to maximize the position gain K_z but ω_{1z} cannot be much larger than 1 rad/sec if

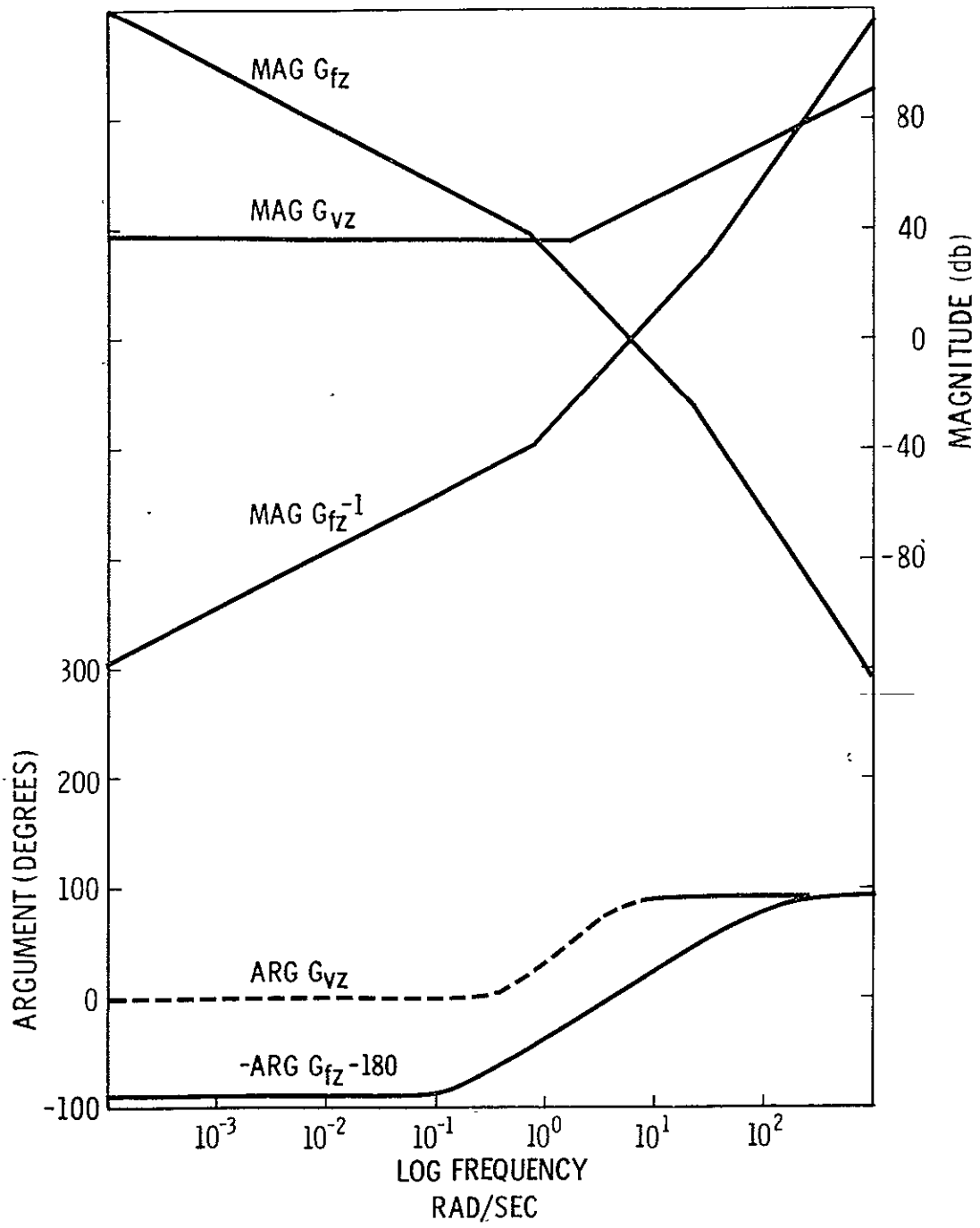

Fig. 3.7.1 Magnitude and phase relationships for a vertical control system using direct lift spoilers.

critical phase considerations are to be satisfied.

3. The application of lagged acceleration feedback only produces a minor improvement in bandwidth and open loop gain ($\omega < \omega_{0z}$).

As a result the acceleration gain $K_{\ddot{z}}$ is assumed to be zero. The control law in equation (3.2 6) then reduces to

$$\delta_{sdc} = \left[K_z \frac{s + K_{iz}}{s} + K_{\dot{z}} s \right] z \tag{3.7-2}$$

The integral compensator gain K_{iz} must be selected so that phase shift introduced by the integral compensator is negligible at ω_{0z}. This condition is satisfied if

$$K_{1z} < \frac{\omega_{0z}}{10.0} \tag{3.7-3}$$

The break frequency ω_{1z} is calculated from the relation

$$\omega_{1\dot{z}} = \frac{K_z}{K_{\dot{z}}} \tag{3.7-4}$$

The mean square spoiler motion as a result of externally and internally generated stochastic disturbances may be bounded using theoren 1 in section 3.5.

$$E(\delta_{sdc}) \leq 2 \left[K_z^2 E(z) + K_{\dot{z}}^2 E(\dot{z}) \right] \tag{3.7-5}$$

Assuming that break frequency ω_{iz} is 1 rad/sec $K_{\dot{z}}$ is equal to K_z and

$$E(\delta_{sdc}) \leq 2 K_z^2 \left[E(z) + E(\dot{z}) \right] \tag{3.7-6}$$

Substituting

$$E(\delta_{sdc})_{max} = 100.0$$

$$E(z) = 100 \text{ ft}^2$$

$$E(\dot{z}) = 25 \text{ ft}^2/\text{sec}^2$$

gives

$$K_z = K_{\dot{z}} \leq 0.63 \text{ degrees/ft}$$

This yields approximately 30 degrees of phase margin and acceptable transient response characteristics. Thus the final gain selection in once again based on effector noise considerations.

While the direct lift technique improves the bandwidth of a vertical position control system its application presents a number of practical difficulties.

1. The spoilers produce high drag. Thus it is desirable to operate as close to the reference setting as possible

2. The variation in z that can be achieved using spoilers is limited by magnitude restrictions on spoiler deflection.

As a result of these problems a hybrid solution which combines the satisfactory low frequency response characteristics of the vertical controller based on pitch with the desirable high frequency properties of direct lift control is adopted. A system based on this configuration is presented in section 5.3

3.8 Summary

The performance limitations imposed on a linear control systems by fixed vehicle and effector characteristics, structural properties of the control law and mean square effector activity have been explored. The results of this investigation have been applied to the synthesis of lateral and vertical position control systems for the SST. While the properties of the linear controllers have been studied in depth nonlinear characteristics which have a profound impact on the nature of the vehicles path must now be considered.

CHAPTER 4

OPTIMIZING TRAJECTORY PERFORMANCE

4. 1 Introduction

In chapter 3 it was demonstrated that the application of corrected inertial position, velocity, lagged acceleration data and direct lift control permits a significant improvement in position control system bandwidth. As a result the sensitivity of the regulated position trajectory to ambient atmospheric disturbances was reduced and the ability of the controller to precisely follow a desired trajectory was increased. Bandwidth cannot be increased indefinitely as a result of considerations such as stability, noise and system nonlinearities. The most important vehicle nonlinearity during landing is saturation. Saturation occurs in all the aerodynamic effectors which produce translational forces and rotational moments on the vehicle. Additional saturation limits are imposed on variables such as roll angle, roll rate and vertical acceleration by human factors such as passenger comfort. The implications of saturation nonlinearites in control system design are now considered.

4. 2 Trajectory Characteristics and Saturation

The most common form of saturation occurs in the effectors which produce the moments and forces required to effect changes in vehicle state. All the aerodynamic effectors of the SST have magnitude and rate limitations. Effector saturation is particularly serious, resulting in an essentially open-loop condition as long as it persists. The effect of saturation is studied by examining the transfer functions of a system linearized about its current operating point. Consider the block diagram in Fig. 3. 3. 1 and let G_1 represent the effector transfer function. Saturation in effector output magnitude or rate modifies G_1 to

$$G_1 = 0 \tag{4.2-1}$$

As a result, the transfer functions relating C to R and C to D become:

$$C/R = 0 \tag{4.2-2}$$

$$C/D = G_2 \tag{4.2-3}$$

Thus reference control is momentarily lost and the sensitivity of the system to disturbances is increased by the factor $1 + G_0 G_1 G_2 H$. It is therefore desirable to eliminate or prevent saturation.

Saturation may be excited by three sources

1. Reference commands to the control system.
2. External disturbances acting on the vehicle.
3. The combination of reference commands and external disturbances.

Saturation arising from disturbances is controlled by reducing the magnitude of the open-loop transfer function. Thus the magnitude of the environmental disturbances imposes further restrictions on open-loop gain. Saturation resulting from reference inputs is restricted by processing the reference signal. This aspect is now considered in detail.

4.3 Nonlinear Trajectory Generation

The problem of input signal processing may be formulated within the Theory of Optimal Control. For example, consider the linearized dynamical system

$$\dot{x} = f_x x + f_m m \tag{4.3-1}$$

where

- x is an n-dimensional state vector
- m is an m-dimensional input
- f_x is an n x n matrix
- f_m is an n x m matrix

The state vector is subject to a set of limits of the form*

$$|x| \leqq L_x \tag{4.3-2}$$

$$|\dot{x}| \leqq L_{\dot{x}} \tag{4.3-3}$$

L_x and $L_{\dot{x}}$ are n-dimensional vectors. The absence of a limit on a particular element of x is signified by setting the corresponding element of L_x equal to ∞. The problem may be defined as follows:

*The inequality sign signifies that $|x_i| \leqq L_{xi}$ $i = 1, 2, \ldots, n$

Problem Definition: Find a control m and the corresponding trajectory x, which minimizes the integral performance index

$$J = \int_0^T x' Mx \, dt \tag{4.3-4}$$

subject to the nonholonomic constraint

$$\dot{x} = f_x x + f_m m \tag{4.3-5}$$

and the hard constraints

$$\left.\begin{aligned} |x| &< L_1 \\ |\dot{x}| &< L_2 \end{aligned}\right\} \tag{4.3-6}$$

where

$$\left.\begin{aligned} L_1 &< L_x \\ L_2 &< L_{\dot{x}} \end{aligned}\right\} \tag{4.3-7}$$

The matrix M is positive semi-definite.

The object of the optimization is to transfer the vehicle to the vicinity of a terminal state while satisfying the limits imposed by Eq (4.3-5) The inequalities (4.3-6) are introduced to allow for the effects of disturbances on the system by providing some range between undisturbed operating values and saturation constraints.

The solution of this problem is complicated by the presence of the magnitude constraints. As a result, a two-point boundary problem must be formulated and solved. While the optimal control approach produces the best answer, the resulting computational complexity usually leads to a solution which requires a special-purpose, hybrid computer if real-time control is desired. These problems have discouraged the application of optimal-control techniques.

To circumvent the computational difficulties the following approximate technique for generating solutions to the problem defined above is presented. The method is particularly suited to vehicle control problems. Consider the simplified vehicle control system shown in Fig. 4.3. 1. The desired terminal state may be set equal to

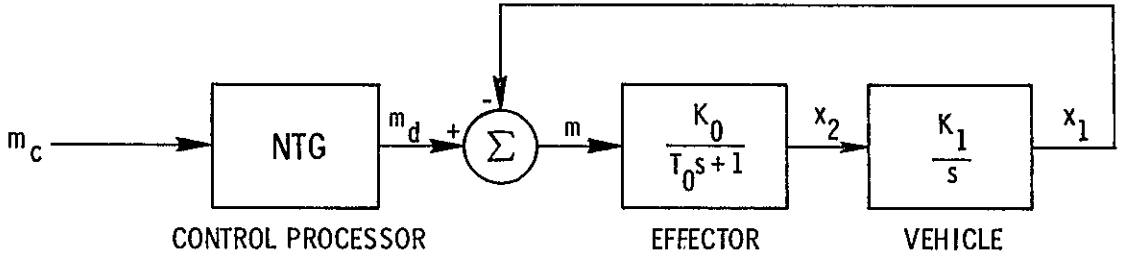

Fig. 4.3.1 Illustrative model of a trajectory control system. The value of x_1 should follow the value of m_d closely.

$$x_1 = m_c \tag{4.3-8}$$

$$x_2 = 0 \tag{4.3-9}$$

The control input is the variable m_d. The effector output x_2 is subject to saturation

$$|x_2| \leq L_0 \tag{4.3-10}$$

$$|\dot{x}_2| \leq L_1 \tag{4.3-11}$$

These limits imply constraints on the vehicle state of the form

$$|\dot{x}_1| \leq |L_0 K_1| \tag{4.3-12}$$

$$|\ddot{x}_1| \leq |L_1 K_1| \tag{4.3-13}$$

Suppose that the natural frequency of the system in Fig. 4.3.1

$$\omega = \left[\frac{K_0 K_1}{T_0}\right]^{1/2} \tag{4.3-14}$$

is large compared to the bandwidth of the input m_c, and the damping ratio

$$\xi = \frac{1}{2}\left(\frac{1}{T_0 K_0 K_1}\right)^{1/2} \tag{4.3-15}$$

is greater than 1. Then the output satisfies

$$\begin{aligned} x_1 &\approx m_d \\ x_2 &\approx \frac{\dot{m}_d}{K_1} \end{aligned} \tag{4.3-16}$$

provided that

$$|\dot{m}_d| \leq |L_0 K_1| \tag{4.3-17}$$

$$|\ddot{m}_d| \geq |L_1 K_1| \tag{4.3-18}$$

The variable m_d may be identified with the trajectory r. Thus the limits on the state variable x imply corresponding constraints on r if saturation within the control loop is to be avoided. A requirement is consequently established for a device which

1. Controls the bandwidth of the input signal
2. Modifies the input signal by constraining the maximum amplitudes of its first and second derivatives.

A device having the desired properties is illustrated in Fig. 4.3. 2. The device will be referred to as a nonlinear trajectory generator. A linearized model of the NTG is obtained by removing the magnitude limits. The transfer function then becomes

$$\frac{m_d}{m_c} = \frac{K_1}{s^2 + K_2 K_1 s + K_1} \tag{4.3-19}$$

The bandwidth of the transfer function is modified by varying the natural frequency ω_t and is normally equal to the crossover frequency of the open-loop transfer function of the control system. The natural frequency depends upon the value of K_1

$$\omega_t = K_1^{1/2} \tag{4.3-20}$$

The damping ration ξ_t is normally larger than 1

$$\xi_t = \frac{K_2 K_1^{1/2}}{2} \tag{4.3-21}$$

or

$$K_2 = \frac{2\xi_t}{K_1^{1/2}} \tag{4.3-22}$$

The limits impose the following constraints on the outputs of the NTG

$$|m_d| \leqq S_0 \tag{4.3-23}$$

$$|\dot{m}_d| \leqq S_1 \tag{4.3-24}$$

$$|\ddot{m}_d| \leqq S_2 \tag{4.3-25}$$

Saturation of m_d automatically sets $\dot{m}_d$ equal to zero; similarly, saturation of $\dot{m}_d$ sets $\ddot{m}_d$ to zero. Thus the requirements imposed by saturation are satisfied.

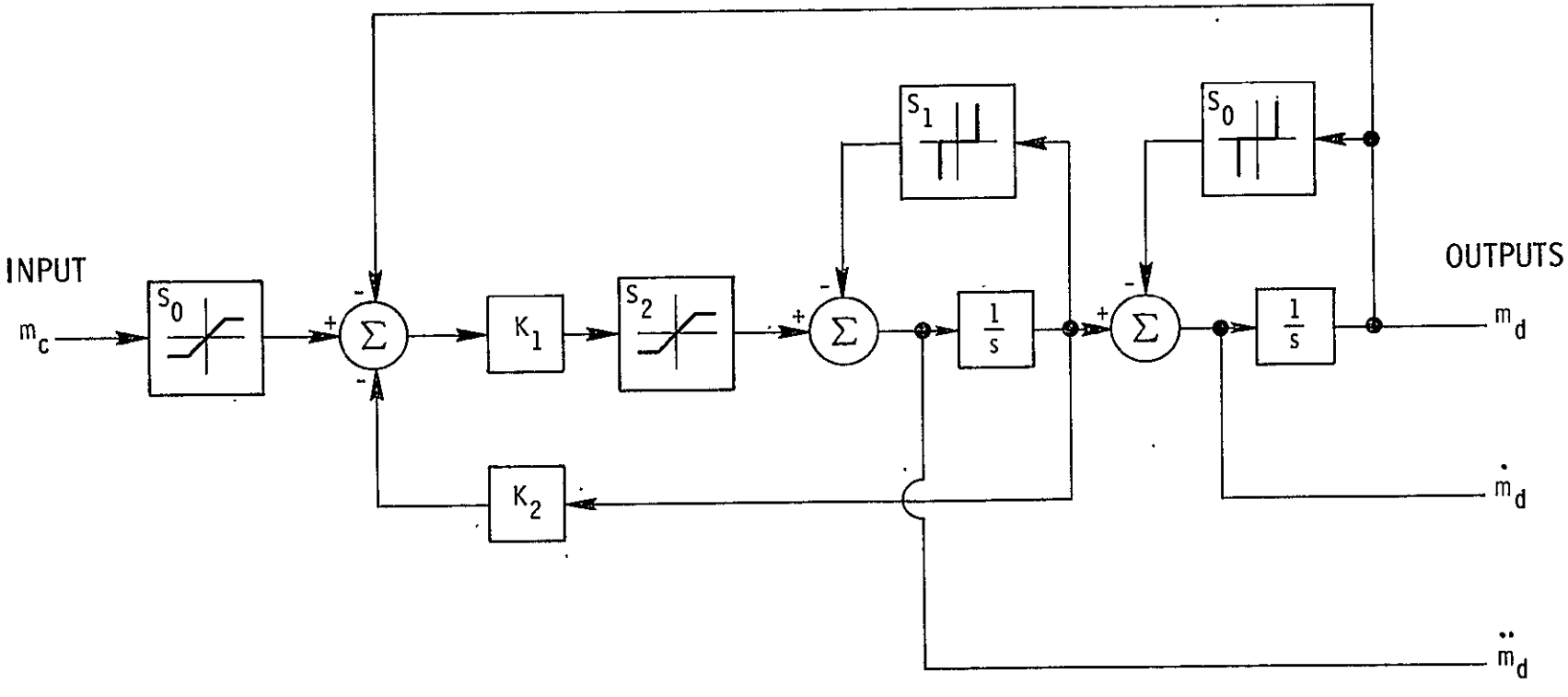

Fig. 4.3.2 Block diagram representation of a second-order nonlinear trajectory generator (NTG).

The availability of first and second derivatives of the output plays an important role in the construction of control systems capable of precisely following a trajectory, as is shown later in the sections on vertical and lateral control system synthesis.

4.4 Generalized Trajectory Control

The effectiveness of the approximate solution described in section 4.3, depends upon the ability of the controlled system to precisely follow the generated trajectory. Trajectory precision has already been improved by

1. Increasing the bandwidth of the control system.
2. Controlling the bandwidth, damping ratio and saturation limits of the Nonlinear Trajectory Generator.

The closed-loop transfer function between the reference input R and the controlled output of Fig. 3.2.1 was stated earlier to be

$$\frac{C}{R} = \frac{G_0 G_1 G_2}{1 + G_0 G_1 G_2 H} \tag{4.4-1}$$

It is of interest to consider the asymptotic behavior of this transfer function as the magnitude of the open-loop transfer function varies. Two cases are of interest

(a) $$G_0 G_1 G_2 H \ll 1$$

$$\frac{C}{R} \to G_0 G_1 G_2 \tag{4.4-2}$$

(b) $$G_0 G_1 G_2 H \gg 1$$

$$\frac{C}{R} \to \frac{1}{H} . \tag{4.4-3}$$

In the first case it is apparent that the advantages of feedback are lost if the open-loop magnitude is significantly less than one. In the second case the output C will not equal the input R unless H is identically one. This problem may be avoided by operating on the input with H so that Eq (4.4-1) becomes

$$\frac{C}{R} = \frac{G_0 G_1 G_2 H}{1 + G_0 G_1 G_2 H} \tag{4.4-4}$$

Consequently, precision trajectory control is achieved by producing a modified control signal which is a linear transformation of the desired trajectory. Typically, H has the form

$$H = 1 + K_{\dot{x}} s + K_{\ddot{x}} s^2 \tag{4.4-5}$$

where $K_{\dot{x}}$ and $K_{\ddot{x}}$ are constants. The form of H in the present application implies that the first and second derivatives of the reference signal must be generated to provide the correct compensation. However, differentiation of the input can be avoided by utilizing the signals available from the nonlinear trajectory generator. The signals from the nonlinear trajectory generator are shown in Fig. 4.3.2 and this utilization is indicated in Fig. 4.4-1. The input R_c to the control system has the required form

$$\begin{aligned} R_c &= R_d + K_{\dot{x}} \dot{R}_d + K_{\ddot{x}} \ddot{R}_d \\ &= \left(1 + K_{\dot{x}} s + K_{\ddot{x}} s^2\right) R_d \\ &= H R_d \end{aligned} \tag{4.4-6}$$

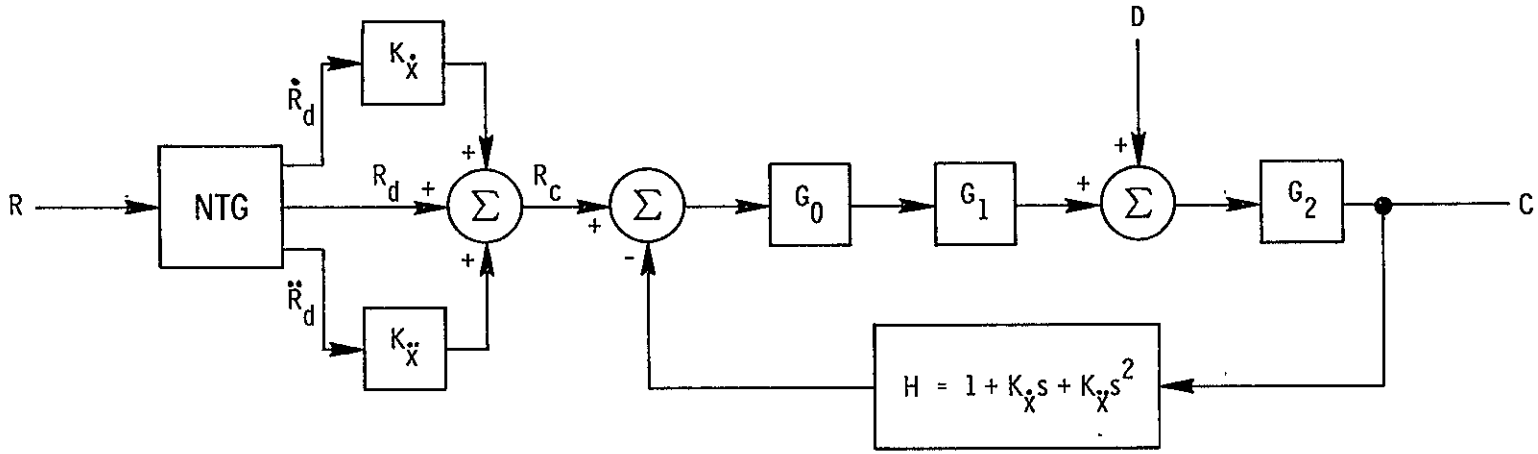

Fig. 4.4.1 Block diagram of a control system incorporating generalized trajectory control.

CHAPTER 5

LATERAL AND VERTICAL CONTROL SYSTEM CONFIGURATIONS

5.1 Introduction

Chapters 3 and 4 have discussed the theoretical considerations associated with inertially stabilized position control system analysis and synthesis. The task of the designer is to amalgamate these various concepts in a final design configuration. This chapter presents up to date modernized control system block diagrams and response characteristics.

5.2 Lateral Position Control System

Lateral control is effective while the vehicle is acquiring and tracking the localizer center plane. During the decrab maneuver lateral position control is abandoned and lateral control responsibility is shifted to the Decrab Controller.* Lateral control is again resumed by the Rollout Control System* after touchdown. Rollout control has not been investigated to date.

Lateral position control is achieved by turning the vehicle in a coordinated fashion ($\beta \approx 0$) using roll angle φ as the primary control variable based on the relationships

$$\dot{\psi} \approx \frac{g \tan\varphi}{v_p} \qquad (5\ 2\text{-}1)$$

$$\dot{y} \approx v_p \sin\varphi \qquad (5.2\text{-}2)$$

Since the maximum amplitudes of φ and ψ are normally less than 45 degrees during the acquisition maneuver the response characteristics of the lateral control system and the linearized model shown in Fig. 5.2.1 are quite similar. The properties of the roll autopilot are described in appendix D. The parameter values associated with the control law are given in table 5.2-1. Bode diagrams of the open and closed loop position controllers are shown in Figs. 5.2.2 and 5.2.3. One characteristic problem associated with the lateral control system is evident in Fig. 5.2.2. Since

*See reference 26.

Table 5.2-1 Lateral Control System Parameters

GAINS		
K_y	Lateral position gain	0.080 deg/ft
$K_{\dot{y}}$	Lateral velocity gain	0.800 deg/ft/sec
$K_{\ddot{y}}$	Lateral acceleration gain	2.000 deg/ft/sec^2
K_{iy}	Integral compensator gain	0.050 rad/sec
CONSTANTS		
T_a	Lateral acceleration filter time constant	0.100 seconds
SATURATION LIMITS	IMPOSED BY VEHICLE LIMITS	IMPOSED BY NTG OR CSP
y	∞	∞
$\dot{y}$	±244 000 ft/sec	±244.000
$\ddot{y}$	± 18.60 ft/sec^2	± 8.000 ft/sec^2
ϕ	± 30.000 degrees	± 30.000 degrees
$\dot{\phi}$	± 43.790 deg/sec	± 10.000 deg/sec
$\ddot{\phi}$	± 21.890 deg/sec^2	± 10.000 deg/sec^2
NTG PARAMETERS		
ϕ_{aq}	Acquisition roll limit	20.000 deg
$\dot{\phi}_{aq}$	Acquisition roll rate limit	7.500 deg/sec
$\ddot{\phi}_{aq}$	Acquisition roll acceleration limit	7 500 deg/sec^2
INTEGRAL COMPENSATOR LIMITS		
L_{iy}	y integral compensator limit	2.0 degrees

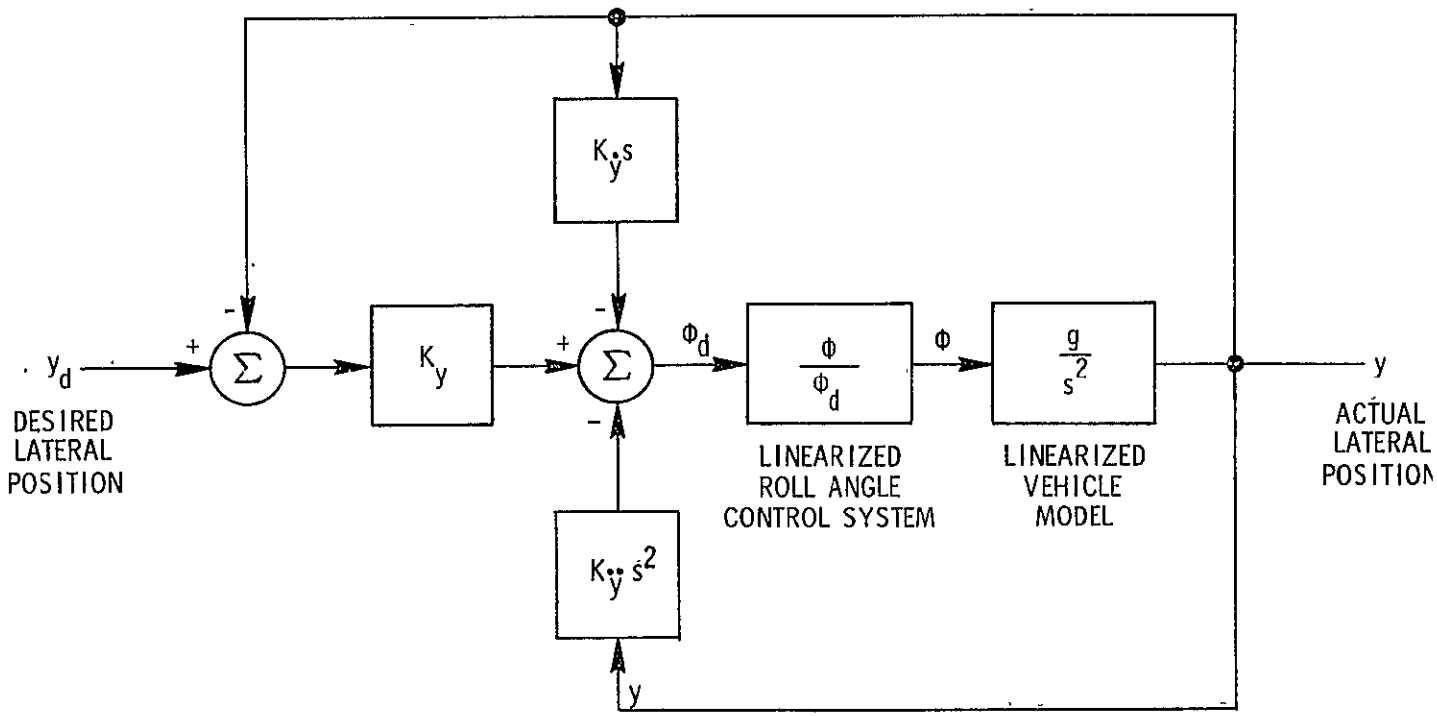

Fig. 5.2.1 Linearized model of lateral control system.

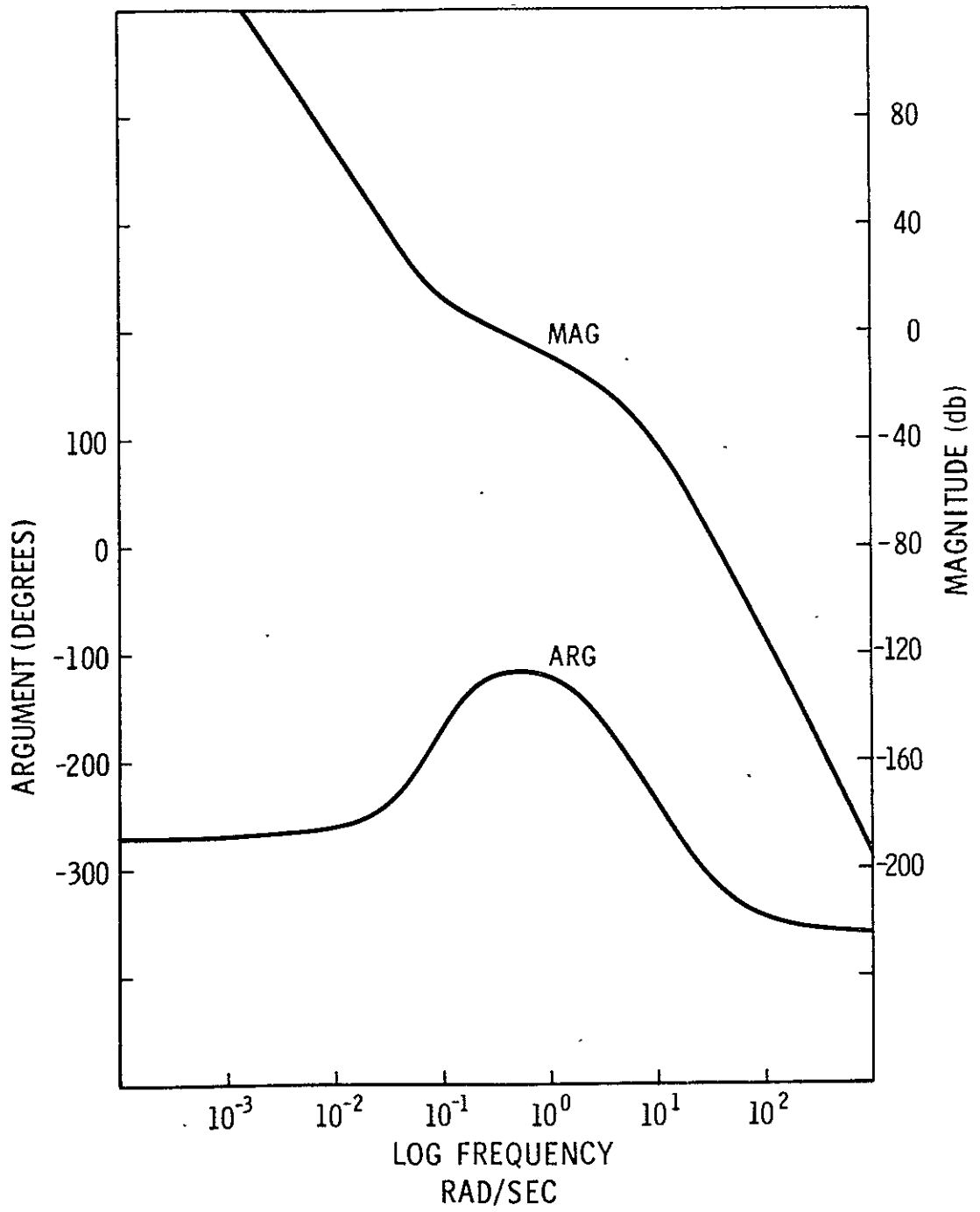

Fig. 5.2.2 Open-loop transfer function of the linearized lateral control system.

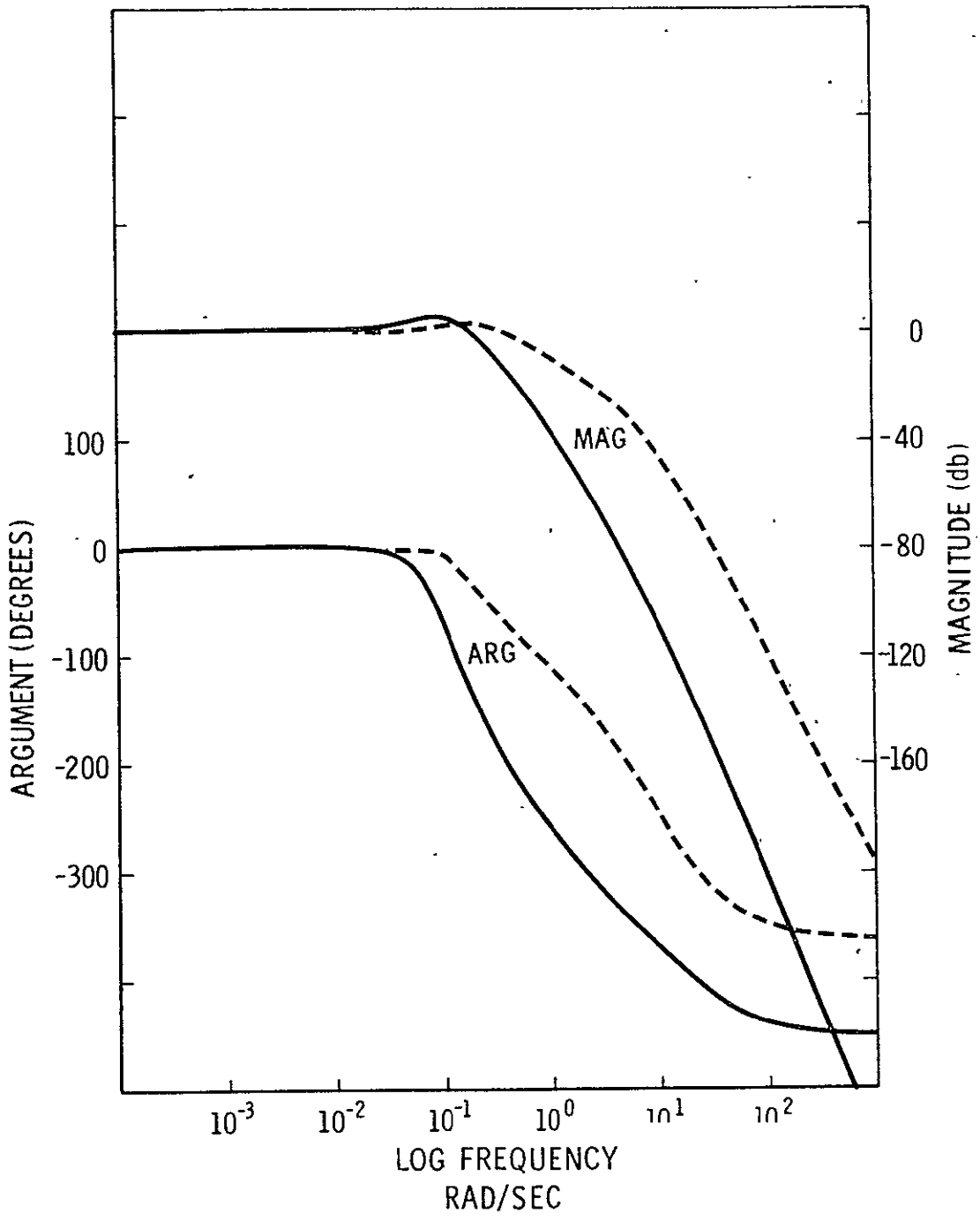

Fig. 5.2.3 Closed-loop frequency response characteristics to errors in position (solid lines) and reference inputs (dotted lines) with feedforward compensation.

the phase angle associated with the open loop transfer function approaches -270 degrees as ω approaches zero the lateral position control system is CONDITIONALLY STABLE. Control system stability depends upon the location of the crossover frequency ω_{0y}. The value of ω_{0y} depends upon the gains K_y, $K_{\dot{y}}$, $K_{\ddot{y}}$, K_{iy} and the magnitude characteristics of the roll control system. If ω_{0y} is sufficiently small the lateral control system will be unstable. While it is possible to adjust the control system parameters to obtain system stability saturation and trigonometric nonlinearities may effectively reduce the open loop gain to a level where a substained oscillation can occur. This problem is circumvented by limiting the output of the integrator in the proportional plus integral compensator so that the integrator will be in hard saturation whenever large values of roll are commanded. Integrator saturation effectively removes the integrator from the system reducing the phase lag to a safe maximum of 180 degrees at low frequencies. The step response of the linearized system appears in Fig. 5.2.4. The effect of generalized trajectory control, discussed in section 4.4, on closed loop bandwidth and step response is also shown. The wide bandwidth to reference inputs ensures that the lateral control system will be able to follow the desired trajectory precisely (in the absence of disturbances).

The lateral position control system performs a sequence of distinct tasks during an automatic landing. The important features are identifed as

1. Acquisition of the ILS Localizer center plane.
2. Tracking the ILS Localizer center plane
3. Momentary termination of lateral position control during the decrab maneuver.
4. Resumption of position control during rollout.

In order to accomplish these tasks the control system must transfer the aircraft from a linear path inclined with respect to the localizer reference plane to a path in the plane. The vehicle remains on this second path until rollout is completed.

Lateral position control is subject to important limitations imposed by passenger comfort. These limitations apply to roll and roll rate. The trajectories generated by NTG_y must reflect the effects of these limitations. A convenient approach to lateral reference trajectory generation is based on the theory of time optimal control. A complete discussion of the synthesis of quasi-time-optimal trajectories is presented in chapter 6 of reference 26. The reference trajectories shown in Fig. 5.2.5 satisfy the relationships

$$|\varphi_c| \leq \varphi_{aq} < \varphi_{max} \tag{5.2-3}$$

$$|\dot{\varphi}_c| \leq \dot{\varphi}_{aq} < \dot{\varphi}_{max} \tag{5.2-4}$$

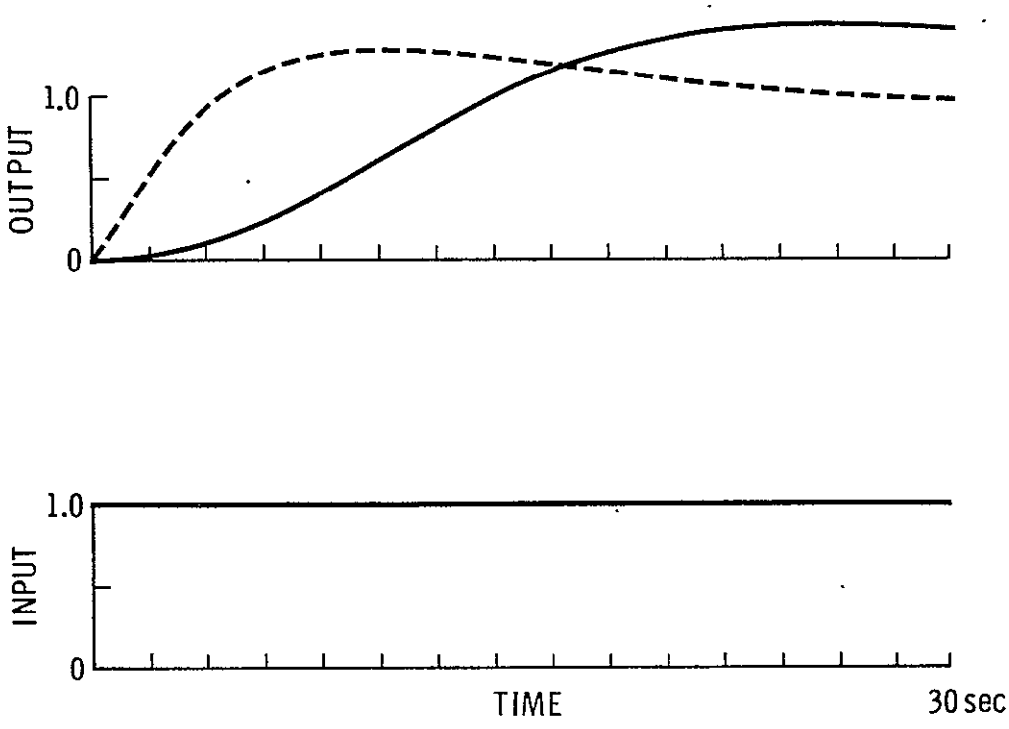

Fig. 5.2.4 Response of the linearized lateral position control system to step inputs in position error (solid lines) and desired position (dotted lines) with feedforward compensation.

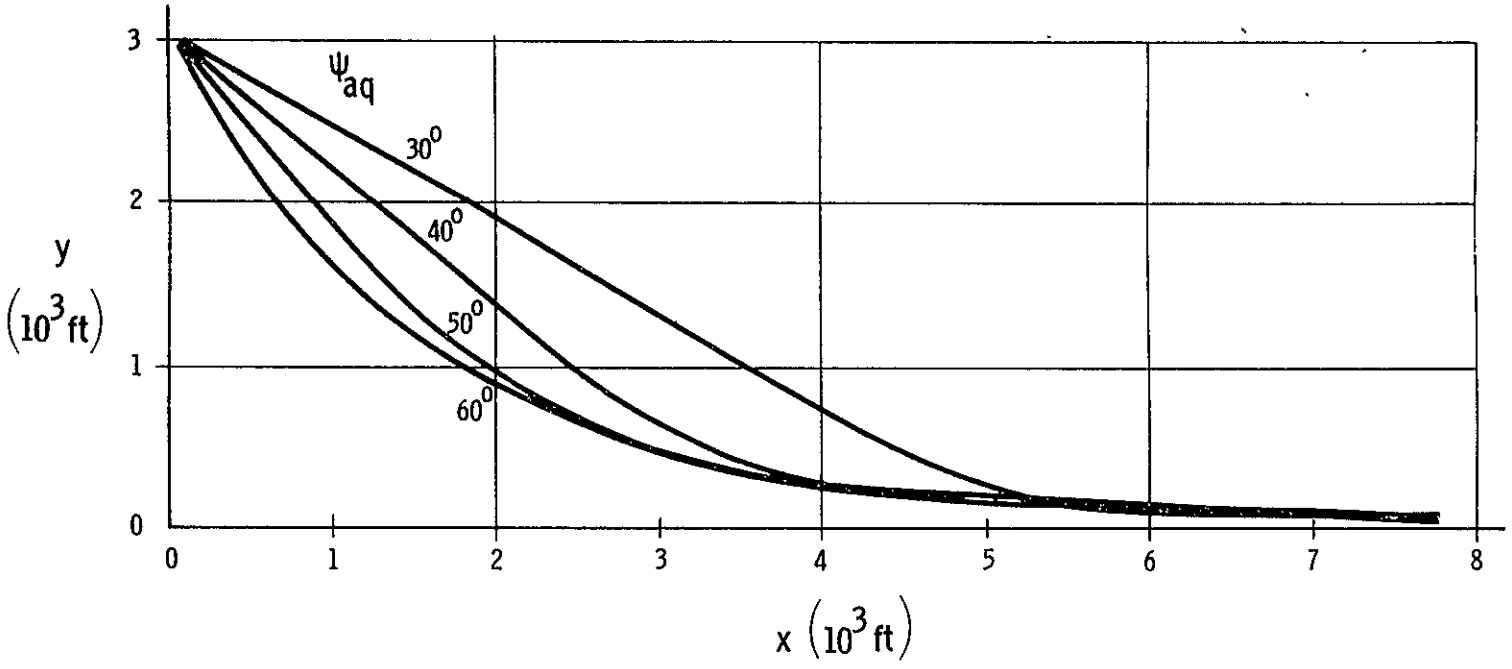

Fig. 5.2.5 Acquisition control system responses for various initial heading angles. These responses demonstrate ability to acquire the localizer beam from a broad range of initial flight path headings.

where φ_{max} and $\dot{\varphi}_{max}$ are the largest permissible roll and roll rate magnitudes respectively. φ_{aq} and $\dot{\varphi}_{aq}$ are constants. The absolute inequality in equations (5. 2-3) and (5. 2-4) provide a roll angle and angular rate margin for counteracting the effects of environmental disturbances, tracking errors and inertial data corrections which are gradually applied during acquisition as shown in section 2. 5. The character of the trajectory and the wide bandwidth of the control system to reference inputs ensures that the aircraft follows the desired trajectory with a high degree of precision as shown in Fig. 5 2. 6. Thus, if the environmental disturbances are moderate, the aircraft is able to fly the y reference path without exceeding the maximum roll angle and roll rates. If the disturbances are very large, however, the commanded values φ_c and $\dot{\varphi}_c$ may exceed the maximum permissible values φ_{max} and $\dot{\varphi}_{max}$. In order to prevent excess roll and roll rate a nonlinear Command Signal Processor CSP_φ is utilized. The structure of CSP_φ is illustrated in Fig. 4. 3. 2. The natural frequency of the CSP defined by equation (4. 3-20) and is adjusted so that linear response bandwidth of the CSP is much greater than the bandwidth of the roll control system. As a result the output φ_d of CSP_φ is essentially equal to the input φ_c subject to the constraints

$$|\varphi_d| < \varphi_{max} \tag{5. 2-5}$$

$$|\dot{\varphi}_d| < \dot{\varphi}_{max} \tag{5. 2-6}$$

Thus, in absence of saturation, the CSP introduces neglibible effects on the linear response characteristics of the position control system It should be emphasized that CSP_φ will normally operate in an unsaturated state thus ensuring minimum sensitivity to disturbances A comprehensive schematic diagram of the lateral position control system is shown in Fig. 5. 2. 7.

5. 3 Vertical Position Control System

Vertical control is maintained during all the phases of an automatic landing prior to touchdown.

Vertical position control is achieved by modifying the vehicle pitch θ and angle of attack α using the pitch angle control system and direct lift spoilers. The basic vertical plane relationship is

$$\dot{z} \approx v_p \sin(\alpha - \theta) \tag{5. 3-1}$$

The analysis of the vertical control system is based on the linearized model shown in Fig. 5. 3-1. Since the perturbations in θ and γ are small during the landing procedure the response characteristics of the actual control system are quite similar to

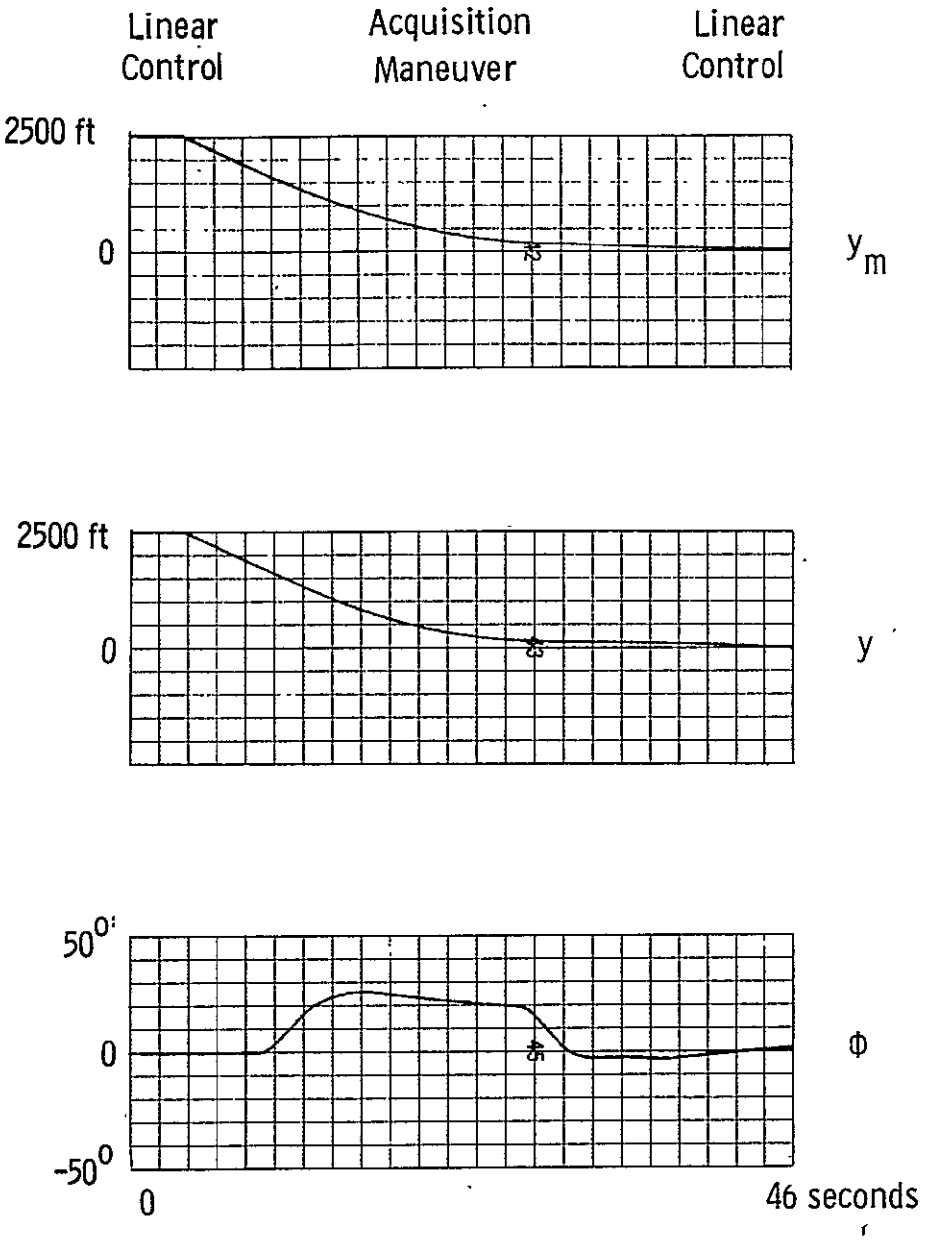

Fig. 5.2.6 Typical acquisition control system response showing the reference trajectory y_m, the actual path y and the roll angle ϕ . ($\psi_o = 45^o$).

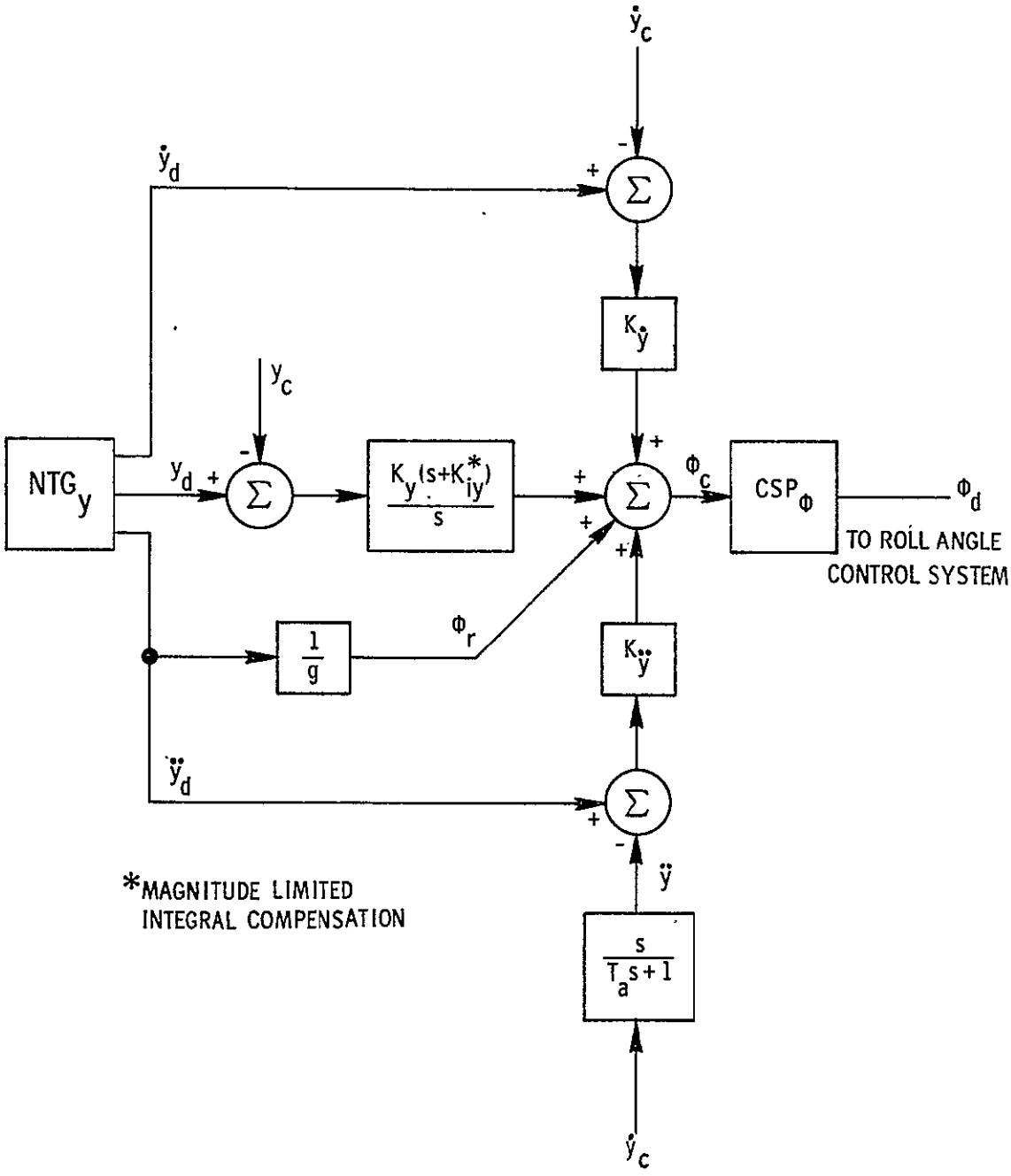

Fig. 5.2.7 Improved lateral position control system with nonlinear trajectory generation, roll command signal processing and inertial stabilization.

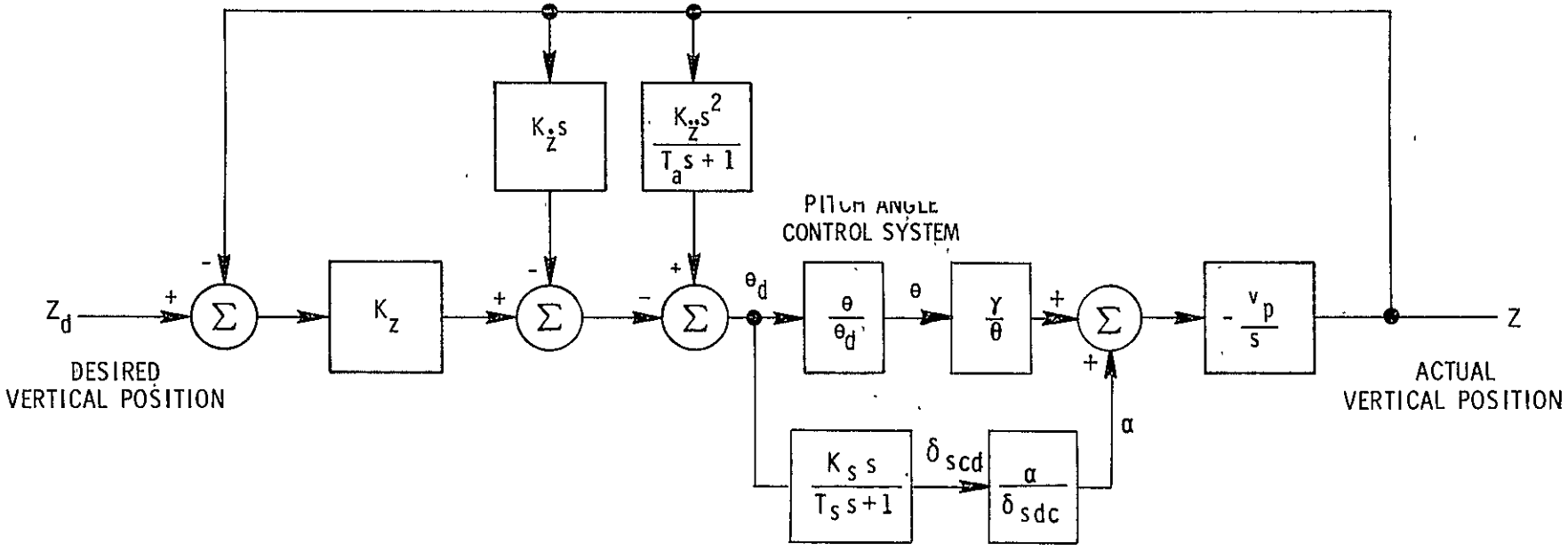

Fig. 5 3. 1 Linearized model of a vertical position control loop.

the linear characteristics. Magnitude and phase characteristics of the open and closed loop transfer functions are shown in Figs. 5. 3. 2 and 5. 3. 3. The step response of the linearized model appears in Fig. 5. 3. 4. The control system parameter values are given in table 5. 3-1. Pitch autopilot design is described in section 5. 11 of reference 26. The important characteristics of the pitch regulator are illustrated in appendix D. The application of direct lift spoilers is illustrated in section 3. 7.

As indicated in section 3. 2 the analysis of the vertical control system in based on the assumption that the perturbation in airspeed u is zero. Thus a critical part of the vertical control system is the automatic throttle. The automatic throttle utilizes airspeed information to generate an engine thrust command which maintains essentially constant airspeed thus satisfying the requirement ($u \approx 0$) for validity of the longitudinal transfer functions derived in appendix C of reference 26. The analysis and design of an automatic throttle, of conventional configuration, is given in appendix E.

The vertical trajectory may be divided into a three distinct segments

1. Transition to the altitude h_{aq} at which the localizer beam center is intersected during the acquisition maneuver.
2. Vertical flight path modification from a level trajectory $h = h_{aq}$ to a descending path tangent to the glideslope centerplane.
3. Reduction in vertical velocity from approximately 10 ft/sec to 2. 5 ft/sec during flareout.

This reference trajectory is shown in Fig. 5. 3. 5. In order to limit vertical acceleration and position errors during transitions 1 and 3 particular care must be exercised in forming the trajectory. Let the vertical path be subject to the constraints

$$|\ddot{z}| \leq \ddot{z}_{max} \qquad (5.\ 3\text{-}2)$$

$$|\dot{z}| \leq \dot{z}_{max} \qquad (5.\ 3\text{-}3)$$

Assuming that precise control is exercised over vertical velocity and acceleration during acquisition and referring to Fig. 5. 3. 5 it is apparent that the following relationships hold for a smooth transition which satifies (5. 3-2) and (5. 3-3).

$$\left|\ddot{z}_d\right| \leq \ddot{z}_{aq} < \ddot{z}_{max} \qquad (5.\ 3\text{-}4)$$

Table 5.3-1 Vertical Control System Parameters

GAINS		
K_z	Vertical position gain	0.063 deg/ft
$K_{\dot{z}}$	Vertical velocity gain	0.126 deg/ft/sec
$K_{\ddot{z}}$	Vertical acceleration gain	0.000 deg/ft/sec^2
K_{iz}	Integral compensator gain	0.050 rad/sec
K_s	Spoiler lead network gain	50.000
CONSTANTS		
T_a	Vertical acceleration filter time constant	0.100 seconds
T_s	Spoiler lead network time constant	5.000 seconds
SATURATION LIMITS	IMPOSED BY VEHICLE LIMITS	IMPOSED BY NTG
z	—	
$\dot{z}$	—	±14.600 ft/sec
$\ddot{z}$	±25.1 ft/sec^2	±12.500 ft/sec^2
θ	—	—
$\dot{\theta}$	± 5.90 deg/sec	—
$\ddot{\theta}$	± 4.92 deg/sec^2	—
NTG PARAMETERS		
ω_z	NTG_z natural frequency	0.500 rad/sec
ξ_z	NTG_z damping ratio	1.000

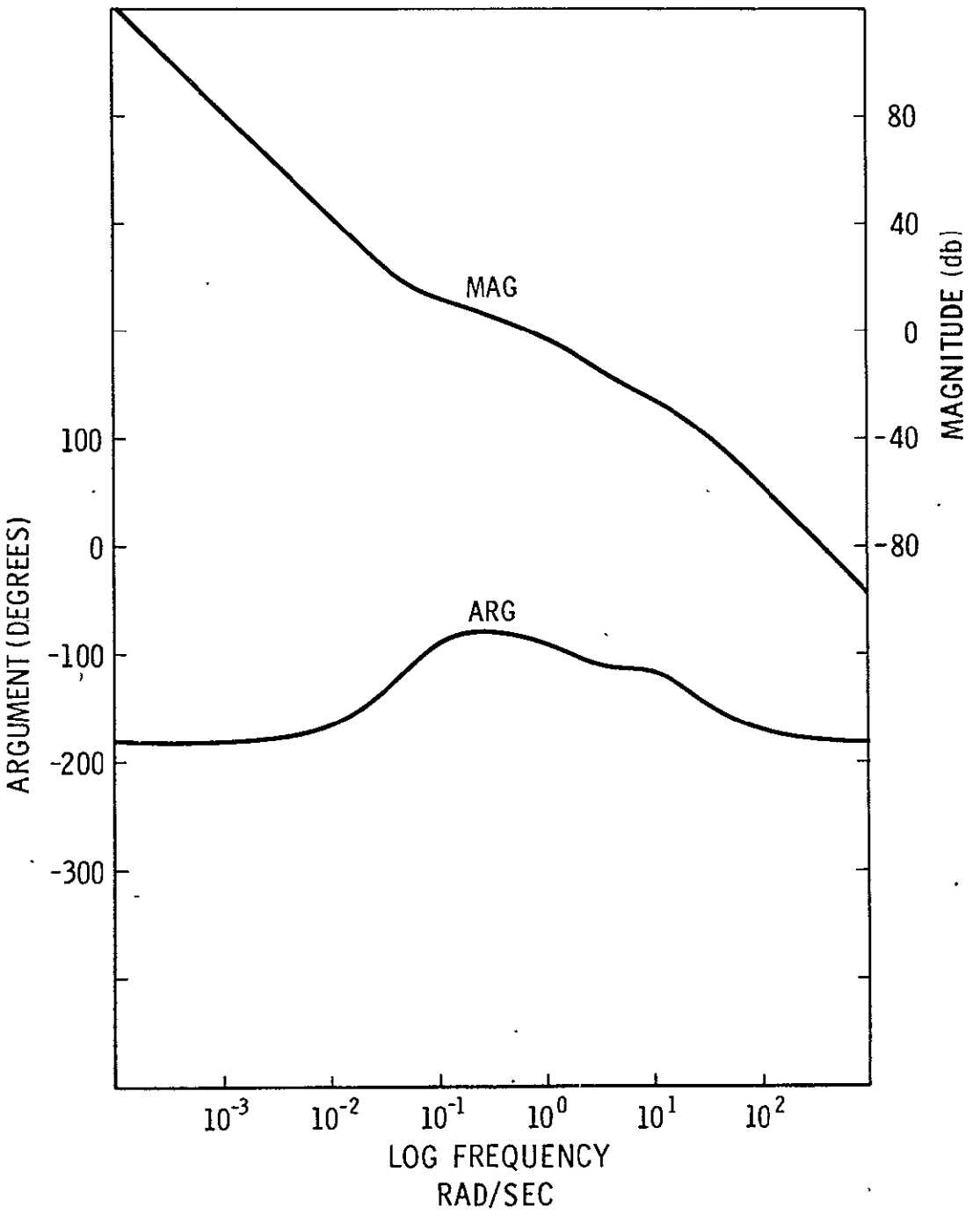

Fig. 5.3.2 Open-loop transfer function of the linearized vertical control system

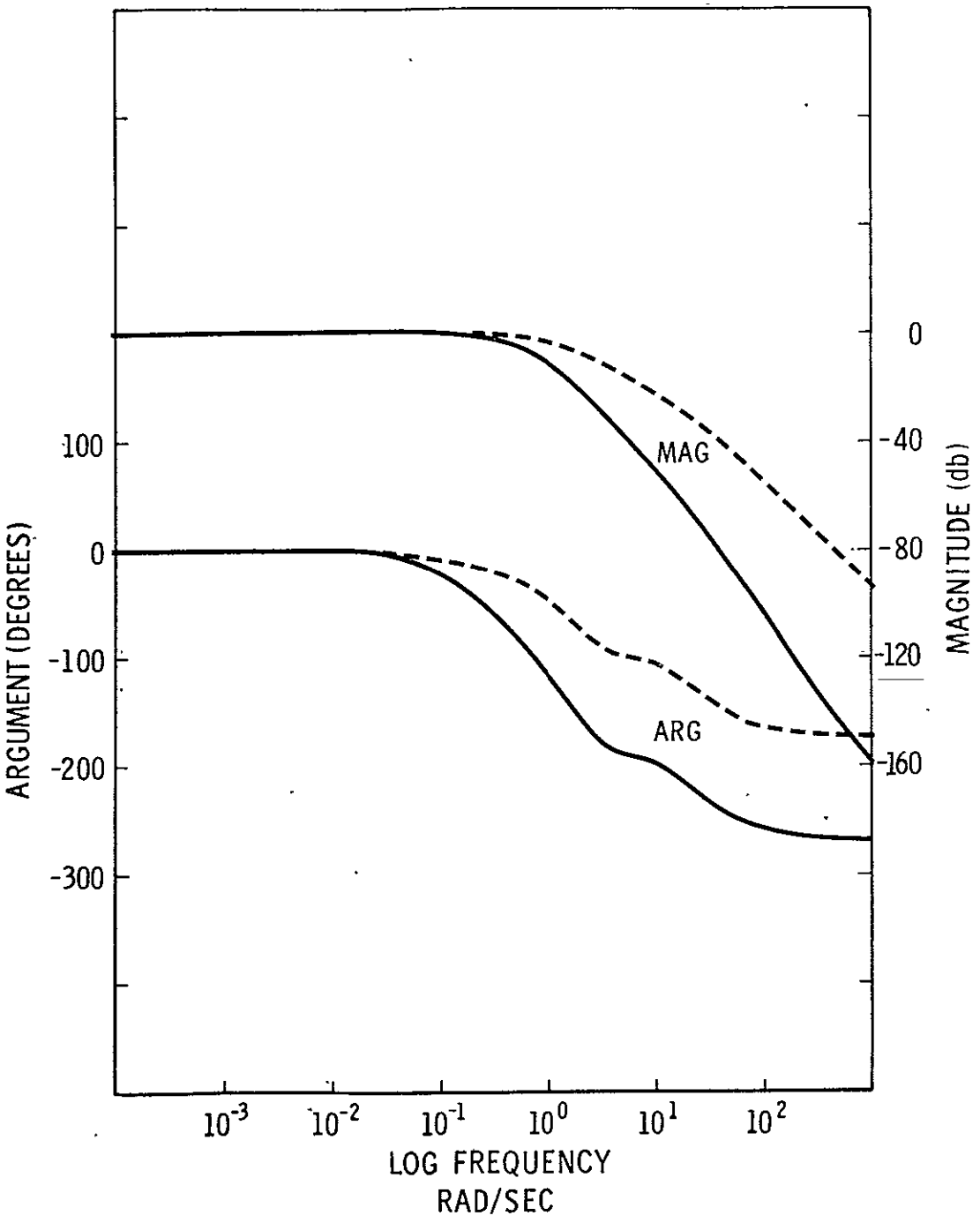

Fig. 5.3.3 Closed-loop frequency response characteristics to errors in position (solid lines) and reference inputs (dotted lines) with feedforward compensation.

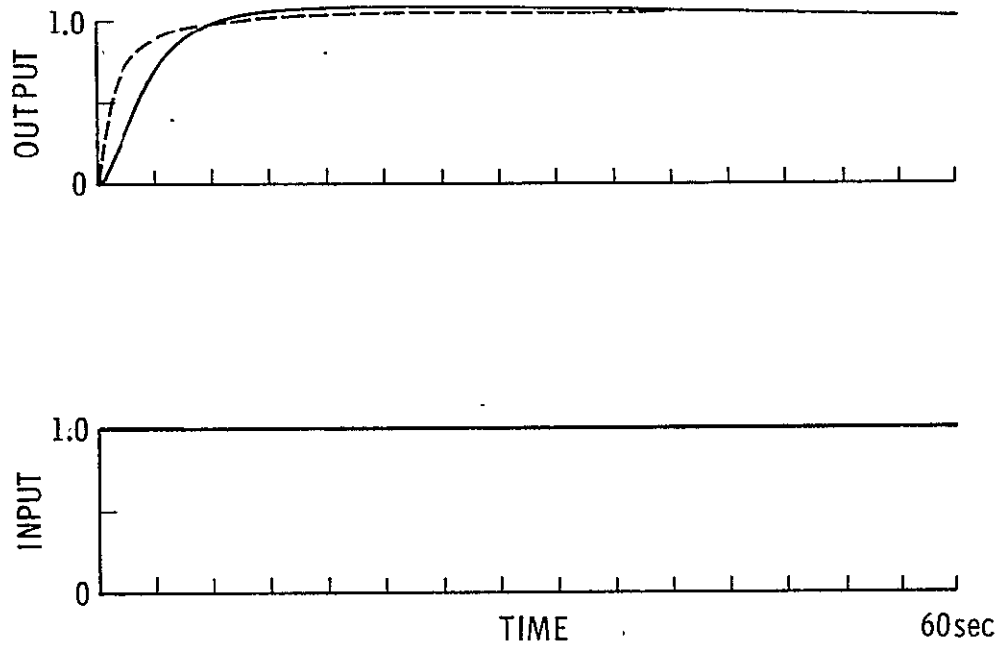

Fig. 5.3.4 Response of the linearized vertical control system to step inputs in position error (solid lines) and reference position (dotted lines) with feedforward compensation.

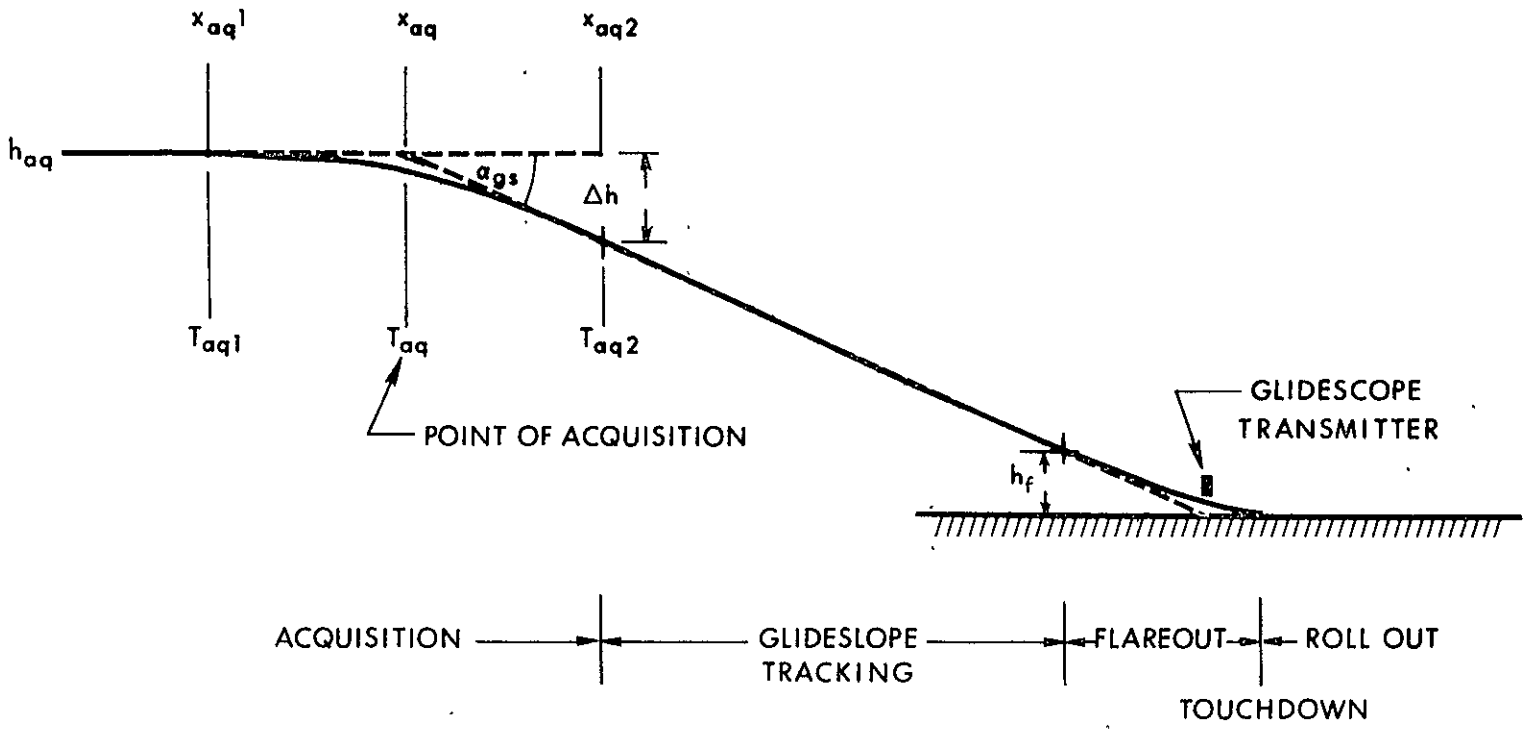

Fig 5.3.5 Nominal vertical trajectory.

$$\Delta h \approx \frac{\ddot{z}_{aq}}{2}\left[\frac{\alpha_{gs}\,\dot{x}}{\ddot{z}_{aq}}\right]^2 \qquad (5.3\text{-}5)$$

$$(x_{aq2} - x_{aq}) \approx \frac{\Delta h}{\alpha_{gs}} \qquad (5.3\text{-}6)$$

$$x_{aq1} - x_{aq2} \approx \frac{\dot{x}^2 \alpha_{gs}}{\ddot{z}_{aq}} \qquad (5.3\text{-}7)$$

where

$\dot{z}_{max}$, $\ddot{z}_{max}$	are the maximum permissible vertical velocity and acceleration
$\ddot{z}_{aq}$	is the desired vertical acceleration during acquisition
α_{gs}	is the glideslope path inclination
$\dot{x}$	is the absolute vehicle velocity in the x direction.
x_{aq}, x_{aq2}, x_{aq1}, Δh	are defined in Fig. 5.3.5

The value of $x_{aq1} - x_{aq}$ is approximately 700 ft. Thus the path transition 1 should be initiated approximately 3 seconds before the termination of acquisition at time T_{aq}. The absolute inequality in equation (5.3-4) provides an acceleration range for overcoming the effects of atmospheric disturbances, inherent tracking errors and vertical position corrections which are gradually applied as shown in section 2.5. Reference trajectory vertical position velocity and acceleration serve as inputs in the complete control system shown in Fig. 5.3.7. As a result of the broad bandwidth of the vertical regulator to reference inputs precise tracking of the desired vertical path is assured.

Initial deviations from the path described above are corrected using the nonlinear trajectory generator shown in Fig. 4.3.2. The errors in vertical position and velocity are introduced as initial conditions on z_p and $\dot{z}_p$. The resultant outputs of the trajectory generator are added to the reference values z_n shown in Fig. 5.3.7. Thus the initial values of z_d and $\dot{z}_d$ will correspond exactly to the estimated values of z and $\dot{z}$. The response characteristics of the perturbation generator are shown in Fig. 5.3.6.

The flareout trajectory may be synthesized in a similar fashion. As a result of the importance of vertical velocity and acceleration regulation it is common

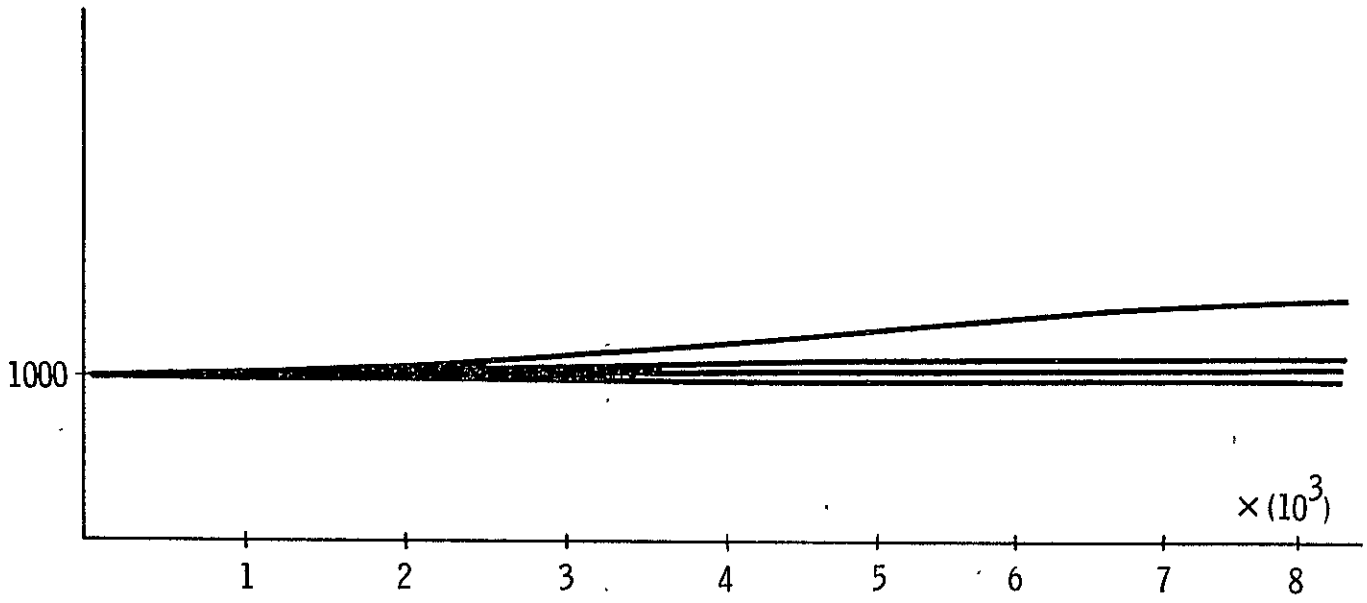

Fig. 5.3.6 Vertical control system responses to desired altitude changes of 0, 50, 100 and 500 ft showing the nonlinear character of the responses generated by the perturbation generator (NTG_z).

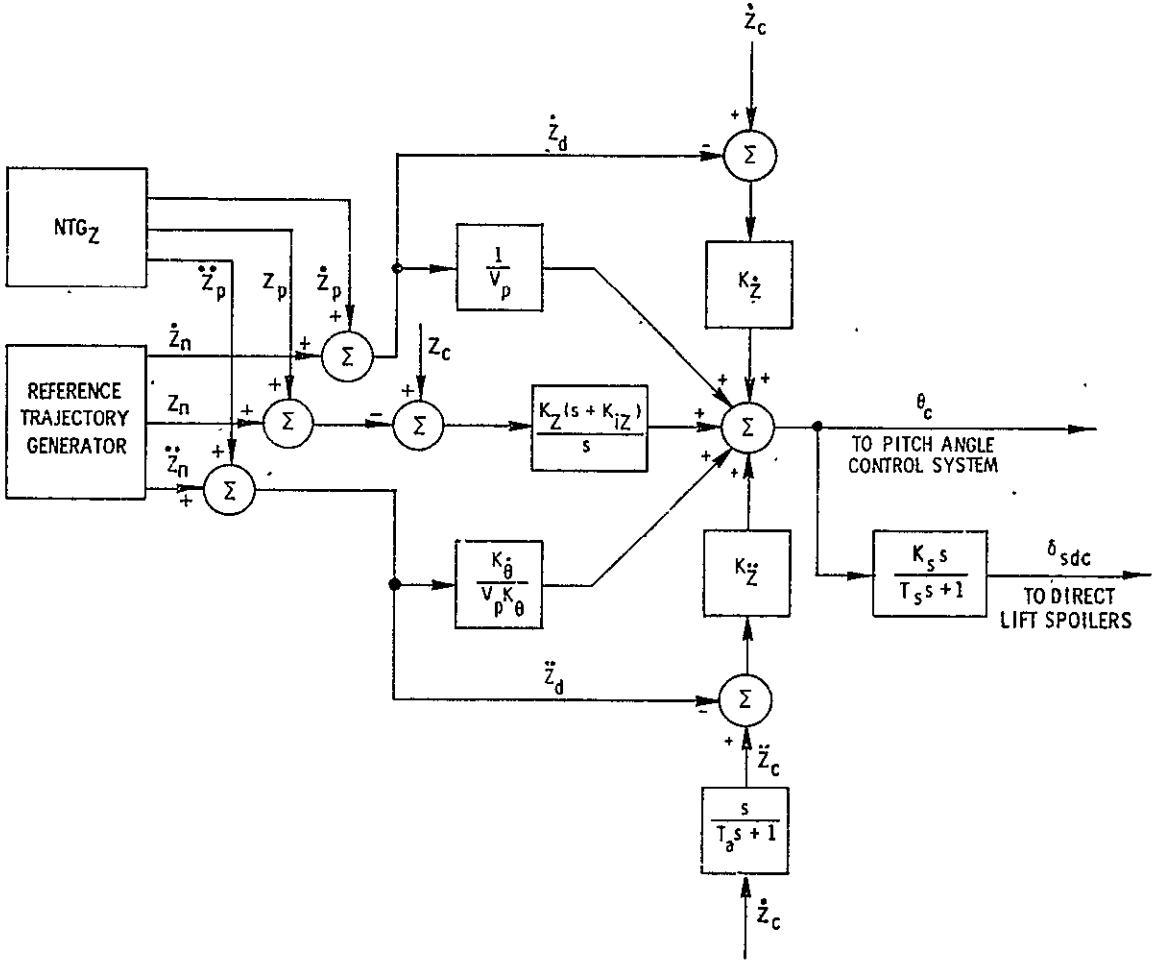

Fig. 5.3.7 Vertical position control system.

to terminate altitude control during flareout. A detailed discussion of flareout may be found in chapter 7 of reference 26

5.4 Summary

Block diagrams and performance data illustrating the current status of the lateral and vertical position control system designs have been presented. The performance of these position controllers will now be compared with the performance of the conventional position control systems presented in appendix C.

CHAPTER 6

A PERFORMANCE COMPARISON OF CONVENTIONAL AND MODERNIZED POSITION CONTROL SYSTEMS

6.1 Introduction

The significance of the innovations which have been introduced in the preceding chapters can only be measured by comparing the performance of the modernized control systems in chapter 5 with a set of conventional control systems. Therefore an effort was directed towards the development of a conventional set of control systems for the SST which reflect the current state of the art in automatic landing system design. The conventional systems have been optimized using the same criteria applied to the inertially stabilized systems (with the exception of effector noise level criteria). The performance achieved by the conventional systems is representative of the capability of systems which provide path control utilizing position information derived from the ILS signal and velocity information based on heading angle for lateral control and beam rate for vertical control. A discussion of conventional path controllers is found in appendix C.

The preceding chapters have shown that significant improvements in performance can be expected in two areas as a result of the application of integrated sensor information and modern control theory. These areas are

1. Reduced sensor noise levels.
2. Decreased sensitivity to environmental disturbances.

The following sections will introduce criteria for measuring the performance increase. The application of these performance measures will demonstrate that significant improvements are indeed achieved by the application of modern techniques.

6.2 Sensitivity to Sensor Noise

The integrated ILS Inertial Sensor described in section 2.4 provides corrected position, velocity and lagged acceleration information. However as a result of the effect of the correction algorithm the velocity and position data is corrupted by ILS noise components superimposed on the corrected position and velocity. The noise components are nonstationary in the statistical sense as indicated in section 2.6. Stationarity may be reestablished by dividing corrected position and velocity by the

appropriate distance to the terminal navigation system antennae. The sensor noise is quantized by comparing $E(\alpha_y^2)$, $E(y_c^2/r_y^2)$ for position and $E(\dot{\alpha}_y^2)$, $E(\dot{y}_c^2/r_y^2)$ for velocity while the vehicle is flown on a path $y = \dot{y} = 0$. The pertinent signals α_y, $\dot{\alpha}_y$, y_c/r_y and $\dot{y}_c/r_y$ are recorded in Fig. 2.7.1. The beam noise is shown in Fig. 2.6.1. The mean square values are tabulated in table 6.2.1. These results show the dramatic reduction in noise amplitude achieved by inertial-ILS integration.

Sensor noise in a conventional automatic landing system is particularly serious as a result of its relatively large amplitude and the absence of any natural attenuating factor such as vehicle inertia which is very effective in the case of atmospheric disturbances. The importance of sensor noise may be inferred from the large perturbations which occur in the vehicle trajectories shown in Figs. 6.2.1 and 6.2.2 as a result of beam noise.

The effects of sensor noise may be quantized by evaluating the statistical averages of the noise generated errors. As a result of the unstationarity indicated above the signals must be divided by the appropriate vehicle to ILS antenna distance. The values of $E(\frac{y}{r_y})$ and $E(\frac{z - z_d}{r_z})$ were generated during simulation and are tabulated in Table 6.2-2. To facilitate the comparison the inertially stabilized variables are identified by the subscript "is" while the conventionally controlled quantities are subscripted "cs".

The reduced sensor noise permits the application of higher feedback gains in the inertially stabilized control system loops compared to the gains in the conventionally stabilized system with similar response characteristics. Increased gains would tend to cancel the effects of sensor noise reduction, however, the important decrease in noise level still leads to a system which is comparatively free from beam noise generated trajectory errors as shown Figs. 6.2.1 and 6.2.2.

6.3 Sensitivity to Random Atmospheric Disturbances

The relationship between controlled output C and disturbance D of the control system in Fig. 3.3.1 is given by

$$\frac{C}{D} = \frac{G_2}{1 + G_0 G_1 G_2 H} \tag{6.3-1}$$

Suppose that a comparison is desired between the responses of two different control systems characterized by variable element transfer functions of the form

$$G_{va} = G_{0a} H_a \tag{6.3.2}$$

$$G_{vb} = G_{0b} H_b \tag{6.3.3}$$

Table 6.2-1

Mean Square Integrated Sensor Parameters

$e(\alpha_y)$ deg	0.224
$e\left(\frac{y_c}{r_y}\right)$ deg	0.100
$e(\dot{\alpha}_y)$ deg	0.224
$e\left(\frac{\dot{y}_c}{r_y}\right)$ deg	0.00511

$$e\left(\frac{y_c}{r_y}\right) \Big/ e(\alpha_y) = 0.446$$

$$e\left(\frac{\dot{y}_c}{r_y}\right) \Big/ e(\dot{\alpha}_y) = 0.022$$

The responses of the control systems to a disturbance D are given by

$$C_a = \frac{G_2}{1 + G_{0a}G_1G_2H_a} D \qquad (6\ 3\text{-}4)$$

$$C_b = \frac{G_2}{1 + G_{0a}G_1G_2H_a} D \qquad (6.3\text{-}5)$$

The ratio of the responses is then

$$\frac{C_a}{C_b} = \frac{1 + G_{0b}G_1G_2H_b}{1 + G_{0a}G_1G_2H_a} = \frac{|1 + G_{ol}|_b}{|1 + G_{ol}|_a} \qquad (6.3\text{-}6)$$

Notice that the ratio of the responses is independent of the characteristics of the disturbance D.

Suppose that C_a/C_b is plotted. Some general conclusions may be derived from the resultant curve.

1. $|C_a/C_b| > 1$ the response magnitude of system b is smaller than that of system a
2. $|C_a/C_b| = 1$ the response magnitudes of the two systems are equal
3. $|C_a/C_b| < 1$ the response magnitude of system a is less than that of system b

As a result it is possible to compare the relative magnitude response characteristics of two systems.

The statistical characteristics of the vehicle response to random disturbances play a key role in system performance valuation. If the spectral characteristics of the noise are assumed to be constant the ratios

$$\frac{e(C_a)}{e(D)}, \quad \frac{e(C_b)}{e(D)} \qquad (6.3\text{-}7)$$

and the relative performance criterion

$$\frac{e(C_a)}{e(C_b)} \qquad (6\ 3\text{-}8)$$

Table 6.2-2

Mean Square Values

Quantity	Inertially Stabilized System	Conventional System
$e(\alpha_y)$ deg	0.114	0.114
$e(\frac{y}{r_y})$ deg	0.038	0.180
$e(\alpha_z)$ deg	0.105	0.105
$e(\frac{z}{r_z})$ deg	0.038	0.120

Derived quantities:

$$e\left(\frac{y_{cs}}{r_y}\right) \Big/ e\left(\frac{y_{is}}{r_y}\right) = 4.7$$

$$e\left(\frac{z_{cs}}{r_z}\right) \Big/ e\left(\frac{z_{is}}{r_z}\right) = 3.2$$

$$E\left(\frac{y_{is}}{r_y}\right) \Big/ E(\alpha_y) = 0.10$$

$$E\left(\frac{y_{cs}}{r_y}\right) \Big/ E(\alpha_y) = 2.50$$

$$E\left(\frac{z_{is}}{r_z}\right) \Big/ E(\alpha_z) = 0.14$$

$$E\left(\frac{z_{cs}}{r_z}\right) \Big/ E(\alpha_z) = 1.30$$

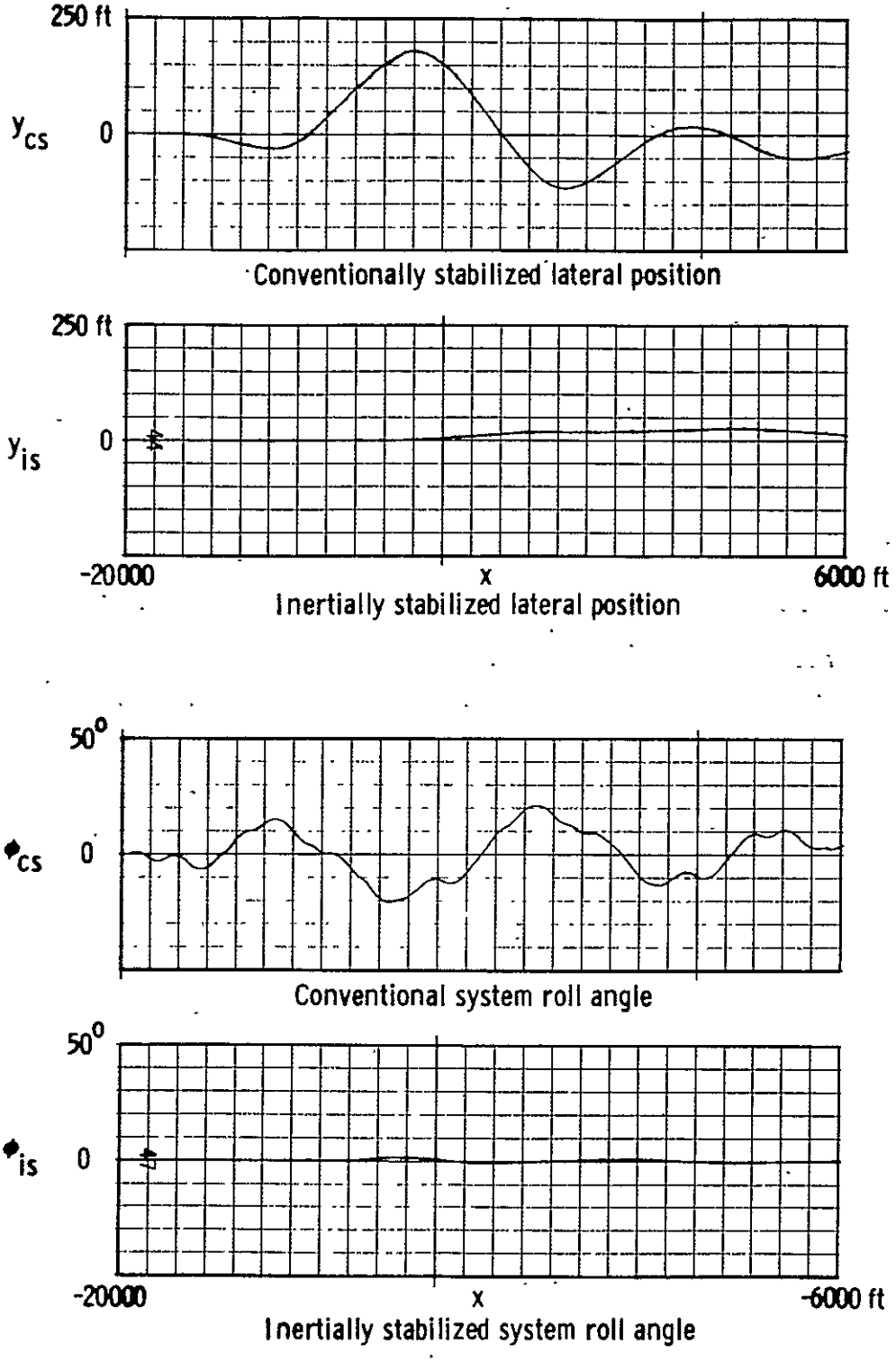

Fig. 6.2.1 Lateral control system response to localizer beam noise.

$\left(e(\alpha_y)\right| = 0.114$ degrees$\Big)$

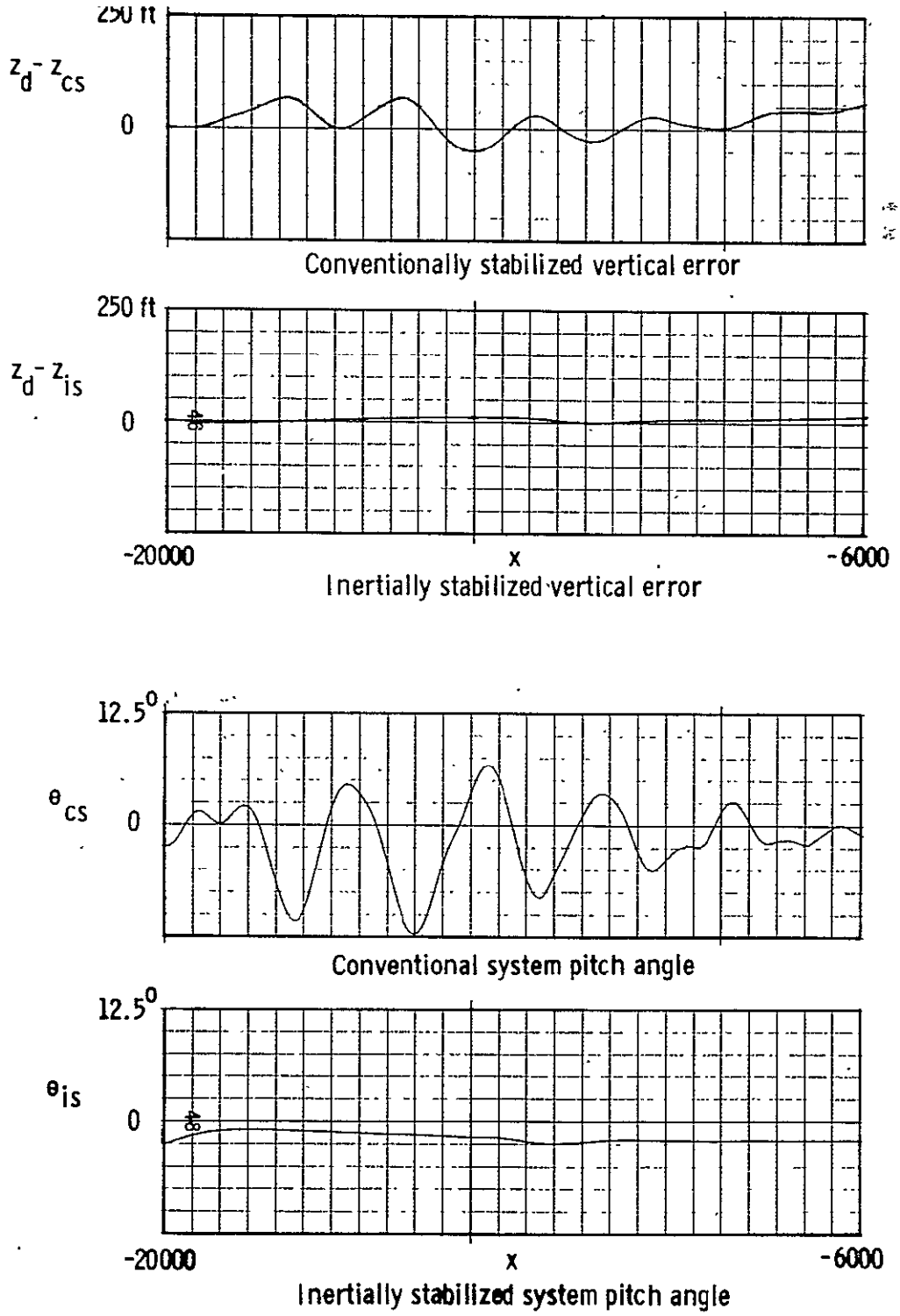

Fig. 6.2.2 Vertical control system response to localizer beam noise. $\left(e(\alpha_z) = 0.121 \text{ degrees}\right)$

may be evaluated. Quantities (6. 3-7) permit the general evaluation of response characteristics once e(D) is defined. The value of (6. 3-8) is very useful for comparing different systems. The calculation of (6. 3-7) and (6. 3-8) is conveniently performed during simulation.

The spectral performance of the lateral position control systems is compared in Fig. 6. 3. 1. A corresponding comparision for the vertical position regulators is shown in Fig. 6. 3. 2. The response of the vehicle to environmental noise (see chapter 8 of reference 26) is illustrated in Figs. 6. 3. 3 to 6. 3. 6. The root mean square values of the controlled variables are summarized in tables 6. 3-1 and 6. 3-2.

6. 4 The Effect of Windshear

Windshear is defined as the derivative of the mean wind velocity with respect to altitude. Shear perpendicular to the runway centerline has a particularly adverse affect on the performance of the lateral position control system. The crosswind w_y is normally countered by the establishment of a crab angle so that

$$v_p \sin\psi = - w_y \tag{6.4-1}$$

Since ψ is small the following approximation is valid

$$v_p \psi \approx - w_y \tag{6.4-2}$$

Windshear is perhaps the most serious disturbance encountered by the lateral position control system. In order to counteract the change in wind velocity with altitide, equation (6. 4-2) must be satisfied at all times. This implies that

$$\dot{\psi} \approx - \frac{\dot{w}_y}{v_p} \tag{6.4-3}$$

The heading rate is related to the roll angle φ by the relation

$$\dot{\psi} \approx \frac{g\varphi}{v_p} \tag{6.4-4}$$

Thus the required roll angle is given by

$$\varphi \approx \frac{\dot{w}_y}{g} \tag{6.4-5}$$

Since $\dot{y}$ and $\ddot{y}$ are small during the localizer tracking phase

$$\varphi \approx K_y \left[\frac{s + K_{iy}}{s}\right] y \tag{6.4-6}$$

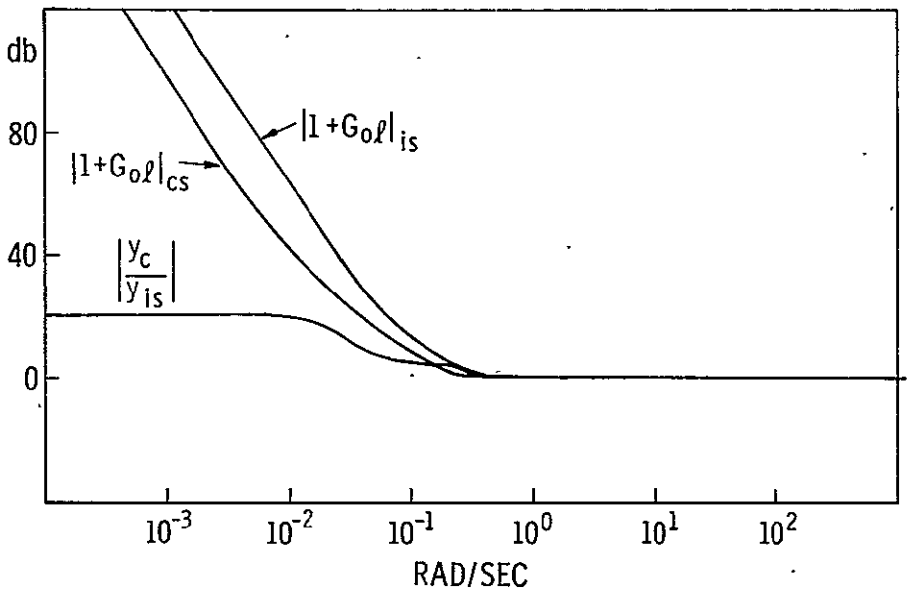

Fig. 6.3.1 Spectral performance of the lateral control systems.

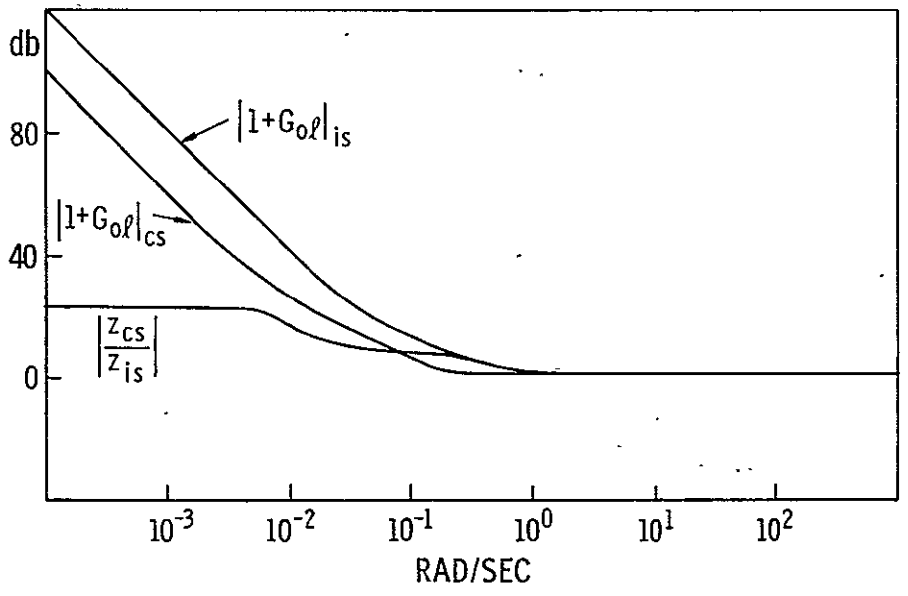

Fig. 6.3.2 Spectral performance of the vertical control systems.

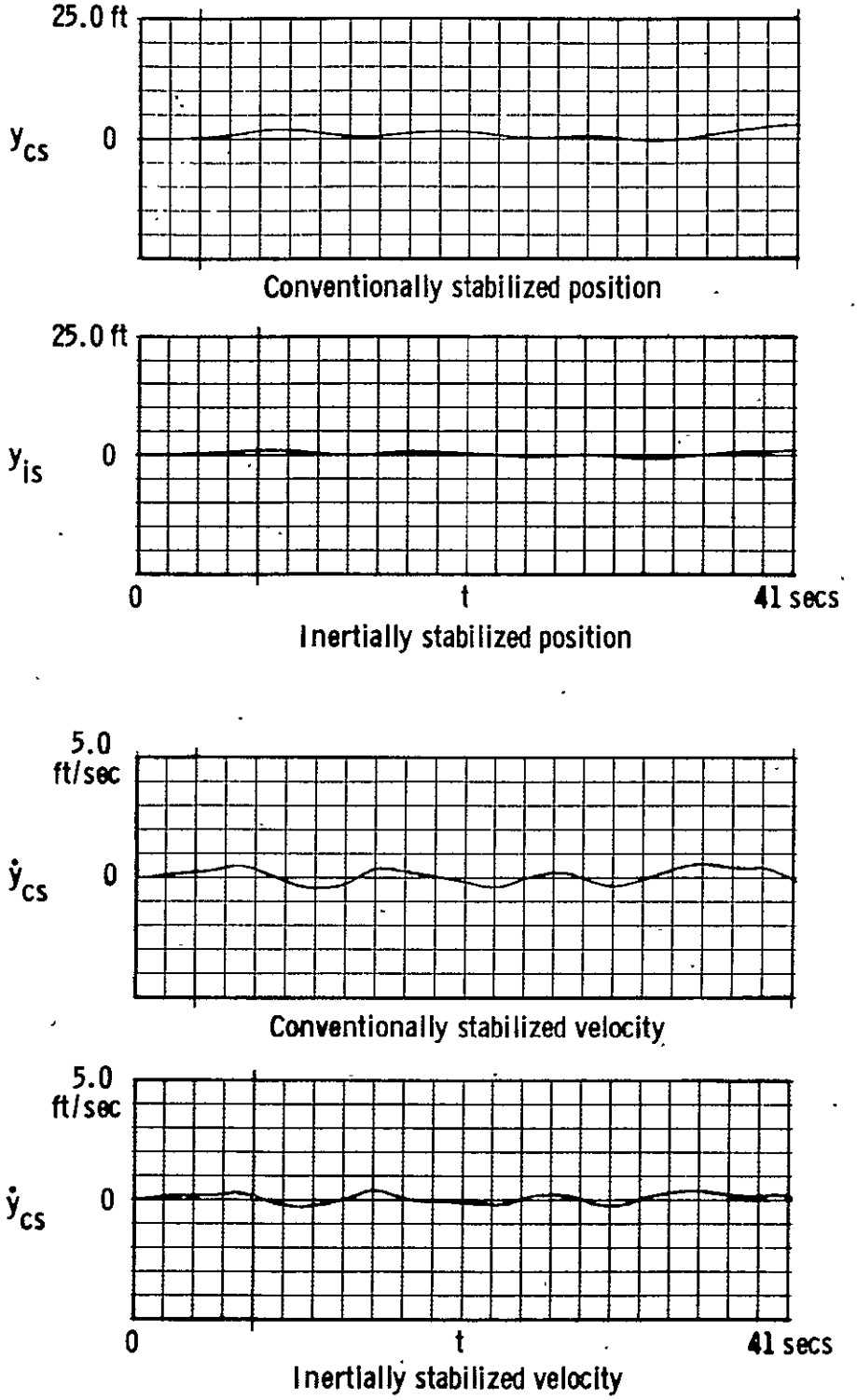

Fig. 6.3.3 Lateral position control system responses to aerodynamic disturbance.
$\left(e(w_n) = 1.47 \text{ ft/sec}\right)$

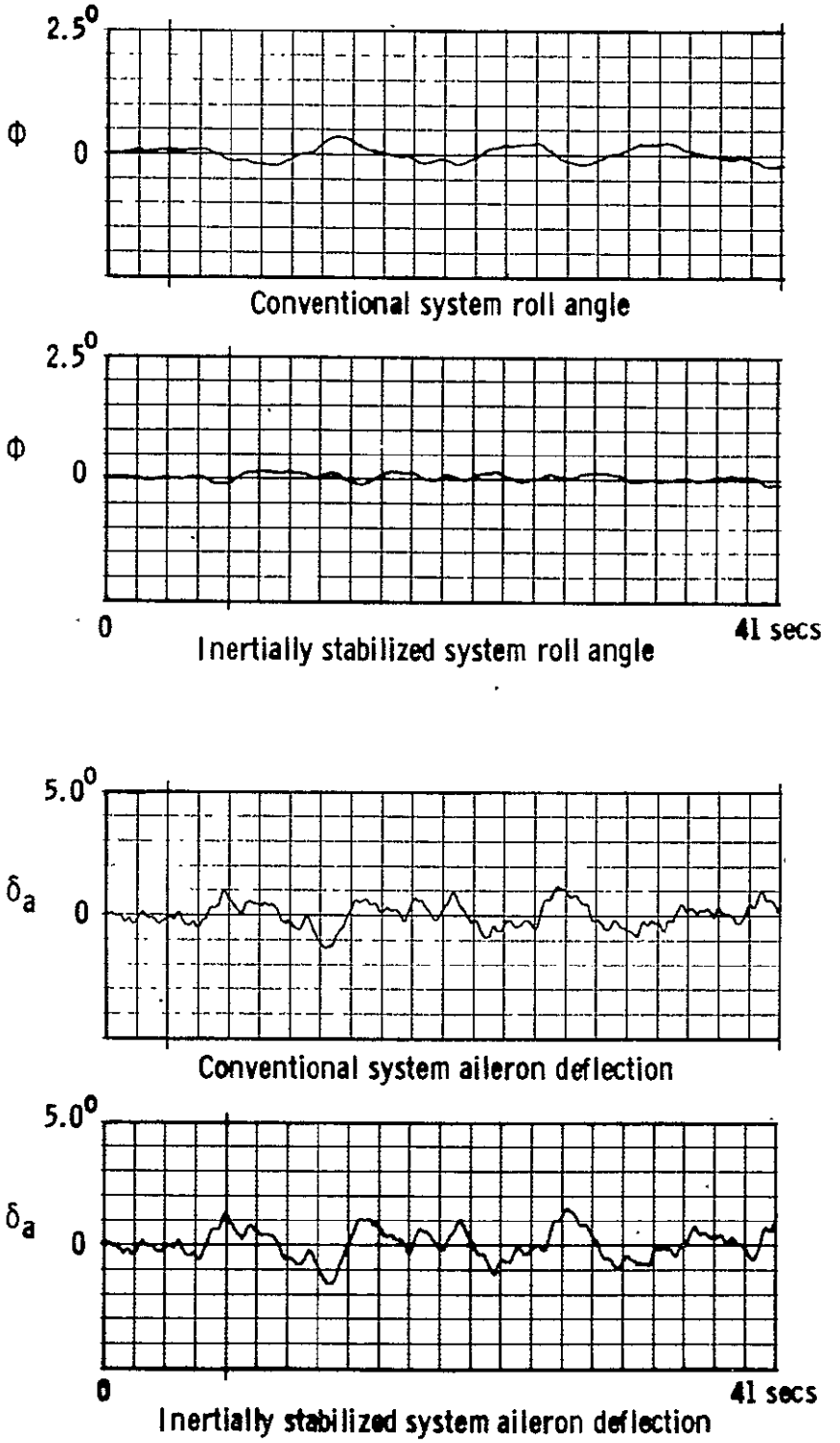

Fig. 6.3.4 Lateral position control system responses to aerodynamic disturbance. $\left(e(w_n) = 1.47 \text{ ft/sec}\right)$

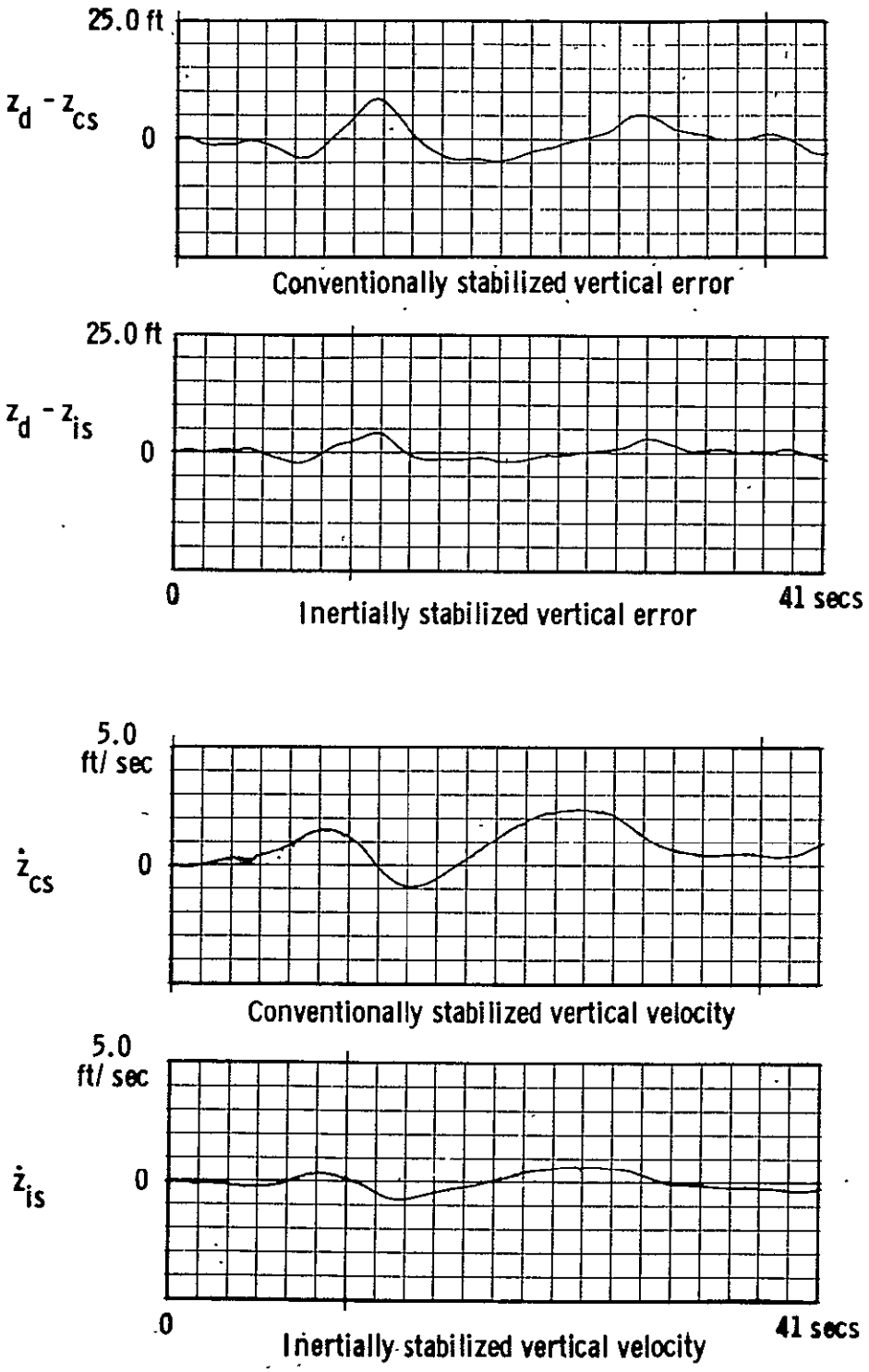

Fig. 6.3.5 Vertical position control system responses in a turbulent environment $\left(\sigma_e(w_n) = 1.46 \text{ ft/sec}\right)$

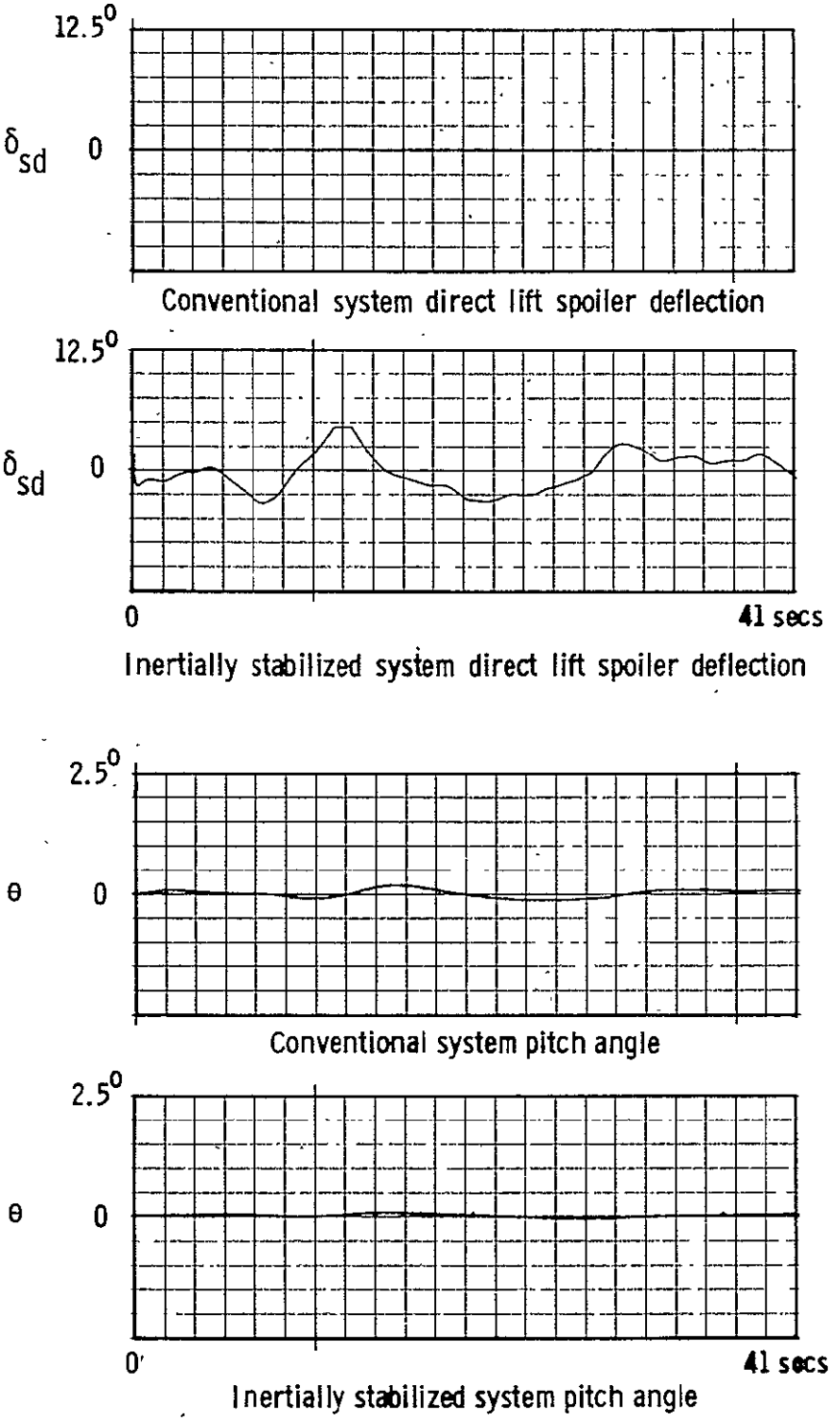

Fig. 6.3.6 Vertical position control system responses in a turbulent environment. $\left(\sigma(w_n) = 1.46 \text{ ft/sec}\right)$

Table 6.3-1

Root Mean Square Lateral Control System Parameter Values From Aerodynamic Noise Tests

Quantity	Inertially Stabilized System	Conventional
$e(w_n)$ ft/sec	2.15	2.15
$e(y)$ ft	0.494	1.11
$e(\dot{y})$ ft/sec	0.192	0.297
$e(\ddot{y})$ ft/sec^2	0.132	0.162
$e(\delta a)$ deg	0.607	0.492

Derived quantities:

$$\frac{e(y_{cs})}{e(y_{is})} = 2.25$$

$$\frac{E(y_{is})}{E(w_n)} = 0.053 \text{ sec}^2$$

$$\frac{E(y_{cs})}{E(w_n)} = 0.266 \text{ sec}^2$$

Table 6.3-2

Root Mean Square Vertical Control System Parameter Values From Aerodynamic Noise Tests

Quantity	Inertially Stabilized System	Conventional System
$e(\dot{w}_n)$ ft/sec	2.22	2.22
$e(e_z)$ ft	3.77	11.81
$e(\dot{z})$ ft/sec	1.00	1.70
$e(\delta e)$ deg	0.656	1.05
$e(\delta_{sd})$ deg	2.25	——

Derived quantities:

$$\frac{e(e_{zcs})}{e(e_{zis})} = 3.14$$

$$\frac{E(e_{zis})}{E(\dot{w}_n)} = 2.87 \text{ sec}^2$$

$$\frac{E(e_{zcs})}{E(\dot{w}_n)} = 28.3 \text{ sec}^2$$

multiplying both sides by s and transposing

$$y \approx \frac{s\varphi}{K_y K_{iy} \left(\frac{1}{K_{iy}} s + 1 \right)} \tag{6.4-7}$$

It is apparent that the steady state value of y will be zero. The time required for the value of y to decay to 0.372 of its initial value is equal to K_{iy}^{-1}. The maximum perturbation in y due to windshear is bounded. An upper bound is given by

$$|y|_{max} \leq \frac{|\dot{w}_y|}{gK_y} \tag{6.4-8}$$

if the response to a step change in wind acceleration is overdamped. Thus the performances of two lateral control systems to windshear are conveniently compared by evaluating (6.4-8) and K_{iy}^{-1}. The results of this comparision are contained in table 6.4-1. The responses of conventionally and inertially stabilized systems are compared in Fig. 6.4.1.

Windshear in the x direction $\dot{w}_x$ produces errors in vertical position in similar fashion. If the perturbation in angle of attack α is assumed to be small and the airspeed is constant the flight path inclination may be approximated by

$$\gamma = \frac{v_p \theta}{v_p + w_x} \tag{6.4 9}$$

The corresponding pitch angle θ is given by

$$\theta = \frac{\gamma(v_p + w_x)}{v_p} \tag{6.4-10}$$

The path inclination angle γ is determined prior to flareout by the constant elevation angle of the glideslope reference plane. Thus the value of θ is constant in the absence of windshear. In the modernized control system the constant component of θ is generated explicitly and applied as a control input as shown in equation 3.2-6. If the acceleration of the air mass in the x direction is not zero the pitch rate must obey the relation

$$\dot{\theta} = \frac{\gamma \dot{w}_x}{v_p} \tag{6.4-11}$$

Suppose that $\dot{w}_x$ is constant. Then the pitch command must contain a component which changes linearly with time in order to satisfy equation (6.4-11). In the

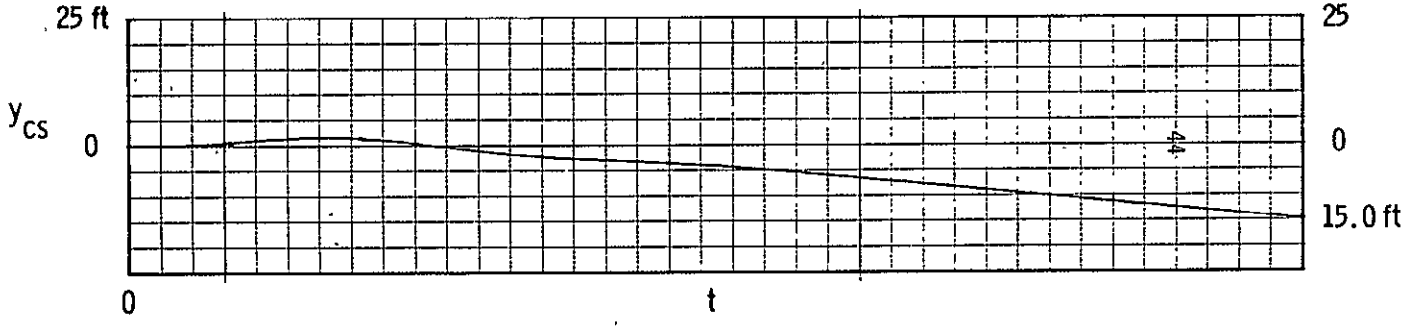

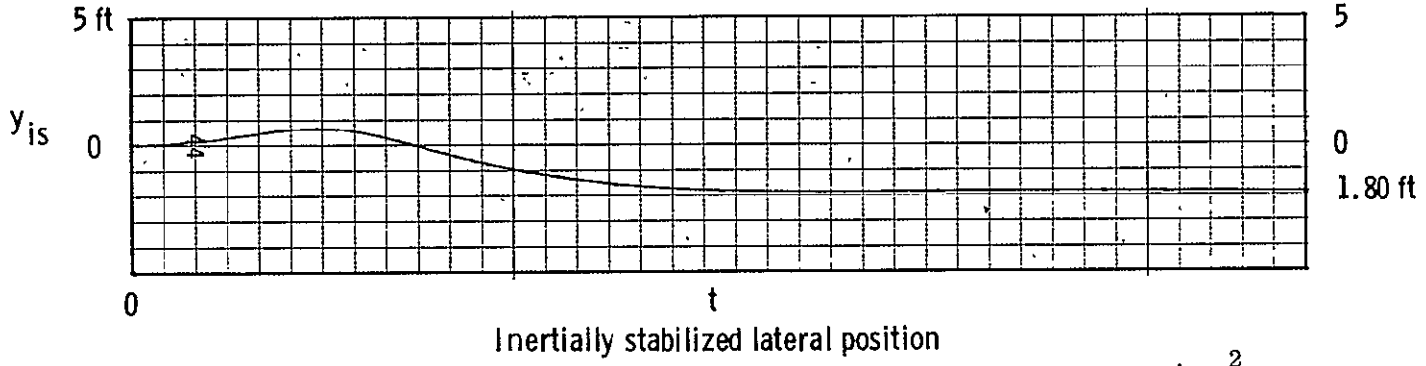

Fig. 6.4.1 Vehicle responses to a step acceleration in air mass of 0.25 ft/sec^2 which could result from windshear near the earth's surface. Note the different scales. The positive y perturbation is due to a minute initial lateral drift velocity. The steady state error is due to roll control system characteristics which are ignored in the linear analysis.

absence of integral compensation the varying component of θ_d would be produced by a corresponding change in vertical error. With integral compensation the error is bounded and is given by the expression

$$(z - z_d) = - \frac{\gamma \dot{w}_x}{v_p K_z K_{iz}} \qquad (6.4\text{-}12)$$

The vertical windshear errors of the conventional and modernized control systems are conveniently compared by computing $(z - z_d/\dot{w}_x)$ as shown in table 6.4.1.

6.5 Touchdown Dispersion

A most important performance index, measures the error between the desired and actual touchdown points. Touchdown errors result from sensor errors (due to noise and inaccuracies) and aerodynamic disturbances. The variation in touchdown in conveniently investigated by considering the fluctuations in the lateral and longitudinal touchdown components independently.

6.6 Lateral Touchdown Dispersion

The variation in lateral touchdown point presents the simpler analytical problem. The errors may be divided into two components, a deviation due to beam and aerodynamic noise effects and a contribution due to windshear. If the various components are uncorrelated the mean square error may be expressed in the form

$$E(e_{ytd}) = R\left(\frac{y}{r_y}, \alpha_y\right) E(\alpha_y) r_{ytd}^2 + R(y, \sigma) E(w_n) + R(y, \dot{w}_y) E(\dot{w}_y) \qquad (6.6\text{-}1)$$

where e_{ytd} is the lateral position at touchdown

r_{ytd} is the distance from the localizer antenna at touchdown

$R(u, v) = E(u)/E(v)$

w_n is the stochasitc component of wind velocity.

The first term on the right hand side of equation (6.6-1) is the mean square value of the lateral position error resulting from localizer beam noise. The second term reflects the effect of turbulence in the atmospheric environment while the effects of windshear are introduced by the last term.

A statistical windshear model was formulated assuming that the wind gradient is constant between h = 200 and h = 0 ft altitude. The mean square value of the deviation in y resulting from windshear may then be inferred from Fig. 6.4-1.

$$R(y, \dot{w}_y) = \frac{9.0}{0.0625} = 144.0 \text{ sec}^4 \quad \text{conventionally stabilized system}$$

$$\frac{1.0}{0.0625} = 16.0 \text{ sec}^4 \quad \text{inertially stabilized system}$$

In order to present the preceding results in a clear fashion the value of $E(\dot{w}_y)$ is assumed to be related to $E(w_n)$ by an expression of the form

$$E(\dot{w}_y) = k_{\dot{w}y} E(w_n) \tag{6.6-2}$$

The value of $k_{\dot{w}y}$ was set equal to 1.000. Equation (6.6-1) may then be rewritten

$$E(e_{ytd}) = R\left(\frac{y}{r_y}, \alpha_y\right)\left[r_{ytd}^2 E(\alpha_y)\right] + \left[R(y, \sigma) + k_{\dot{w}y} R(y, \dot{w}_y)\right] E(w_n) \tag{6.6-3}$$

If it is assumed that the mean square value $E(\alpha_y)$ of the localizer noise is 0.10 degrees^2 (reference 2) equation (6.6-3) may be plotted as a function of $E(w_n)$ using the coefficient values in tables 6.2-2 and 6.3-1. Curves illustrating the variation in $E(e_{ytd})$ as a function of w_n^2 are shown in Fig. 6.6.1.

6.7 Longitudinal Touchdown Dispersion

The analysis of longitudinal touchdown variation presents a more difficult problem. Touchdown occurs at the termination of the flareout maneuver which is generally initiated by sensing elevation above the runway using a radio altimeter. To simplify this investigation it shall be assumed that the error in longitudinal contact point is entirely due to the fluctuations in vertical path as a result glide-slope beam noise, aerodynamic disturbances and radio altimeter error. Assuming that the beam noise, atmospheric disturbances and altimeter error are uncorrelated and the system response to the disturbances is linear the mean square value of the longitudinal contact error may be written in the form

$$E(e_{xtd}^2) = R\left(\frac{z}{r_z}, \alpha_z\right) E(\alpha_z)\, r_f^2\, \alpha_{gs}^{-2} + \left[R(z, \sigma) E(w_n) + \dot{R}_{z\dot{w}x} E(\dot{w}_x)\right] \alpha_{gs}^{-2} + E(e_{hf})\, \dot{z}_{td}^{-2}\, v_p^2 \tag{6.7-1}$$

Table 6. 4-1

Windshear Comparisons

Quantity	Modernized System	Conventional System
$(gK_y)^{-1}$ sec^2	22.2	87.0
K_{iy}^{-1} sec	20.0	200.0
$\frac{\gamma}{V_p K_z K_{iz}}$ sec^2	0.873	0.057

Derived quantities:

$$\frac{(gK_y)_{is}}{(gK_y)_{cs}} = 3.92$$

$$\frac{(K_{iy})_{is}}{(K_{iy})_{cs}} = 10.0$$

$$\frac{(K_z K_{iz})_{is}}{(K_z K_{iz})_{cs}} = 15.3$$

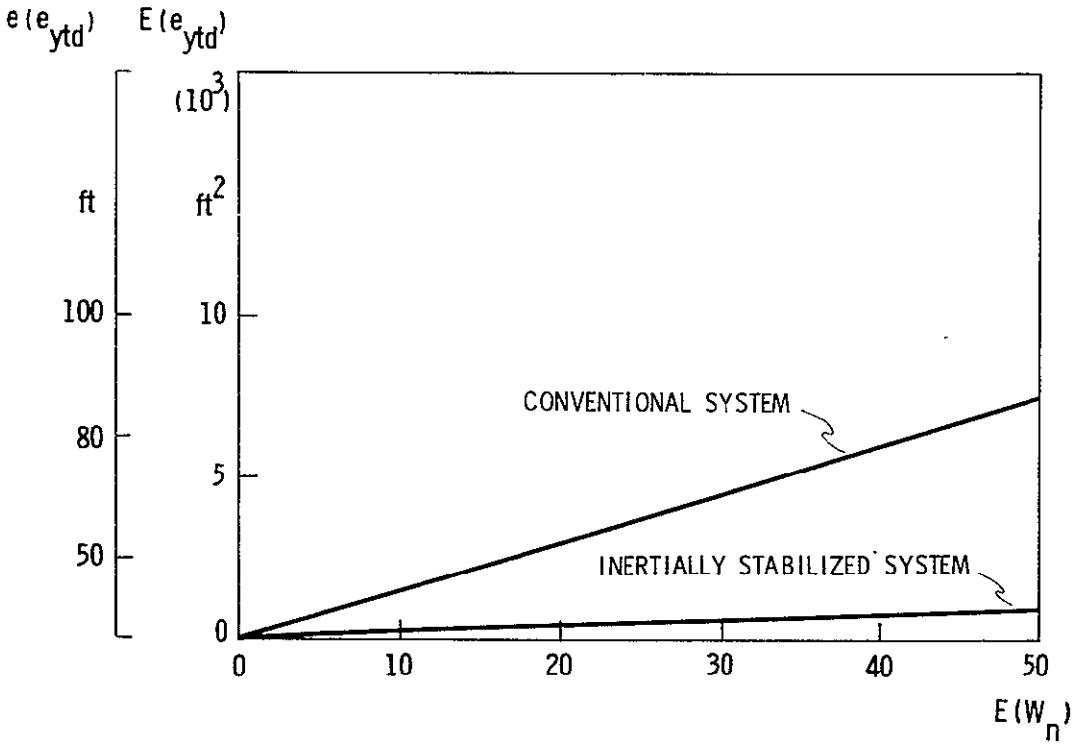

Fig. 6.6.1 Lateral touchdown mean square error versus mean square turbulence intensity.

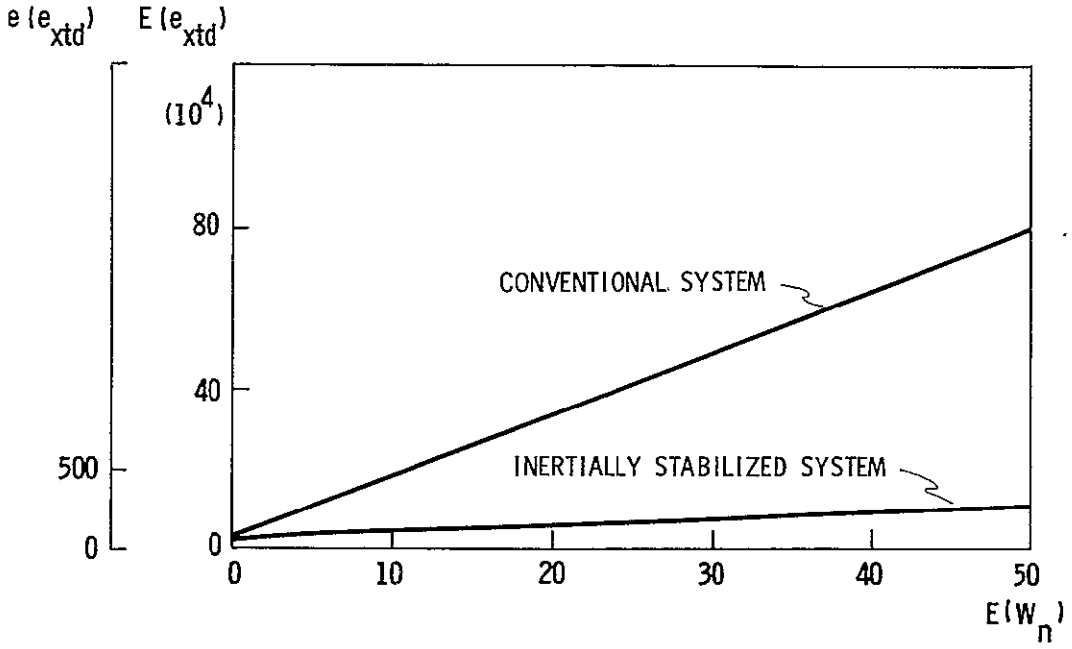

Fig. 6.7.1 Longitudinal touchdown mean square error versus mean square turbulence intensity.

where

e_{xtd} is the difference between the desired and actual touchdown points along the runway.

r_f is the distance from the glideslope antenna at the initiation of flareout.

α_{gs} is the glidepath angle.

w_n is the stochastic component of wind velocity.

e_{hf} is the radio altimeter error.

$\dot{z}_{td}$ is the nominal vertical velocity at touchdown.

The first term on the right hand side of (6. 7-1) is the mean square error resulting from glideslope beam noise; the second term is the contribution due to atmospheric disturbances while the last term represents the contribution as a result of altimeter error.

The properties of equation (6. 7-1) may be illustrated by setting

$$\alpha_{gs} = 0.0437 \text{ radians}$$

$$r_f = 1500 \text{ ft}$$

$$E(e^2_{hf}) = 4.0 \text{ ft}^2$$

$$\dot{z}_{td}^2 = 6.25 \text{ ft}^2/\text{sec}^2$$

The above values may then be used to generate values of 6. 7-1 as a function of w_n which are then summarized in Fig. 6. 7. 1.

6. 8 Root Mean Square Touchdown Area

The results presented in the preceding sections may be applied to illustrate the touchdown performance of an automatic landing system in a graphic fashion. The root mean square touchdown area is defined by a width equal to $2e(e_{ytd})$ and a length equal to $2e(e_{xtd})$. These areas may be drawn using the plotted data in Figs. 6. 6. 1 and 6. 7. 1 as shown in Fig. 6. 8. 1.

Assuming that the deviations in touchdown point are normally distributed the following probability relationships may be written

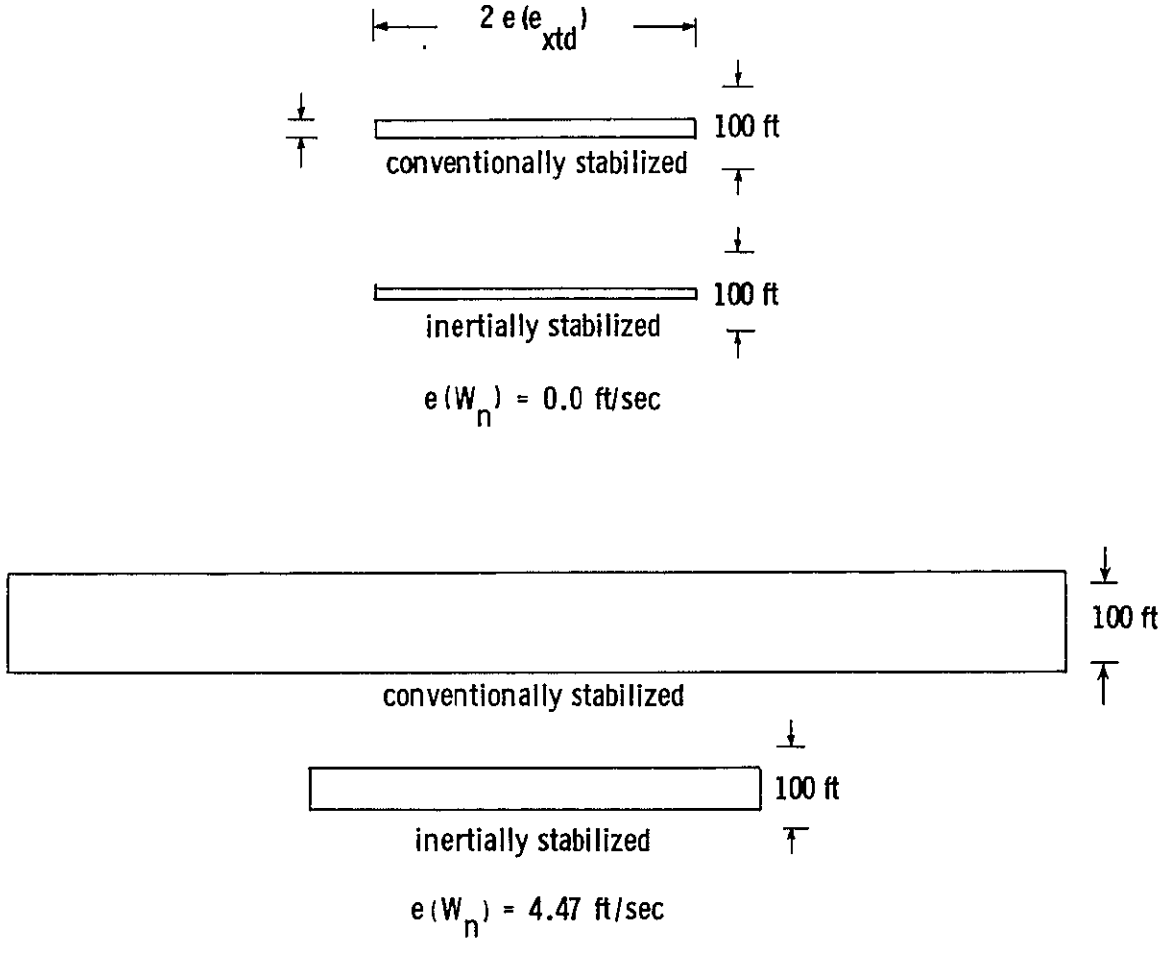

Fig. 6.8.1 Root mean square touchdown areas for various values of mean square turbulence.

$$P\left(e_{ytd} \leq e(e_{ytd})\right) = 0.68$$

$$P\left(e_{ytd} \leq 2.00e(e_{ytd})\right) = 0.96$$

$$P\left(e_{ytd} \leq 2.58e(e_{ytd})\right) = 0.99 \qquad (6.8\text{-}1)$$

Thus, we are assured that an aircraft performing landings in a stationary (in the statistical sense) environment will land within the root mean square area 68% of the time. The maximum permissible deviations in $\dot{y}$ and x at touchdown are nominally defined as 50 ft and 1000 ft, respectively. In the example presented in sections 6.6 and 6.7 lateral error is the critical parameter. The modernized control system performs 99% of the time with root mean square turbulence velocities in excess of 10.0 ft/sec. The conventional system, on the other hand, fails to achieve a satisfactory landing 32% of the time at a modest value of $e(w_n) = 4.0$.

6.9 Summary and Conclusions

The preceding sections of chapter 6 provide the basis for some general conclusions concerning the development status of the NASA/MIT automatic landing system. The lateral control system will be discussed first followed by the vertical position regulator.

If the results in sections 6.2, 6.4 and 6.6 are studied, it is apparent that the most important factors which lead to large lateral touchdown dispersions in a conventional lateral control system are

1. High levels of ILS induced noise in the vehicle position and velocity data.
2. Sensitivity to windshear.

By integrating inertial navigator and ILS information a very significant reduction in measured position and velocity noise components was achieved. As a result the root mean square perturbations in lateral trajectory due to beam noise are reduced by a factor of 4.73 as shown in table 6.2.1.

The lag-free nature and low noise characteristics of the corrected inertial lateral position and velocity data added to the availability of lagged lateral acceleration information provided the basis for a new lateral position control system design which features important increases in the position feedback gain K_y, the velocity gain $K_{\dot{y}}$, the integral compensator break frequency K_{iy} and a new loop closure on lagged inertial acceleration through a gain $K_{\ddot{y}}$. By carefully tailoring

the desired trajectory of the vehicle to prevent effector and/or flight envelope saturation, maximum advantage can be derived from the increased open loop gains and response bandwidth to minimize the effects of atmospheric disturbances Satisfactory lateral reference trajectories are currently synthesized using the nonlinear trajectory generation techniques presented in chapter 6 of reference 26. The combination of increased gains and nonlinear trajectory generation resulted in an approximately 2 times reduction in the root mean square amplitude of the lateral path perturbations due to atmospheric turbulence. The most important reduction occurred in the lateral perturbation at touchdown from windshear. The inertially stabilized system reduced the effect of windshear by a factor of 12.

In section 6. 7 it was shown that the dispersion in the location of the touchdown point along the runway centerline is primarily caused by

1. Errors in the altitude at which the flareout maneuver is initiated.
2. Deviations in the vertical trajectory as a result of atmospheric disturbances.

A reduction in the first source of error is limited by the accuracy of the instrument (usually a radar altimeter) which provides the automatic landing system with runway surface referenced elevation data during the terminal phases of the landing. This error may be reduced by improved instrument accuracy and/or inertial system-altimeter integration using the techniques presented in chapter 2. The work to date has not covered this facet of the landing problem. The effects of the second dispersion generating factor, atmospheric turbulence, may be reduced by increasing the open loop gain and bandwidth of the vertical position control system. The gain and bandwidth of the conventional system are limited by the noise levels in the measured vertical position and velocity data and the inherent physical characteristics of the vehicle. The first limitation is circumvented by combining inertial and ILS information. Sensor integration reduces the root mean square noise in position and velocity by 2 and 45 times respectively (table 2. 6-1). By applying auxiliary direct lift control the limitations imposed by vehicle characteristics are eased and the vertical control system open loop gain and bandwidth may be improved. The root mean square vertical deviations that result from stochastic components in the atmosphere are reduced by a factor of 3 by the improved open loop gain and bandwidth.

The combined improvements in the vertical and lateral position control systems result in a landing system which is able to perform successfully in a much broader range of ambient turbulence and windshear as shown in section 6. 8.

CHAPTER 7

AREAS FOR FURTHER INVESTIGATION

7.1 Areas for Further Investigation

In the course of the program summarized in this report an attempt has been made to elucidate and solve some of the basic problems associated with automatic landing systems. The results presented in the preceding chapter indicate that some major improvements are feasible if inertial and terminal ILS navigation system data is properly combined and the control system design is revised to reflect the improved character of this information In addition to these concrete results many significant problems have been revealed which could not be fully investigated as a result of time and funding limitations. Among the tasks particularly appropriate for future investigation are:

1. Investigate the affect of inertial system quality on landing system performance. Determine the lower limits on inertial system accuracy for satisfactory landing system performance.
2. Study the practical problems introduced by disparities between the locations of the vehicle center of gravity and the inertial navigator.
3. Apply inertial-ILS-DME* filtering techniques to generate improved information along the glidepath.
4. Utilize inertial system data to detect terminal navigation system failure and/or interference caused by overflight.
5. Investigate the feasibility of extrapolating the reference glidepath using inertial navigator information during periods of terminal navigation system failure and/or interference.
6. Study the application of longitudinal direct force generators (dive brakes) to improve the performance of the automatic throttle.
7. Redesign the automatic throttle to incorporate inertial acceleration data.
8. Improve the lateral control system by the application of side force generating effectors.

*DME is not available at some facilities.

9. Optimize the landing abort procedure using variational techniques and design a landing abort control system.

10. Refine the flareout control system design presented in reference 26 to include the latest improvements in vertical control system structure and inertial-radio altimeter data processing.

11. Synthesize an optimal "decrab" maneuver trajectory using mathematical optimization techniques and redesign the decrab control system.

12. Model the vehicle in the rollout configuration and design a rollout control system.

13. Investigate the application of inertial information to monitor and control aircraft takeoff and takeoff abort.

14. Perform flight tests to validate the results obtained using the simulation.

The availability of an on board inertial navigation system offers unique possibilities for flight testing new automatic landing system concepts. Landing system tests have historically been performed at low altitudes utilizing installed ILS facilities. As a result a certain degree of danger has existed in the initial test phases as a result of proximity to the ground. Since an inertial system provides an absolute geographic reference a hypothetical runway may be defined at an elevation above ground. The geometry of the runway, an instrument landing system, DME etc. may be defined. The location of the test vehicle relative to the imaginary airport is then defined by comparing the aircraft's inertial position to the geometrical coordinates of the runway complex. Computations may also be performed to generate the signals received from the simulated ILS and DME (including ILS and DME noise). Thus the aircraft could perform all the phases of an automatic landing at a safe altitude. The effects of turbulence are easily evaluated by locating the runway complex in an unsteady atmospheric environment. Simulation of the effects of wind or windshear is easily accomplished by translating the geographic coordinates of the hypothetical airport. The absence of ground effect and touchdown dynamics would contribute the primary source of error. Once the landing system is operating satisfactorily at high altitudes low altitude tests could be performed using actual ILS and DME information.

APPENDIX A

SPOILER TRANSFER FUNCTION

Derivation of the transfer function relating angle of attack to direct lift spoiler deflection follows

The equations relating α and q to the elevon deflection δ_e and the direct lift spoiler deflection δ_{sd} are given in reference 26.

$$C_{\dot{\alpha}}\dot{\alpha} = C_{\dot{\alpha}u} + C_{\dot{\alpha}q}q + C_{\dot{\alpha}\theta}\theta + C_{\dot{\alpha}\alpha}\alpha + C_{\dot{\alpha}x}\delta_e + C_{\dot{\alpha}\delta_{sd}}\delta_{sd} \quad \text{(A.1-1)}$$

$$C_{\dot{q}}\dot{q} = C_{\dot{q}u}u + C_{\dot{q}q}q + C_{\dot{q}\alpha}\alpha + C_{\dot{q}\delta_e}\delta_e + C_{\dot{q}\delta_{sd}}\delta_{sd} \quad \text{(A.1-2)}$$

where

$C_{\dot{\alpha}}$ is a constant

$C_{\dot{\alpha}x}$ is a constant relating α to the variable x

u is the perturbation in airspeed

α, q are perturbations in the angle of attack and pitch rate respectively

δ_e, δ_{sd} are the deflections of the elevons and direct lift spoilers respectively

Assuming that u is zero as a result of the control effected by the automatic throttle the equations reduce to

$$C_{\dot{\alpha}}\dot{\alpha} = C_{\dot{\alpha}q}q + C_{\dot{\alpha}\theta}\theta + C_{\dot{\alpha}\alpha}\alpha + C_{\dot{\alpha}\delta_e}\delta_e + C_{\dot{\alpha}\delta_{sd}}\delta_{sd} \quad \text{(A.1-3)}$$

$$C_{\dot{q}}\dot{q} = C_{\dot{q}q}q + C_{\dot{q}\alpha}\alpha + C_{\dot{q}\delta_e}\delta_e + C_{\dot{q}\delta_{sd}}\delta_{sd} \quad \text{(A.1-4)}$$

It is desirable to eliminate the pitching moment due to spoiler deflection. This goal is achieved if the elevon is deflected so that

$$\delta_e = - C_{\dot{q}\delta_e}^{-1} \left[C_{\dot{q}\alpha} \alpha + C_{\dot{q}\delta_{sd}} \delta_{sd} \right] \tag{A.1-5}$$

As a result it is possible to set q and θ equal to zero in equations (A. 1-1) and (A.1-2). Substituting for δ_e in equation (A.1-1) gives

$$\begin{aligned} C_{\dot{\alpha}}\dot{\alpha} &= \left[C_{\dot{\alpha}\alpha} - C_{\dot{\alpha}\delta_e} C_{\dot{q}\delta_e}^{-1} C_{\dot{q}\alpha} \right] \alpha \\ &\quad + \left[C_{\dot{\alpha}\delta_{sd}} - C_{\dot{\alpha}\delta_e} C_{q\delta_e}^{-1} C_{q\delta_{sd}} \right] \delta_{sd} \\ &= \bar{C}_{\dot{\alpha}\alpha} \alpha + \bar{C}_{\dot{\alpha}\delta_{sd}} \delta_{sd} \end{aligned} \tag{A.1-6}$$

Rewriting the equation in Laplace transform notation and rearranging terms yields

$$\left[\bar{C}_{\dot{\alpha}} s - \bar{C}_{\dot{\alpha}\alpha} \right] \alpha = \bar{C}_{\dot{\alpha}\delta_{sd}} \delta_{sd} \tag{A.1-7}$$

or

$$\left(\frac{\alpha}{\delta_{sd}} \right)_{q=0} = \frac{\bar{C}_{\dot{\alpha}\delta_{sd}} / \bar{C}_{\dot{\alpha}\alpha}}{C_{\dot{\alpha}} / \bar{C}_{\dot{\alpha}\alpha} s - 1} \tag{A.1-8}$$

Using the stability derivatives

$$\begin{aligned} C_{\dot{\alpha}} &= - 4.630 \\ C_{\dot{\alpha}\alpha} &= 3.235 \\ C_{\dot{\alpha}\delta_e} &= 0.288 \\ C_{\dot{\alpha}\delta_{sd}} &= - 0.731 \\ C_{\dot{q}\delta_e} &= - 0.079 \\ C_{\dot{q}\alpha} &= - 0.043 \\ C_{\dot{q}\delta_{sd}} &= 0.000 \end{aligned}$$

and equation (A. 1-5) gives

$$C_{\dot{\alpha}\alpha} = 3.080$$

$$C_{\dot{\alpha}\delta_{sd}} = -0.731$$

The transfer function (A.1-7) is then

$$\left[\frac{\alpha}{\delta_{sd}}\right]_{q=0} = \frac{0.237}{1.510s + 1.000} \qquad \text{(A.1-9)}$$

APPENDIX B

B.1 Proof of Theorem 1

Let the time average be defined

$$\mathcal{E}(x^2) = \lim_{T\to\infty} \frac{1}{T} \int_0^T x^2 dt \tag{B.1}$$

and let the time averages of the squares and cross products of the elements a_i $i = 1, n$ exist. Consider the first two elements of the sequence.

$$\mathcal{E}\left((a_1 + a_2)^2\right) = \mathcal{E}(a_1^2) + \mathcal{E}(a_2^2) + 2\mathcal{E}(a_1 a_2) \tag{B.2}$$

$$\mathcal{E}\left((a_1 - a_2)^2\right) = \mathcal{E}(a_1)^2 + \mathcal{E}(a_2^2) - 2\mathcal{E}(a_1 a_2) \tag{B.3}$$

Since the left hand sides of B.2 and B.3 are positive semi-definite

$$\mathcal{E}(a_1^2) + \mathcal{E}(a_2^2) \geq 2\mathcal{E}(a_1 a_2) \tag{B.4}$$

Therefore

$$\mathcal{E}\left((a_1 + a_2)^2\right) \leq 2\left(\mathcal{E}(a_1^2) + \mathcal{E}(a_2^2)\right) \tag{B.5}$$

Now suppose that the theorem holds for the first k terms (k<n) so that

$$\mathcal{E}\left(\left(\sum_{i=1}^{k} a_i\right)^2\right) \leq 2\sum_{i=1}^{k} \mathcal{E}(a_i^2) \tag{B.6}$$

Then for k + 1 terms

$$\mathcal{E}\left(\left(\sum_{i=1}^{k} a_i + a_{k+1}\right)^2\right) \leq 2\sum_{i=1}^{k+1} \mathcal{E}(a_i^2) - \mathcal{E}(a_{k+1}^2) + \sum_{i=1}^{k} \mathcal{E}(a_{k+1}\, a_i)$$

$$\geq 0 \tag{B.7}$$

$$\mathcal{E}\left(\left(\sum_{i=1}^{k} a_i - a_{k+1}\right)^2\right) \leqq 2\sum_{i=1}^{k+1}\mathcal{E}(a_i^2) - \mathcal{E}(a_{k+1}^2) - \sum_{i=1}^{k}\mathcal{E}(a_{k+1}a_i)$$

$$\geqq 0 \qquad \text{(B.8)}$$

therefore:

$$\mathcal{E}\left(\left(\sum_{i=1}^{k+1} a_i\right)^2\right) \leqq 2\sum_{i=1}^{k+1}\mathcal{E}(a_i^2) \qquad \text{(B.9)}$$

then, by mathematical induction:

$$\mathcal{E}\left(\sum_{i=1}^{n}(a_i^2)\right) \leqq 2\sum_{i=1}^{n}\mathcal{E}(a_i^2) \qquad \text{(B.10)}$$

QED.

APPENDIX C

CONVENTIONAL AUTOMATIC LANDING SYSTEM DESIGN

C.1 Introduction

The most common type of automatic landing system uses information derived from the ILS localizer and glide-path receivers to provide the position error data required for acquisition and flight along the reference line defined by the intersection of the ILS localizer and glide-slope center planes. Conventional systems provide essentially linear position control relative to this reference line. This appendix describes lateral and vertical control system designs which are based on the conventional approach.

C.2 Conventional Lateral Position Control System

In the lateral channel the coupler output provides the reference input to the roll autopilot. Roll angle serves as the lateral control variable, since the heading rate $\dot{\psi}$ is roughly proportional to roll angle ϕ

$$\dot{\psi} = \frac{g \tan \phi}{v_p} \qquad \text{(C.2-1)}$$

and the lateral velocity y is proportional to heading angle relative to the path (in the absence of a cross wind).

$$\dot{y} = v_p \sin \psi \qquad \text{(C.2-2)}$$

where g is the gravitational constant and v_p is the path velocity. A schematic diagram of a conventional LATERAL control system is shown in Fig. C.2.1 where:

K_y is an adjustable position feedback gain.

$K_{\dot{y}}$ is an adjustable rate feedback gain.

K_{iy} is the integral compensator gain.

T_r is the ILS Receiver Time Constant.

T_v is the velocity lead network time constant.

d_{loc} is the estimated distance to the localized antenna.

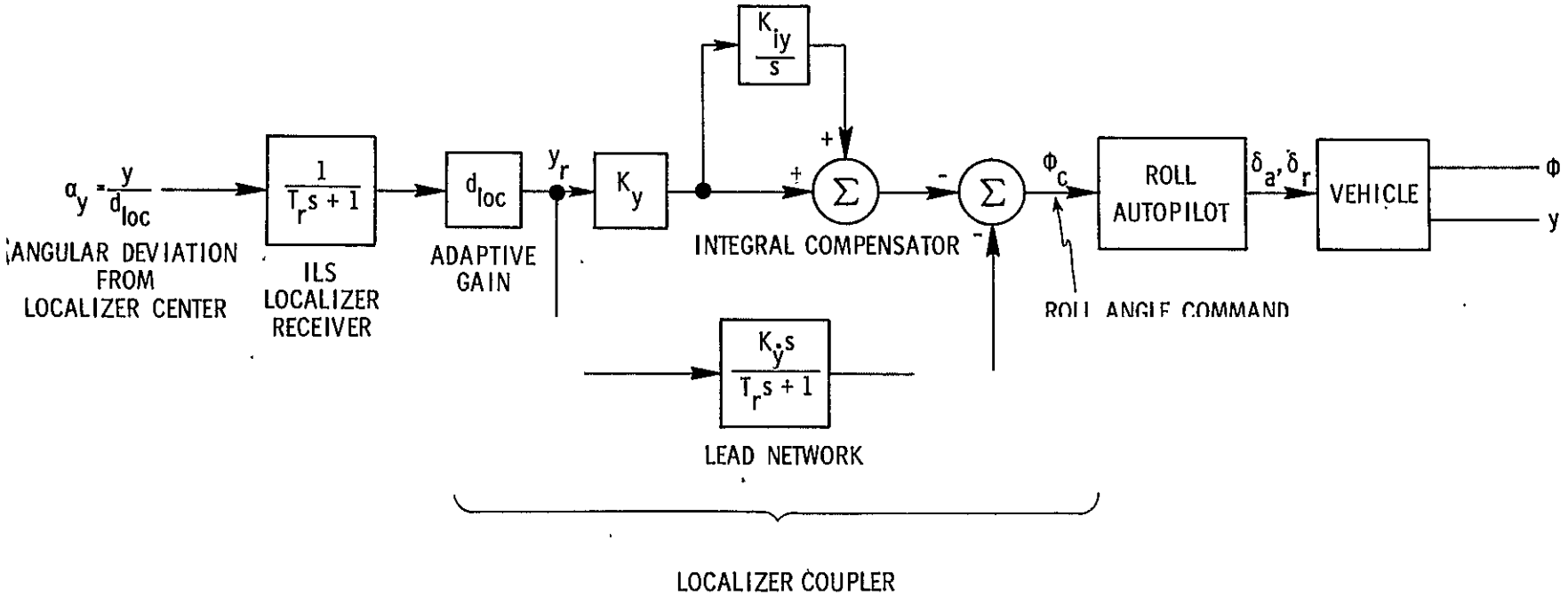

Fig. C.2.1 Conventional lateral position control system.

Position information relative to the localizer beam center is obtained by multiplying the angular deviation (radians) provided by the localizer receiver by the distance d_{loc} to the localizer antenna. This position information is multiplied by the gain K_y to close the position control loop.

The integral compensator operates on y to provide a roll command which maintains the correct crab angle when the aircraft is operated in a varying cross wind as well as correcting for any individual errors in trim.

The lead network generates a signal proportional to the rate of change of lateral position; this signal provides dynamic response compensation as indicated above. This compensation may be augmented by heading feedback due to the relation in Eq (C.2-2).

The open-loop transfer characteristics of the control system are shown in Fig. C.2.2, which uses the linearized vehicle transfer functions in Appendix B, ref 26, the roll angle control system in Appendix D and the parameter values in Table C.3-1. The closed-loop transfer function is shown in Fig. C.2.3. A linearized response appears in Fig. C.2.4.

C.3 Conventional Vertical Position Control System

Vertical position control is achieved by applying the output of the vertical coupler as a reference input to the pitch autopilot as shown in Fig. C.3.1 where

K_z is an adjustable position feedback gain.

$K_{\dot{z}}$ is an adjustable velocity feedback gain.

K_{iz} is an adjustable integral compensator gain.

T_r is the ILS receiver time constant.

T_v is the velocity lead network time constant.

d_{gs} is the estimated distance to the glide-slope antenna.

α_{gs} is the angular deviation from the glide-path center.

z_{gs} is the vertical coordinate of the glide-path center.

x is the distance to the glide-slope antenna.

z is the vertical distance between the aircraft and the glide-path center.

The vertical component of velocity $\dot{z}$ is approximately proportional to the pitch θ.

$$\dot{z} \approx -v_p\theta$$

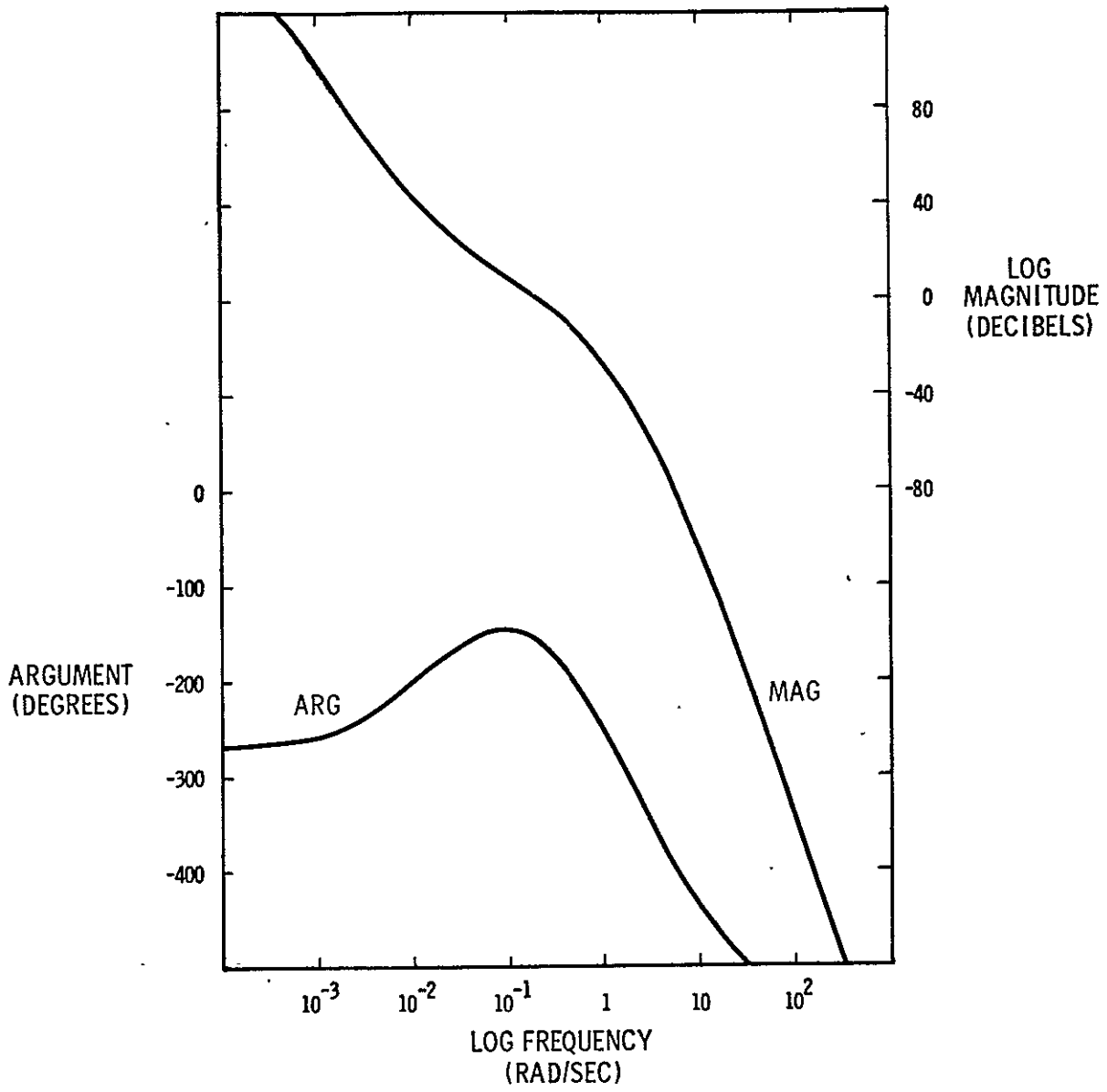

Fig. C.2.2 Open-loop transfer function of a conventional lateral position control system.

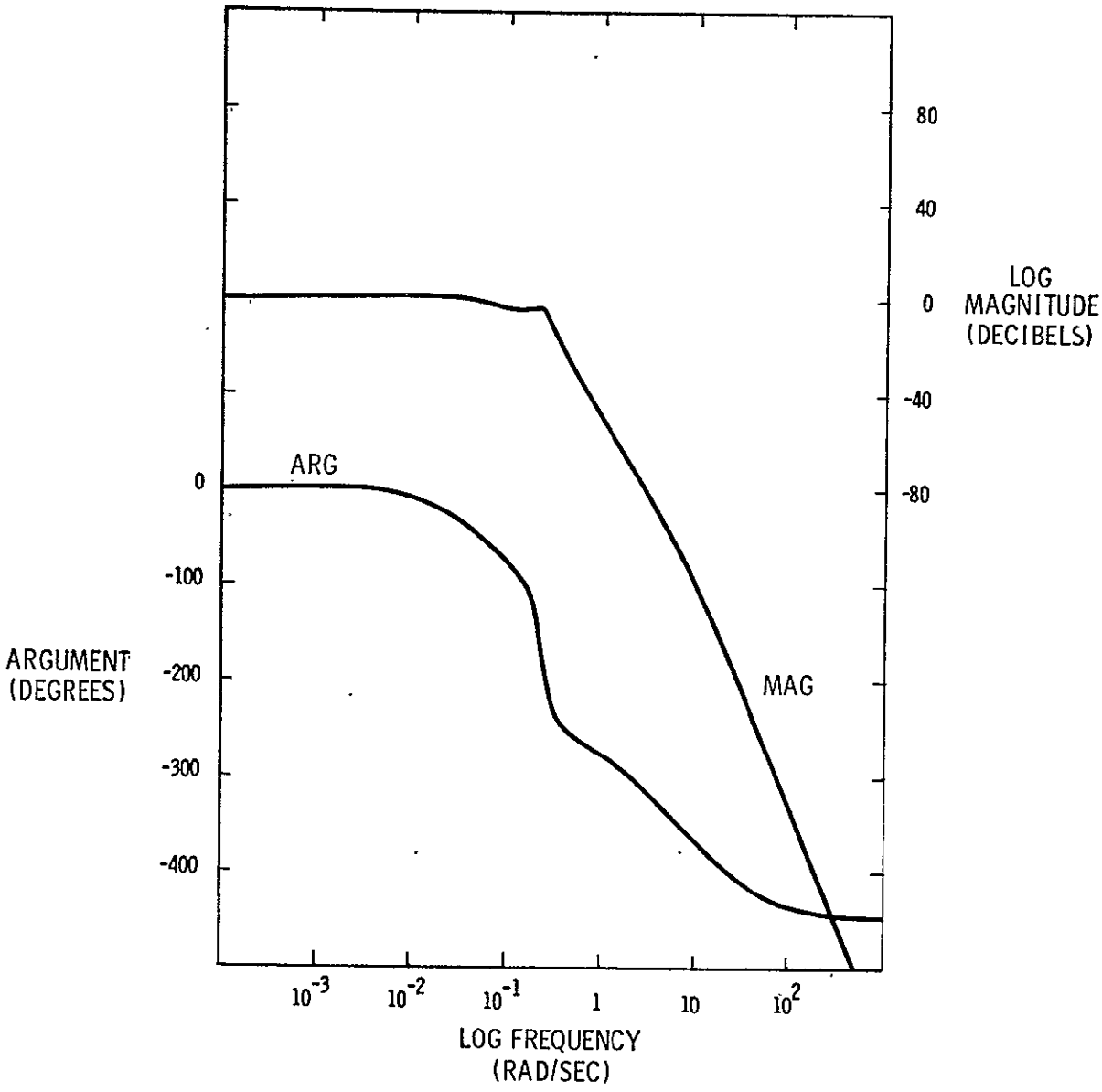

Fig. C.2.3 Closed-loop transfer function $\frac{y}{y_d}$ for a conventional lateral position control system.

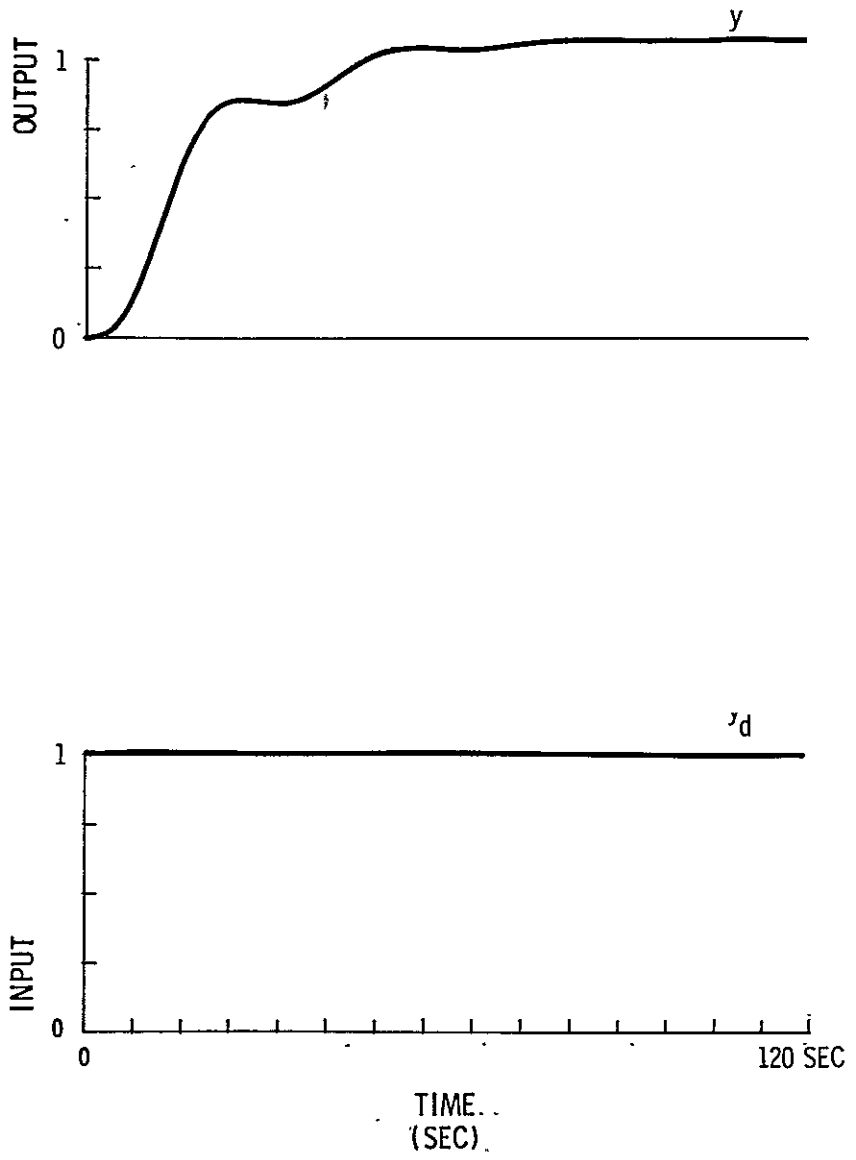

Fig. C.2.4 Unit-step response of the linearized conventional lateral position control system.

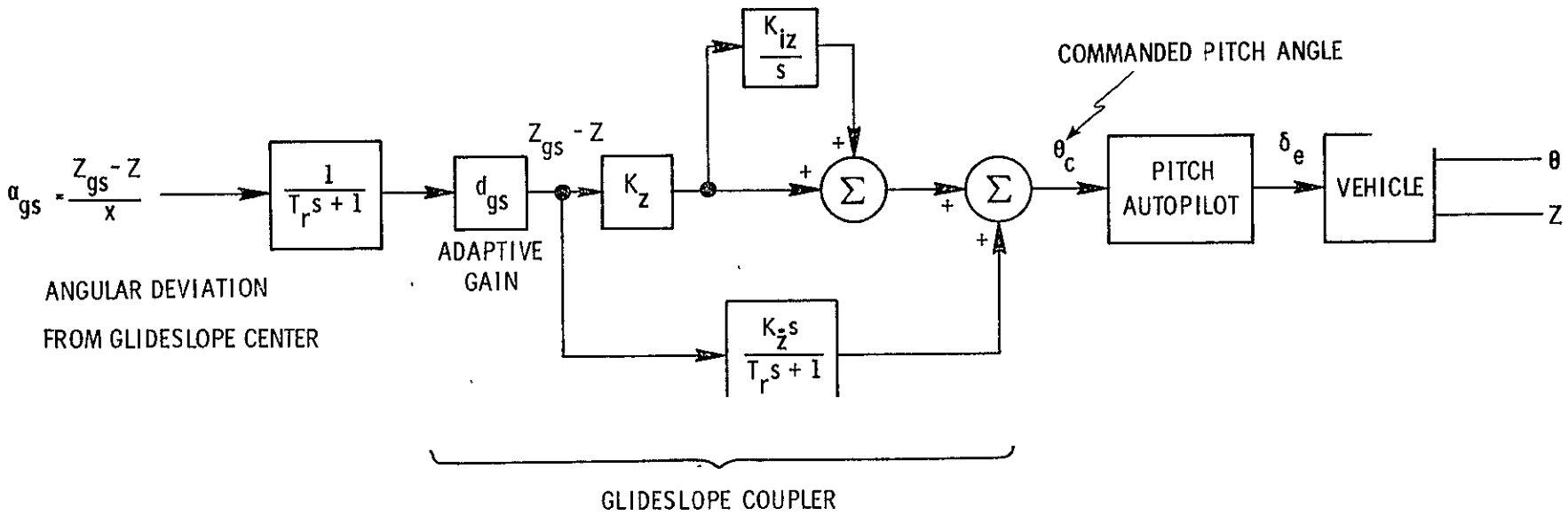

Fig. C.3-1 Conventional vertical position control system.

The vertical distance between the aircraft and the glide-path center is obtained by multiplying the angular deviation (radians) from the ILS glide-slope receiver by the estimated distance to the glide-slope transmitter. This is then multiplied by a gain K_z to close the position loop.

The integral compensator provides the constant component of θ which is required for flight down an inclined path with zero position error as well as correcting for trim. The velocity lead network provides a signal proportional to the rate of change of vertical position for dynamic compensation.

The open-loop transfer function of the control system is shown in Fig. C.3.2 and is generated using the vehicle transfer function in Section C.5, the pitch angle control system in Section 5.11 and the parameter values in Table C.3-1 of ref 26. The closed-loop transfer function is shown in Fig. C.3.3, and the unit-step response of the linear model appears in Fig. C.3.4.

Table C.3-1 Parameter Values for Conventional ILS Coupler

GAINS		
K_y	lateral position gain	0.0205 deg/ft
$K_{\dot{y}}$	lateral velocity gain	0.410 deg/ft/sec
K_{iy}	y intrgral compensator gain	0.005 sec
K_z	vertical position gain	0.041 deg/ft
$K_{\dot{z}}$	vertical velocity gain	0.205 deg/ft/sec
K_{iz}	z integral compensator gain	0.005 sec
CONSTANTS		
T_r	ILS receiver time constant	0.40 secs
T_v	velocity filter time constant	1.00 secs

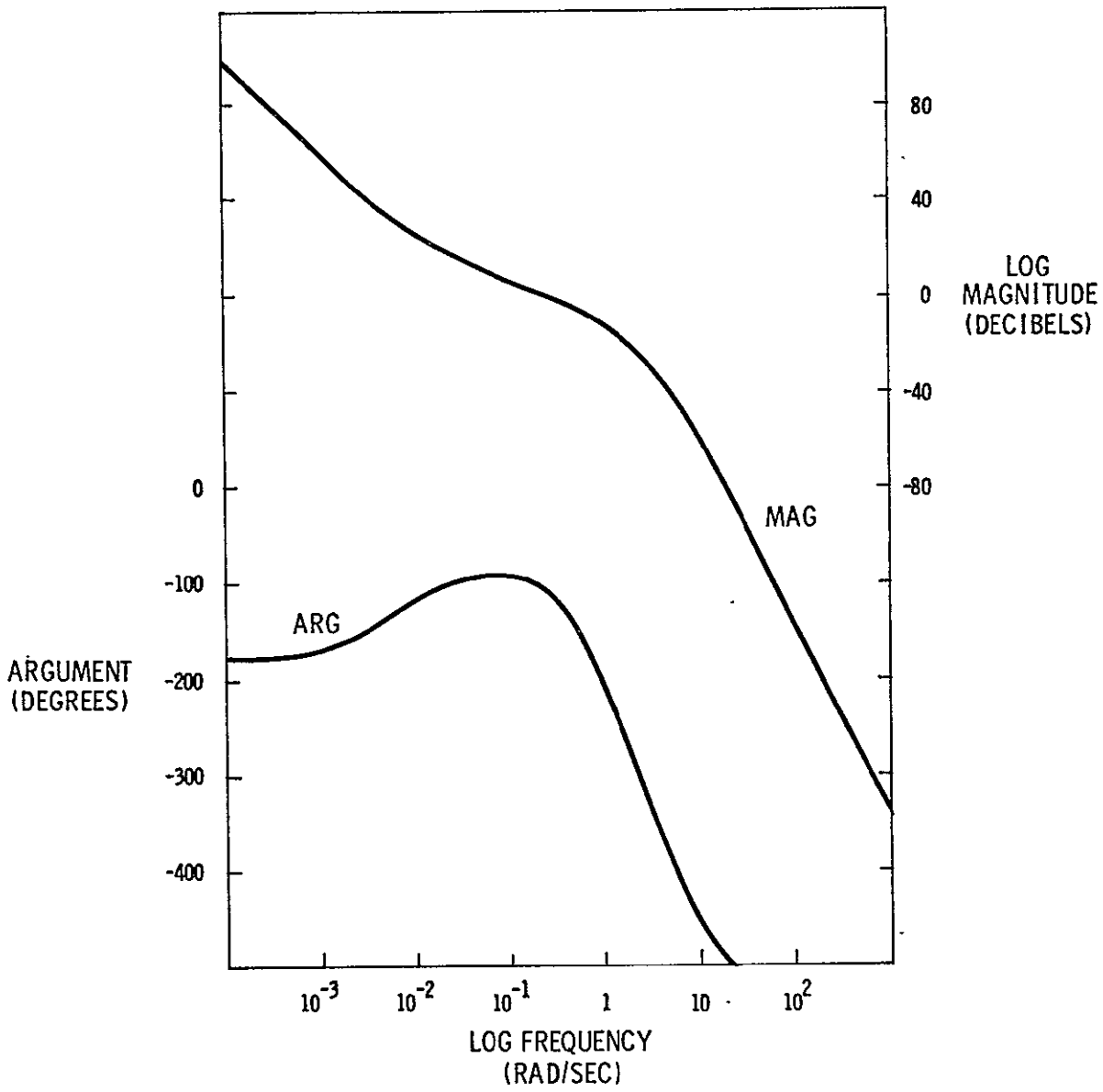

Fig. C.3.2 Open-loop transfer function of a conventional vertical position control system.

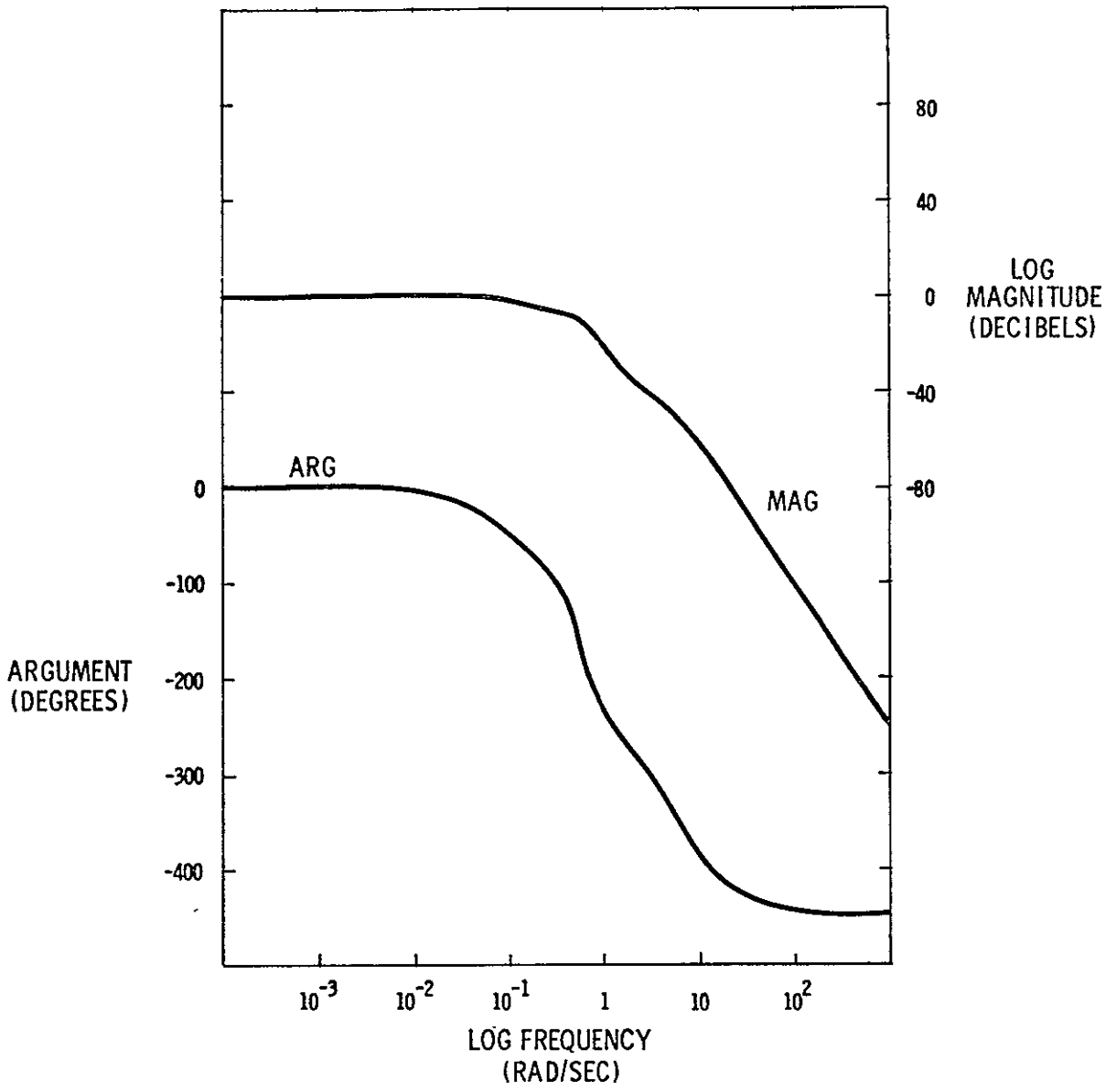

Fig. C.3.3 Closed-loop transfer function $\frac{z}{z_d}$ of a conventional vertical position control system.

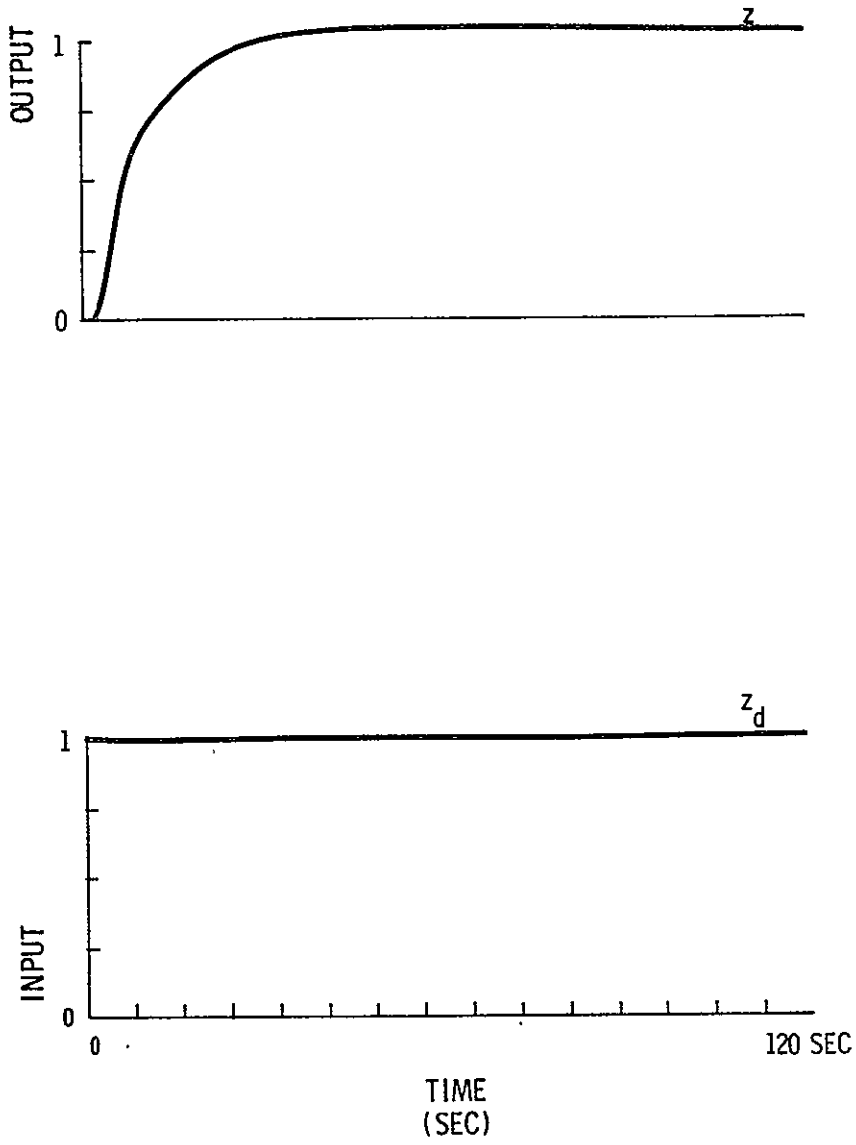

Fig. C.3.4 Unit-step response of the linearized conventional vertical position control system .

APPENDIX D

ATTITUDE CONTROL SYSTEMS

D. 1 Introduction

As indicated in chapter 3 control of roll angle φ and pitch angle θ plays an essential role in the construction of the lateral and vertical position control systems. A complete discussion of roll and pitch control is found in chapter 5 of reference 26. The roll and pitch control system designs are summarized here for completeness.

D. 2 Roll Angle Control System Design

A linearized model of the roll control system is shown in Fig. D. 2. 1. The open and closed loop magnitude and phase frequency domain characteristics are shown in Figs. D. 2. 2 and D. 2. 3 and the linearized system step response is shown in Fig. D. 2. 4. The complete roll control schematic in Fig. D. 2. 5 includes a lateral Stability Augmentation System (SAS) which generates the rudder deflections required for turn coordination. ($\beta = 0$) Since the control system, with integral compensation ($K_{i\varphi} \neq 0$), is conditionally stable and the roll control system is subject to saturation the integral compensator output must be limited to ensure stable operation. The parameter values associated with Fig. D. 2. 4 are given in Table D.2-1.

D. 3 Pitch Angle Control System Design

The pitch angle control system appears in linearized form in Fig. D. 3. 1. Phase and magnitude frequency domain characteristics of the linearized model are shown in Figs. D. 3. 2 and D. 3. 3. The step response of the linearized system is shown in Fig. D. 3. 4. The complete pitch control system is shown in Fig D. 3. 5. The parameter values associated with Fig. D. 3. 5 are shown in table D. 2-1.

Table D. 2-1 Roll and Pitch Angle Control System Parameters

PARAMETER	VALUE
K_{ϕ}	1.000
$K_{\dot{\phi}}$	2.000
$K_{i\phi}$	0.000
K_1	3.000
K_2	0.170
K_3	0.374
K_4	2.000
K_5	2.000
K_6	3.000
K_7	2.000
K_8	0.666
K_9	0.534
T_1	1.000
T_2	0.500
T_4	2.000
T_7	1.000
L_1	10.000
K_{θ}	7.100
$K_{\dot{\theta}}$	16.250

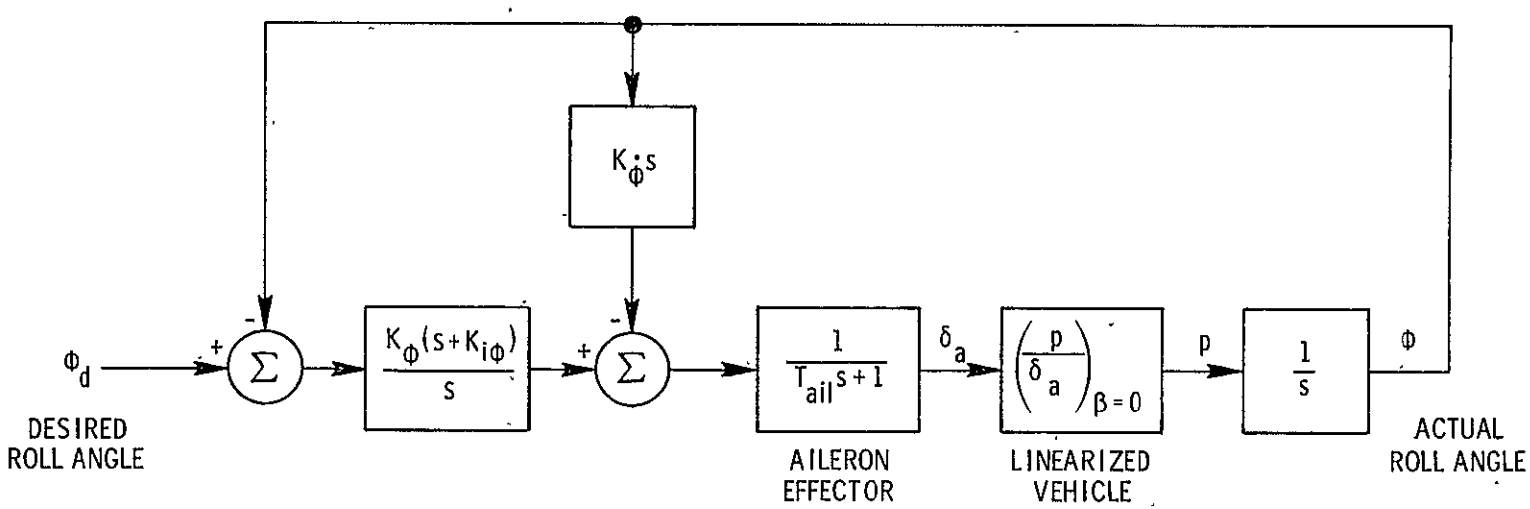

Fig. D. 2. 1 Linear model of the roll angle control system.

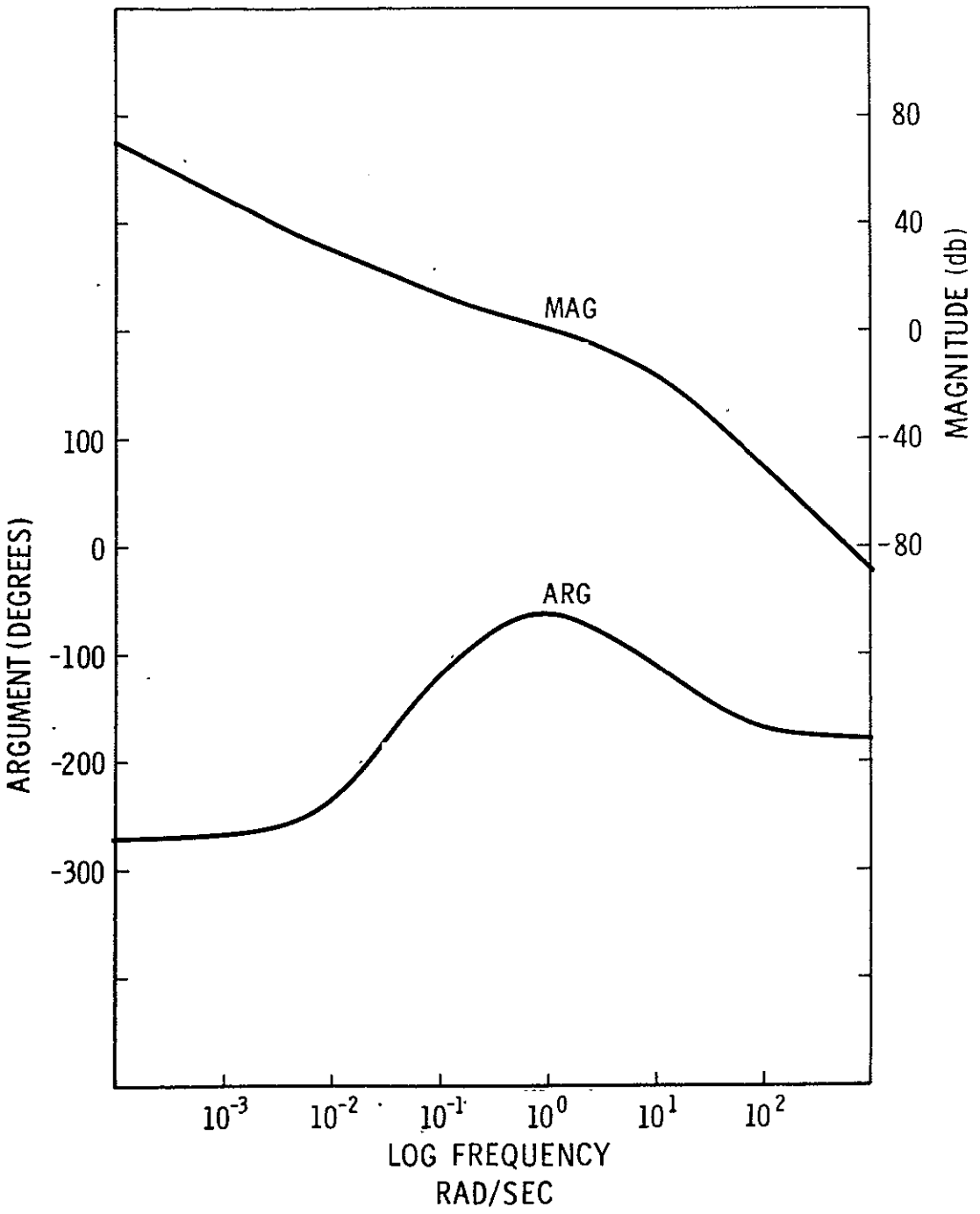

Fig. D.2.2 Open-loop transfer function of the roll control system.

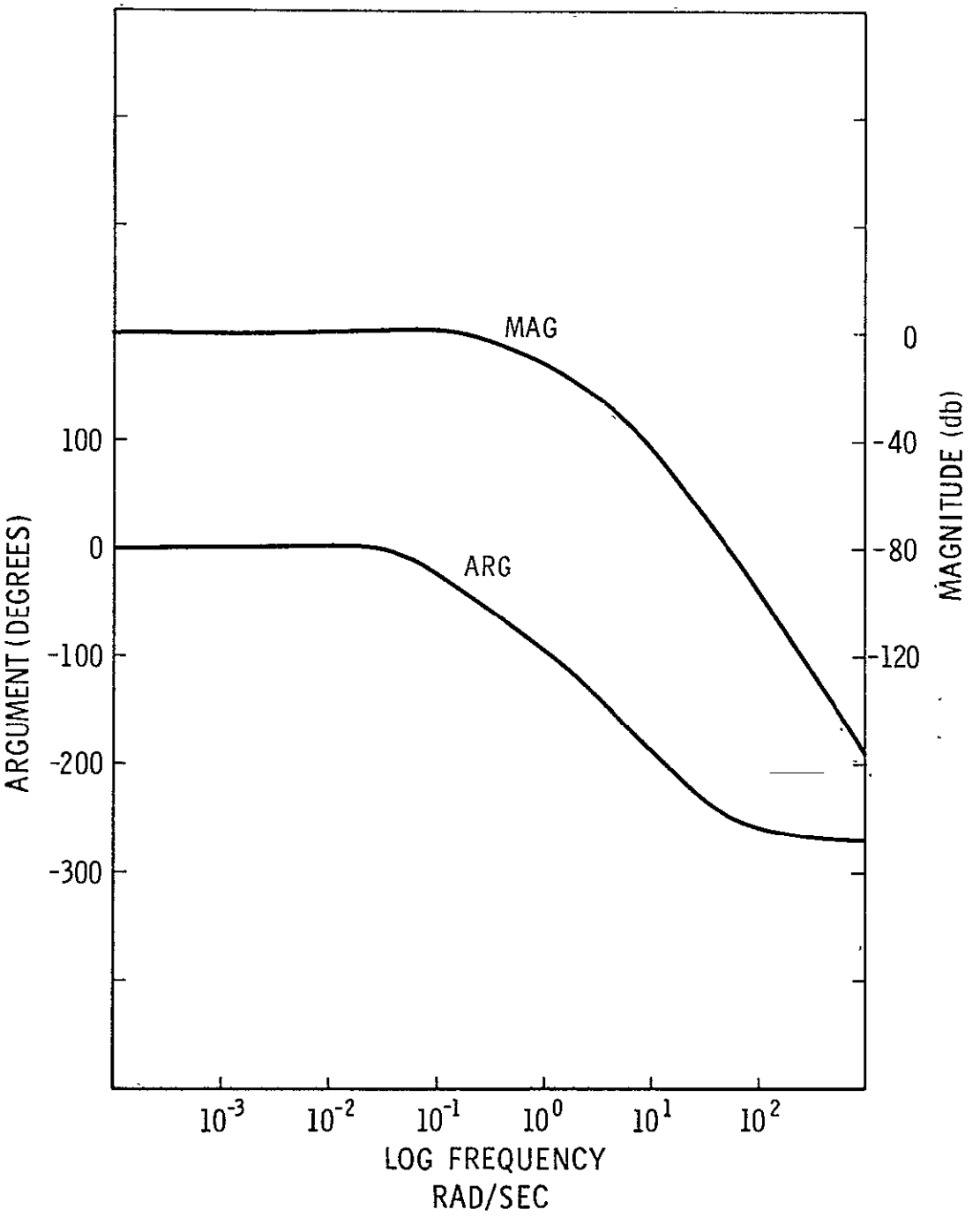

Fig. D.2.3 Closed-loop transfer function of the roll control system.

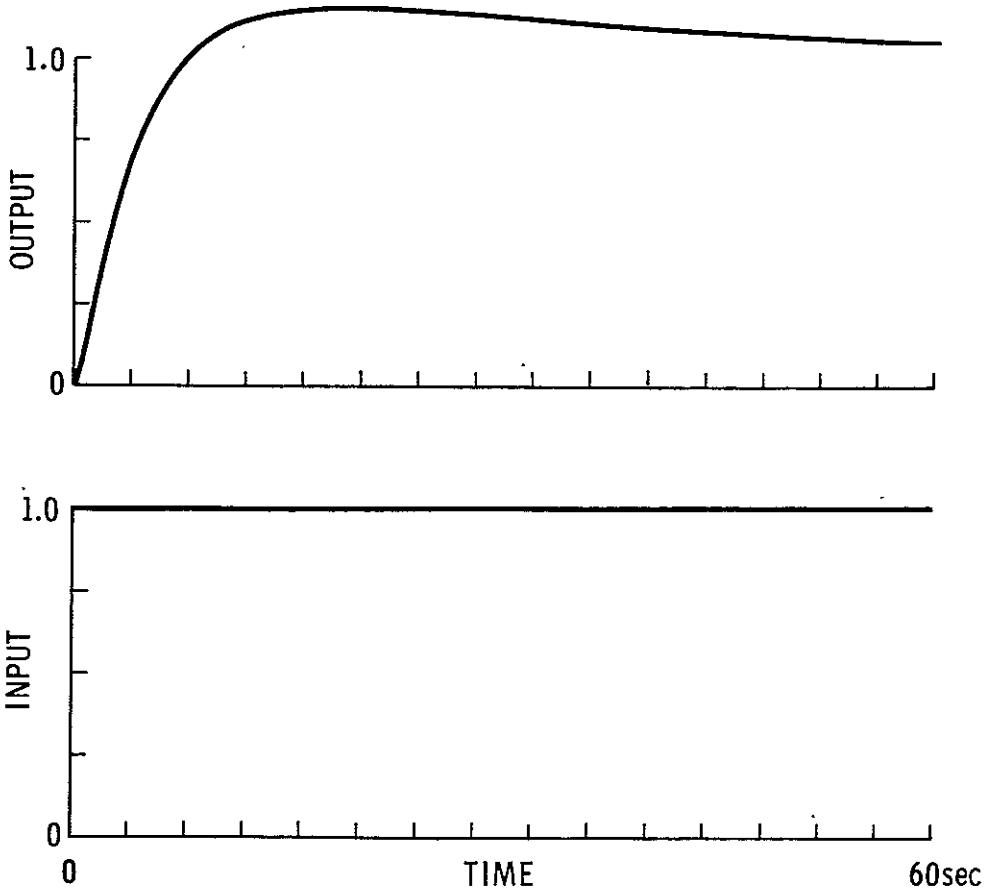

Fig. D.2.4 Unit step response of the linearized roll angle control system.

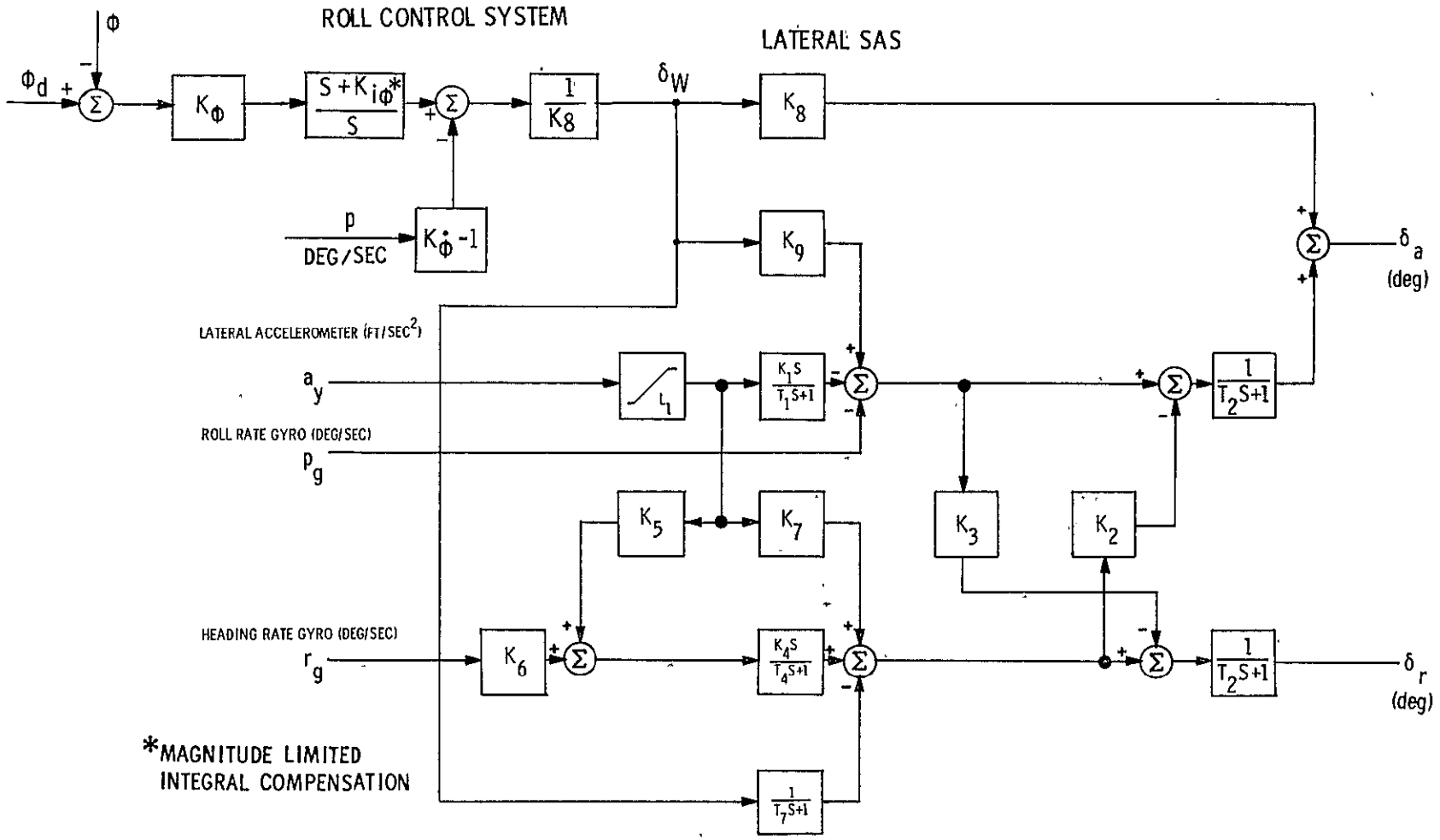

Fig. D. 2. 5 Roll angle control system with lateral SA

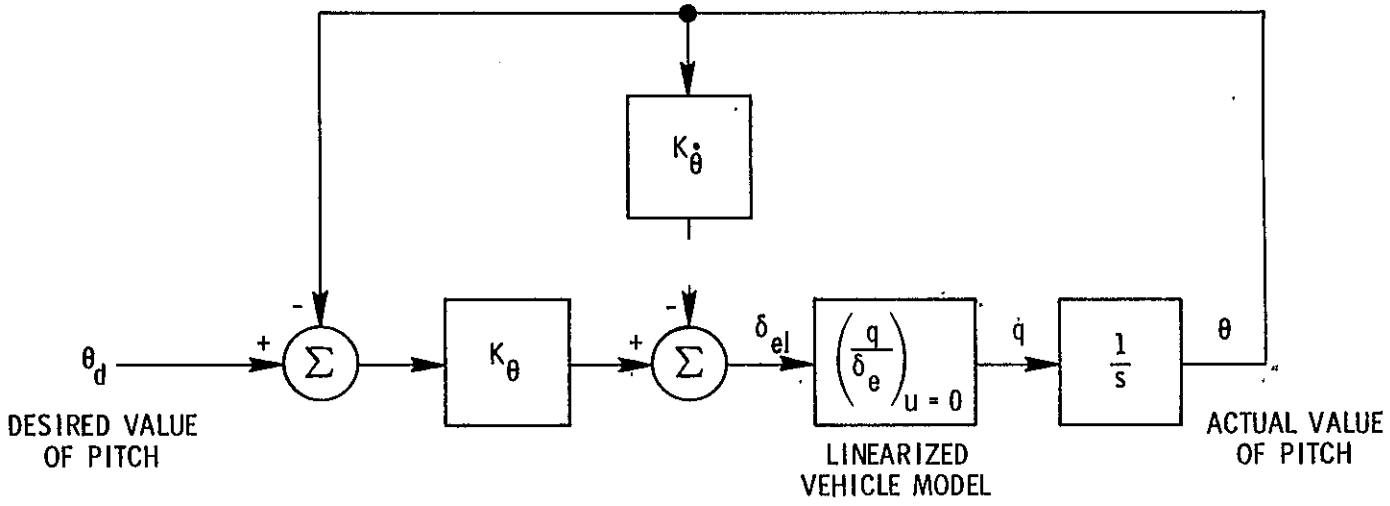

Fig. D. 3. 1 Linearized model of a pitch attitude control system.

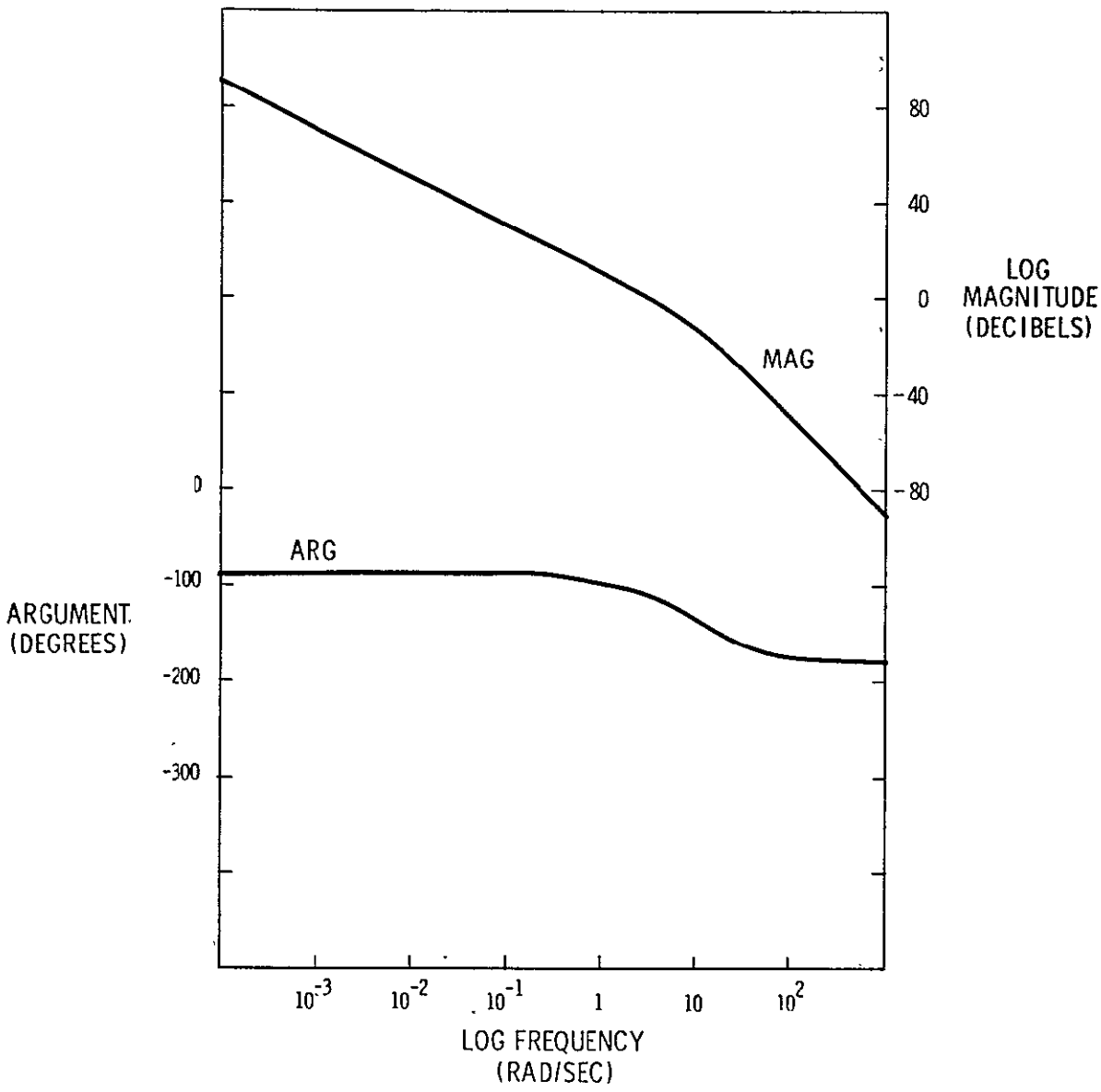

Fig. D.3.2 Open-loop transfer function of the pitch control system.

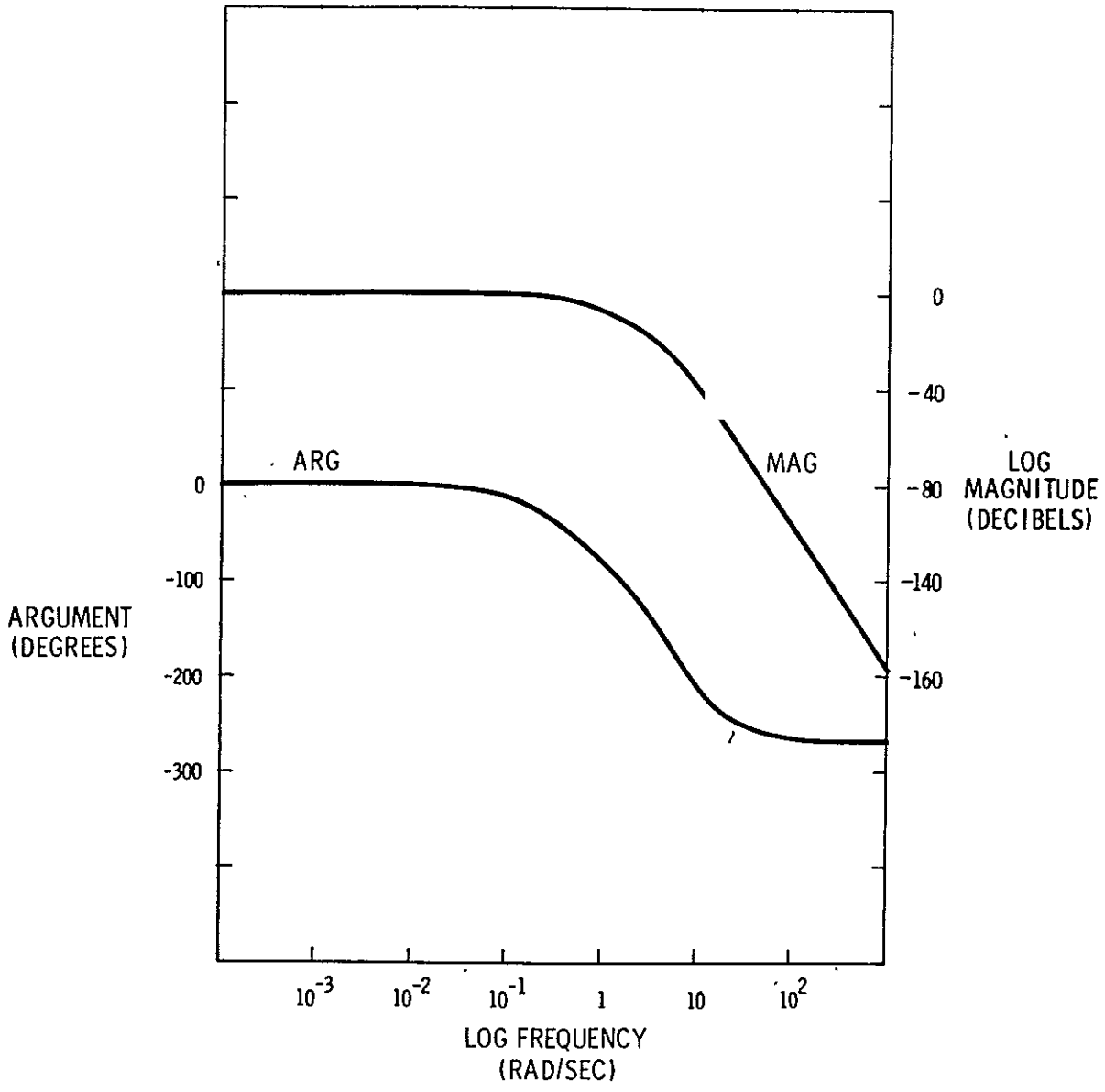

Fig. D.3.3 Closed-loop transfer function of the pitch control system.

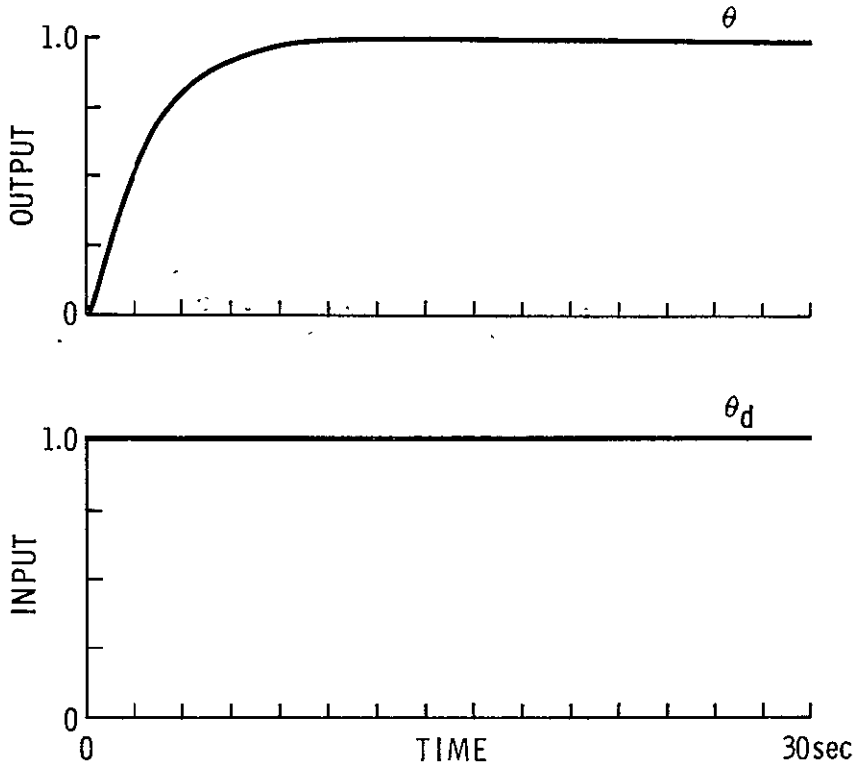

Fig. D.3.4 Unit step response of the linearized pitch angle control system.

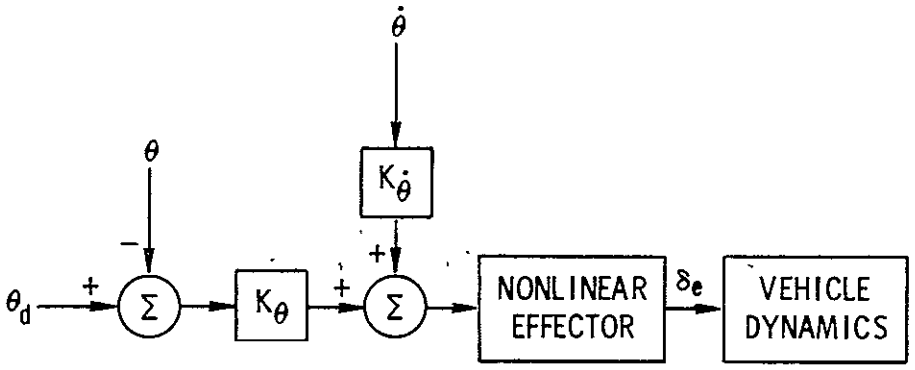

Fig. D.3.5 Pitch attitude control system.

APPENDIX E

AIRSPEED CONTROL SYSTEM

E. 1 Introduction

The basic nonlinear vehicle equations were derived in chapter 8. Linearization about the nominal operating condition provides for application of the techniques of linear control system analysis and synthesis.

E. 2 Derivation of the Airspeed-Thrust Transfer Function

The longitudinal variables u, α, q are related by a coupled set of linear differential equations in the perturbation quantities as follows:

$$C_{\dot{u}}\dot{u} = C_{\dot{u}u}u + C_{\dot{u}\alpha}\alpha + C_{\dot{u}\theta}\theta + C_{\dot{u}\delta_T}\delta_T \qquad \text{(E. 2-1)}$$

$$C_{\dot{\alpha}}\dot{\alpha} = C_{\dot{\alpha}u}u + C_{\dot{\alpha}\alpha}\alpha + C_{\dot{\alpha}q}q + C_{\dot{\alpha}\theta}\theta + C_{\dot{\alpha}\delta_e}\delta_e + C_{\dot{\alpha}\delta_T}\delta_T \qquad \text{(E. 2-2)}$$

$$C_{\dot{q}}\dot{q} = C_{\dot{q}u}u + C_{\dot{q}\alpha}\alpha + C_{\dot{q}q}q + C_{\dot{q}\delta_e}\delta_e + C_{\dot{q}\dot{\alpha}}\dot{\alpha} + C_{\dot{q}\delta_T}\delta_T \qquad \text{(E. 2-3)}$$

where, for example, $C_{\dot{u}u}$ is the coefficient of the u perturbation in the $\dot{u}$ equation. Airspeed control is achieved by throttle manipulation; the resulting thrust variation couples into the pitch and lift equations. To obtain an approximate transfer function relating u and δ_T, the longitudinal equations are simplified for the moment by assuming that the pitch control system maintains a zero pitch rate through elevator manipulation.

The simplified equations are:

$$C_{\dot{u}}\dot{u} = C_{\dot{u}u}u + C_{\dot{u}\alpha}\alpha + C_{\dot{u}\delta_T}\delta_T \qquad \text{(E. 2 4)}$$

$$C_{\dot{\alpha}}\dot{\alpha} = C_{\dot{\alpha}u}u + C_{\dot{\alpha}\alpha}\alpha + C_{\dot{\alpha}\delta_T}\delta_T + C_{\dot{\alpha}\delta_e}\delta_e \qquad \text{(E. 2 5)}$$

$$0 = C_{\dot{q}u}u + C_{\dot{q}\alpha}\alpha + C_{\dot{q}\dot{\alpha}}\dot{\alpha} + C_{\dot{q}\delta_T}\delta_T + C_{\dot{q}\delta_e}\delta_e \qquad \text{(E. 2-6)}$$

These equations may be rewritten in Laplace notation in the form

$$G_{uu}u + G_{u\alpha}\alpha \quad = G_{u\delta_T}\delta_T \qquad \text{(E. 2-7)}$$

$$G_{\alpha u}u + G_{\alpha\alpha}\alpha + G_{\alpha\delta_e}\delta_e = G_{\alpha\delta_T}\delta_T \qquad \text{(E. 2-8)}$$

$$G_{qu}u + G_{q\alpha}\alpha + G_{q\delta_e}\delta_e = G_{q\delta_T}\delta_T \qquad \text{(E. 2-9)}$$

where the G_{uu}, $G_{u\alpha}$ .... are polynomials in s.

Defining the characteristic polynomial

$$\Delta = G_{uu}\left[G_{\alpha\alpha}\,G_{q\delta_e} - G_{\alpha\delta_e}\,G_{q\alpha}\right] - G_{u\alpha}\left[G_{\alpha u}\,G_{q\delta_e} - G_{\alpha\delta_e}\,G_{qu}\right]$$

permits a simultaneous solution of (E. 2-7, 8, 9) for the transfer function

$$\left[\frac{u}{\delta_T}\right]_{q=0} = \frac{G_{u\delta_T}\left[G_{\alpha\alpha}\,G_{q\delta_e} - G_{\alpha\delta_e}\,G_{q\alpha}\right] - G_{u\alpha}\left[G_{\alpha\delta_T}\,G_{q\delta_e} - G_{\alpha\delta_e}\,G_{q\delta_T}\right]}{\Delta}$$

E. 3 Numerical Value of Airspeed-Thrust Transfer Function

The numerical value for the transfer function developed in the previous section incorporating coefficient values appropriate to the Boeing B2707-200 is

$$\left[\frac{u}{\delta_T}\right]_{q=0} = \frac{0.0000824\,(s + 0.668)}{(s + 0.653)\,(s + 0.053)}$$

E. 4 Airspeed Control System Design

The design of the airspeed control system is shown in block diagram form in Fig. E. 4, 1. Airspeed and a lagged acceleration are the feedback signals supplied. The first blocks in the forward loop comprise a proportional plus integral network

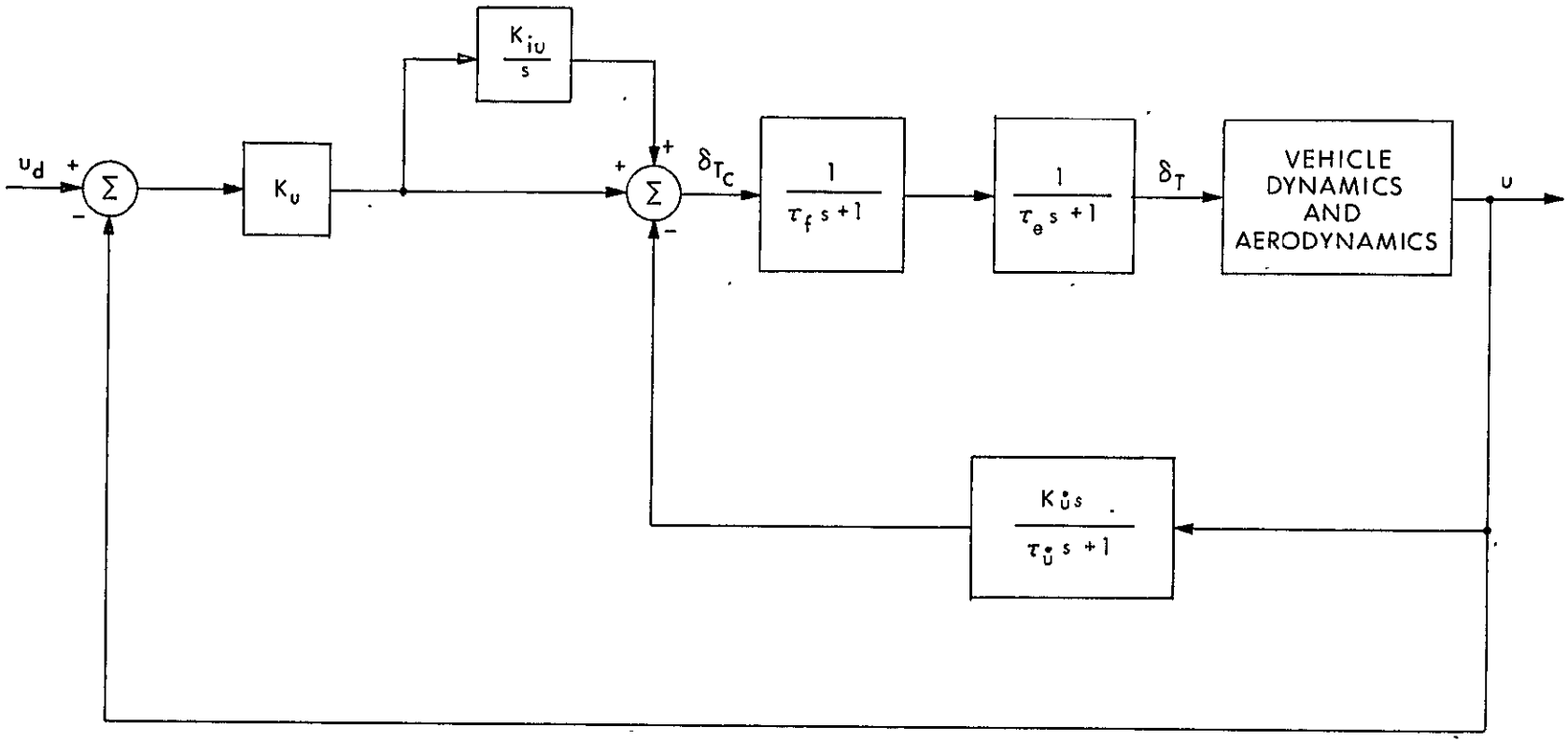

Fig. E.4.1 Airspeed control system block diagram.

to provide compensation. A first order filter is provided to limit high frequency throttle activity and a first order equation models the turbine engine thrust lag. The engine time constant was assumed to be 4 seconds. The time constants in the filter and the acceleration feedback loop were each set at 1/10 second.

The root locus for the inner (acceleration) loop is shown in Fig. E. 4. 2. The closed loop poles were chosen on the real axis, as shown, and the corresponding value for the gain was

$$\underline{K_{u_\bullet} = 10,200}$$

With this value for $K_{u_\bullet}$ and with $K_{iu} = 0$ the root locus for the outer loop is shown in Fig. E. 4. 3. The dominant closed loop poles were selected to give a damping ratio of about $\zeta = 0.7$. The corresponding value for K_u was

$$\underline{K_u = 5,650}$$

The control system was incorporated with the above gains into the digital simulation, which includes the full nonlinear aircraft equations of motion, and subsequently no changes were found to be necessary. The simulation also determined that a satisfactory compromise value for the P + I compensation gain was

$$\underline{K_{iu} = 0.02}$$

E. 5 Airspeed Control System Transfer Functions

Define

$$G = \left[\frac{1}{\tau_f s + 1}\right]\left[\frac{1}{\tau_e s + 1}\right]\left[\frac{u}{\delta_T}\right]_{q=0}$$

$$H = \left\{K_u\left[\frac{s + K_{iu}}{s}\right] + \left[\frac{K_{u_\bullet} s}{\tau_a s + 1}\right]\right\}$$

$$\frac{u}{u_d} = \frac{G}{1 + GH}\left[\frac{s + K_{iu}}{s}\right]K_u$$

For the design gains, a computer program has factorized the above transfer functions and developed the corresponding Bode plots.

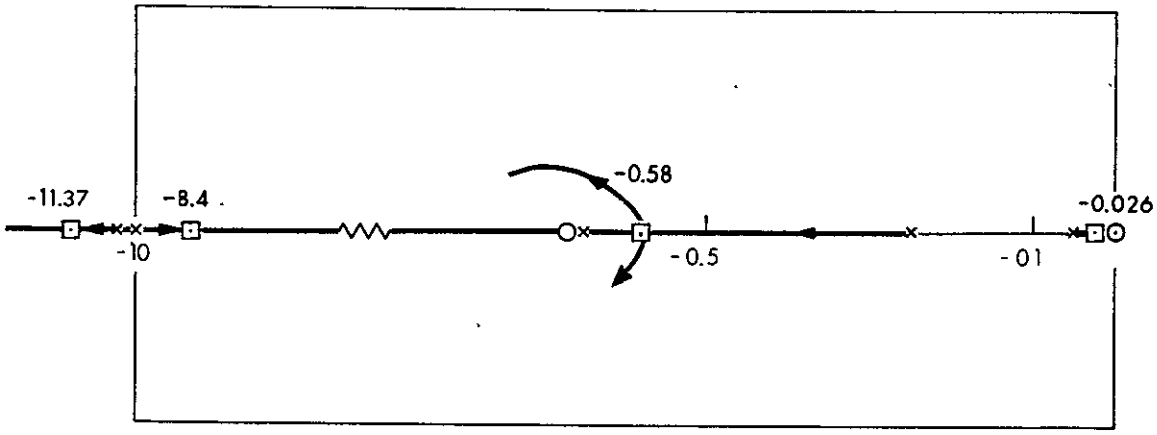

Fig. E.4.2 Root locus of the inner (acceleration) loop of the airspeed control system.

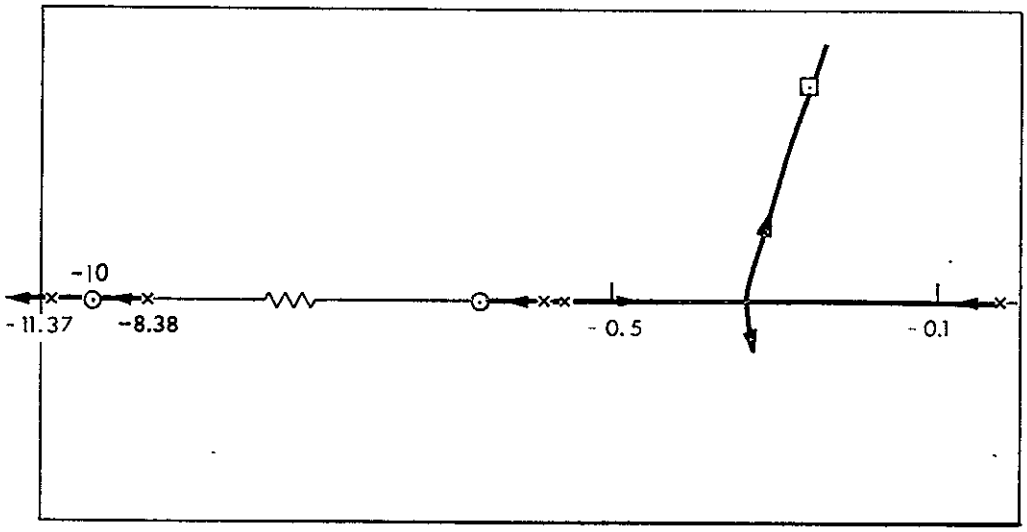

Fig. E 4.3 Root locus of the airspeed control system with $K_{\dot{u}}=10,200$ and $K_{iu}=0$. (Root loci not to scale)

$$G = \frac{0.000206\,(s + 0.668)}{(s + 10)\,(s + 0.25)\,(s + 0.653)\,(s + 0.053)}$$

$$H = \frac{107{,}650\,(s + 0.02)\,(s + 0.5)}{s(s + 10)}$$

$$\frac{u}{u_d} = \frac{1.162\,(s + 0.02)\,(s + 0.67)\,(s + 10)}{(s + 0.0194)\,(s + 0.253 \pm 0.253i)\,(s + 0.65)\,(s + 8.40)\,(s + 11.38)}$$

The vehicle transfer function, G, is plotted in Fig. E. 5. 1, the feedback function, H, in Fig. E. 5. 2, and the closed loop transfer function, u/u_d, in Fig. E. 5. 3. The unit step response of the transfer function u/u_d is shown in Fig. E.5. 4.

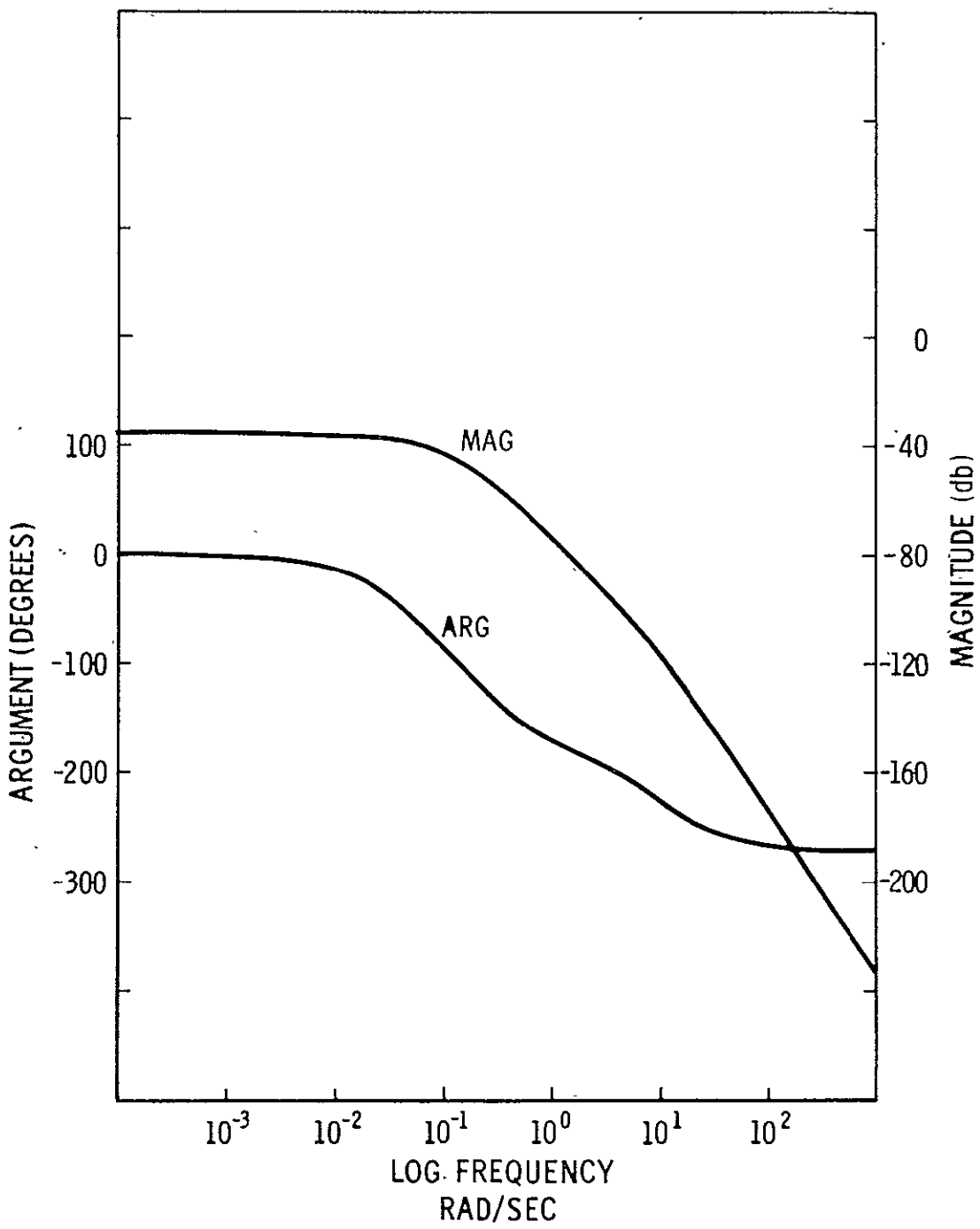

Fig. E.5.1 Bode plot of G(S).

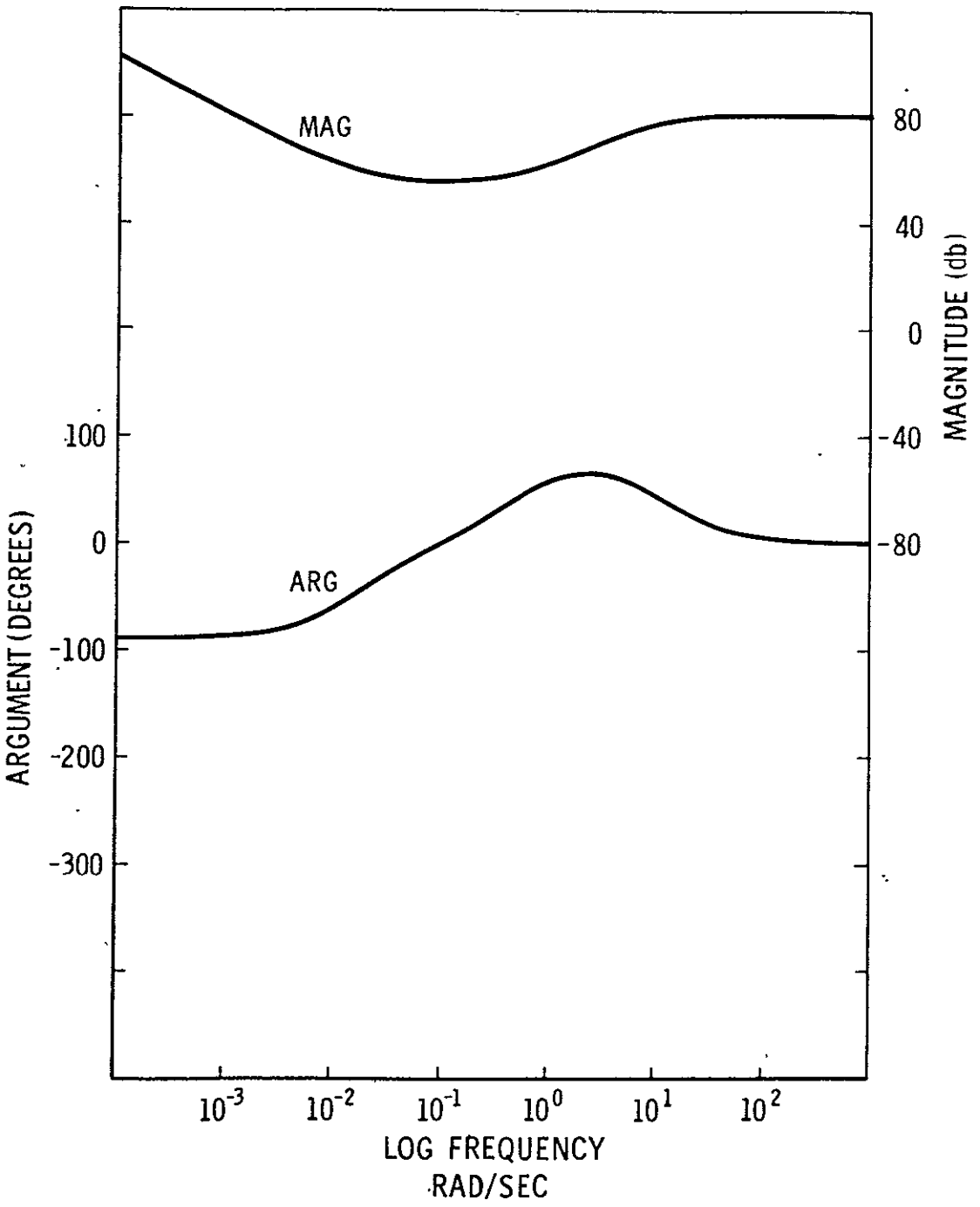

Fig. E 5.2 Bode plot of H(S).

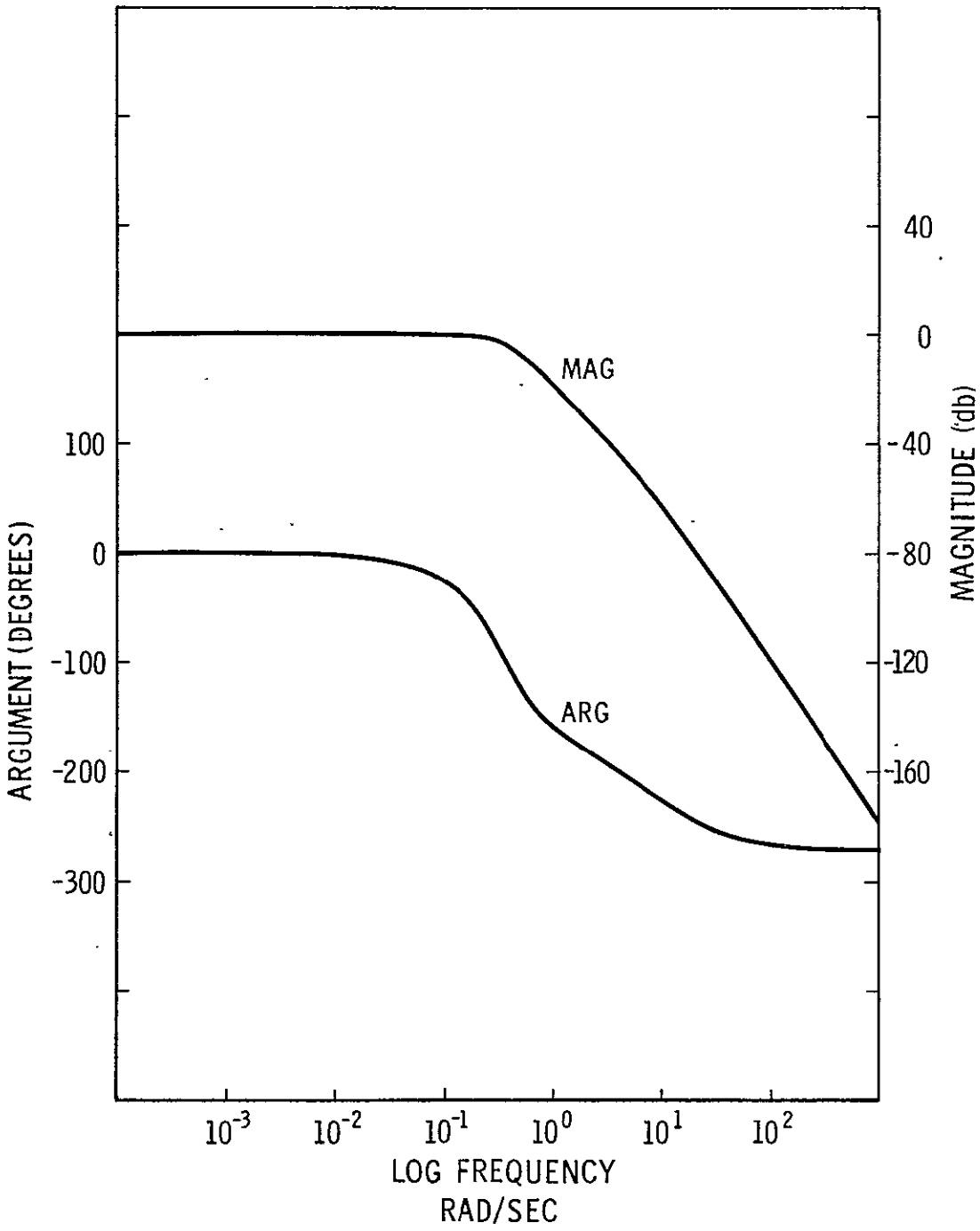

Fig. E.5.3 Bode plot of transfer function, u/u_d.

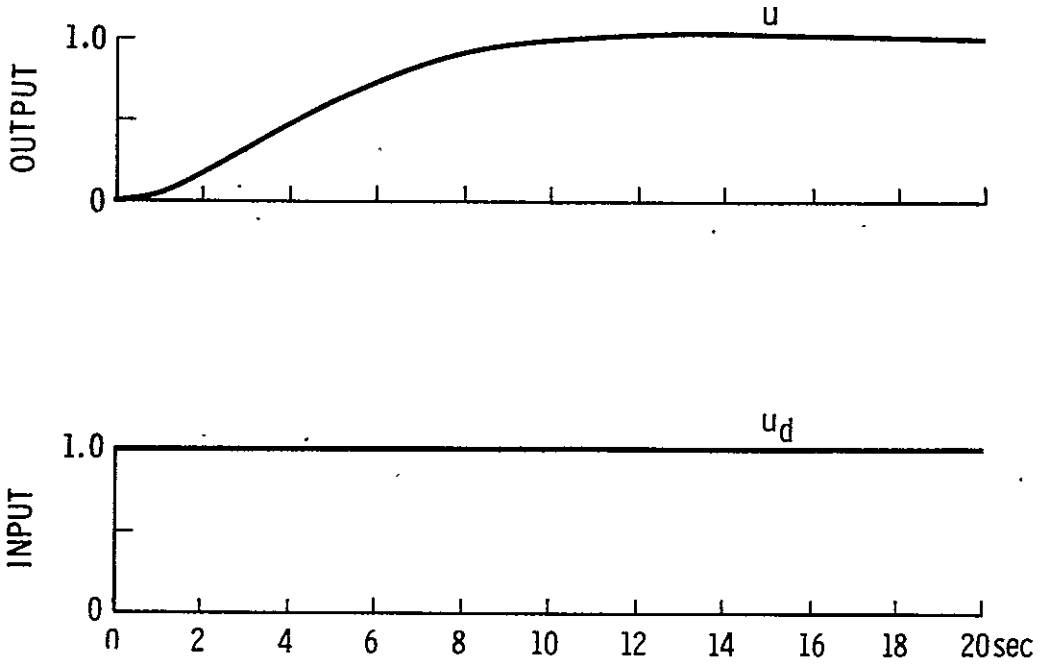

Fig. E.5.4 Step response of u/u_d.

REFERENCES

1 Vice, J. R. and Muir, J. C., Final Report - Evaluation of the BLEU Automatic Landing System, FAA Report AD 600829 December 1963.

2 Analog Computer Study of a Category III ILS, Airborne and Ground Equipment Standards, The Bendix Corporation - Eclipse-Pioneer Division FAA Project No. AD 1091, September 1964.

3 Standard Performance Criterion for Autopilot/Coupler Equipment Radio Technical Commission for Aeronautics Paper No. 31-63/ DO-118 March 14, 1963.

4 Analytical Study of ILS Beam Characteristics for the Systems Research and Development Service, The Bendix Corporation, Eclipse-Pioneer Division. Appendix to ref 3.

5 Blakelock, J. H., Automatic Control of Aircraft and Missiles, John Wiley and Sons, 1965.

6 Etkin, B., Dynamics of Flight, Stability and Control, John Wiley and Sons, 1959.

7 Broxmeyer, C., Inertial Navigation Systems, McGraw Hill, 1964.

8 McDonald, D., "Nonlinear Techniques for Improving Servo Performance," Proceedings of the National Electronics Conference 1950, pp. 400-421.

9 Hopkins, A. M., "A Phase Plane Approach to the Compensation of Saturating Servomechanisms," Transactions of the AIEE, 1951, pp. 631-639.

10 Neiswander, R. S. and MacNeal, R. H., "Optimization of Nonlinear Control Systems by Means of Nonlinear Feedbacks," Transactions of the AIEE, 1953, Part 2.

11 Bogner, I. and Kazda, L. F., "An Investigation of the Switching Criteria for Higher Order Contactor Servomechanisms," Transactions of the AIEE, 1964, Part 2, pp. 118-127.

12 Chang, S. S. L., "Optimum Switching Criteria for Higher Order Contactor Servomechanisms," Transactions of the AIEE, 1955, Part 2, pp. 273-276.

REFERENCES (Cont)

13 Kalman, R. D., "Analysis and Design Principles of Second and Higher Order Saturating Servomechanisms," Transactions of the AIEE, 1955, Part 2, pp. 294-310.

14 Neiswander, R. S., "An Experimental Treatment of Nonlinear Servomechanisms," Transactions of the AIEE, 1956, Part 2, pp. 308-316.

15 Rozonoer, L. I., "L. S. Pontryagin Maximum Principle in the Theory of Optimum Systems," Automatika i Telemekhanika, Vol. 20, Nos. 10-12, November 1959.

16 Pontryagin, L. S., Boltyanskii, V. G., Gamkrelidze, R. V., and Mishehenko, E. F., The Mathematical Theory of Optimal Processes, John Wiley and Sons, 1963.

17 Bryson, A. E. and Ho, Y. C., Optimal Programming, Estimation, and Control, Mimeographed lecture notes, Harvard University, February 1965.

18 Merriam, C. W., Optimization Theory and the Design of Feedback Control Systems, McGraw-Hill, 1964.

19 Boeing letter 9-7310-00-11, November 1967.

20 Willich, W., "B-2707 Stability Derivatives as Mechanized in the Phase IIC Full Mission Profile Simulation," Boeing Report No. D6A10485-1, November 1966, Revision to the above report, No. 2707-AERO-5, January 1967.

21 Etkin, B., "Theory of the Flight of Airplanes in Isotropic Turbulence - Review and Extension," AGARD Report No. 372, April 1961.

22 Kalman, R. E., "A New Approach to Linear Filtering and Prediction Problem," Journal of Basic Engineering, Transactions of the ASME, March 1960.

23 Kalman, R. E. and Bucy, R. S., "New Results in Linear Filtering and Prediction Theory," Journal of Basic Engineering, Transaction of the ASME, March 1961

24 Battin, R. H., "A Statistical Optimizing Navigation Procedure for Space Flight, Report R-341, M. I. T. Instrumentation Laboratory, Cambridge, Mass., May 1962.

25 Brock, L. D., "Application of Statistical Estimation to Navigation Systems," Report R-414, M. I. T. Instrumentation Laboratory, Cambridge, Mass., June 1965.

26 Broxmeyer, C., MacKinnon, D., and Madden, P., "Application of Inertial Navigation and Modern Control Theory to the All-Weather Landing Problem", Report R-613, M. I. T. Instrumentation Laboratory, Cambridge, Mass., June 1968.

N69-33436

IMPROVING AUTOMATIC LANDING SYSTEM PERFORMANCE USING MODERN CONTROL THEORY AND INERTIAL MEASUREMENTS

Duncan MacKinnon

Massachusetts Institute of Technology
Cambridge, Massachusetts

January 1969